Norwegian University
of Life Sciences

**Master's Thesis 2018 30 ECTS**
Faculty of Science and Technology
Espen Olsen

# A study of the performance of two wall attached PV systems in a Nordic climate

Linn Tabita Milde
Industrial Economics and Technology Management
Faculty of Science and Technology

# Preface

The study reported in this work was based on an initiative promoted by the Institute for Energy Technology (IFE), to analyze the performance of wall applied PV systems in a Nordic climate. I am grateful for the opportunity to conclude my degree in Industrial Economics and Technology Management with a master thesis in cooperation with such an established scientific community. The experience has been inspirational.

First of all, I want to thank my supervisor at IFE, Dr. Josefine Helene Selj, for her invaluable guidance and dedication. Further, I would like to thank my supervisor at the Norwegian University of Life Sciences (NMBU), Dr. Ing. Espen Olsen, for his time and crucial advice.

I also want to thank Mari Benedikte Øgaard, Åsmund Skomedal, Bent Thomassen, Bjørn Aarseth and the others at the Solar Energy Department at IFE, for their contributions and assistance while conducting the experiments. I am forever thankful for the time you set aside to help me.

I must give thanks to my lovely office comrades at IFE for all our coffee/tea breaks and all the fun we had together during this experience. Also, I want to thank the people in the Department for Energy System Analysis for their warm welcoming and conversations, and my fellow students in room TF210 and TF211 at NMBU.

Finally, I want to thank my parents, siblings and friends for their optimism and support throughout this period. A special thanks to those who read and commented on my final result.

Ås, 12.05.2018

Linn Tabita Milde

# Sammendrag

Mengden installert PV i Norge øker. Bygningsfestet og bygningsintegrerte solceller har blitt populære, og markedet for næringsbygg øker. Det er viktig å ta hensyn til den potensielle produksjonen når det installeres et PV system. Designet til systemet burde passe med bygningens struktur, omgivelser, og lokasjon. I tillegg er lønnsomheten viktig når man skal velge hvilket system man skal bygge.

Poenget med studiet er å analysere opptredenen til to veggmonterte systemer ved Kjeller i Norge, og finne ut hvordan de blir påvirket i et Nordisk klima. Det første systemet er et 1.30 $kW_p$ Polykrystallinsk (pc-Si) PV system og det andre er et 1.32 $kW_p$ Kobber-indium-gallium-selenid (CIS) PV system. Produksjons- og værdata fra teststedet, mellom 1. februar 2017 og 31. januar 2018, er brukt i analysen. Den gjennomsnittlige årlige sluttytelse, referanseytelse, utnyttelsesgrad og system effektivitet er beregnet for begge systemene.

Over evalueringsperioden er det funnet ut at CIS systemet produserer 14% mer energi enn pc-Si systemet. Dette er uforventede resultater fordi forskjellen i installert effekt er liten. Tapene til systemene er analysert i en kvantitativ undersøkelse for å avdekke mekanismene som påvirker systemenes prestasjon, og for å finne ut hvorfor CIS systemet presterte bedre enn pc-Si systemet. System- og array-fangst-tapene ble estimert, i tillegg til tapene grunnet tilsmussing, irradians, temperatur og vekselretter. En pulset solsimulator er i tillegg brukt for å studere prestasjonsendringene til modulene på grunn av degradering og light soaking effekten.

I løpet av evalueringsperioden var den gjennomsnittlige årlige referanseytelsen 811.7 h/år, og sluttytelsen til pc-Si og CIS systemene var henholdsvis 623.1 h/år og 697.6 h/år. Målingene utført med solsimulatoren viste at CIS modulene hadde forbedret seg grunnet light soaking effekten. Den målte installerte effekten til pc-Si systemet var 1.28 $kW_p$ og den målte installerte effekten til CIS systemet var 1.39 $kW_p$.

Det ble oppdaget at CIS systemet presterte dårligere enn pc-Si systemet på grunn av det lokale klimaet. Dette ble oppdaget gjennom estimering av temperatur- og irradianstapene, samt array-fangst-tapene. Systemtapene var større for pc-Si systemet enn for CIS systemet, med tap i endelig ytelse på henholdsvis 84.2 h/år og 35.8 h/år. Dette er antageligvis på grunn av den overdimensjonerte vekselretteren.

Resultatene viser at CIS systemet produserte mer elektrisitet per $kW_p$ enn pc-Si systemet. Av analysen ser det ut som dette delvis er en konsekvens av light soaking effekten og vekselretteren.

# Abstract

The amount of installed PV in Norway is increasing. Building applied and building integrated PV has become popular, and the market for commercial buildings is growing. The potential production is important to consider when installing a PV system. The design of the system should agree with the building structure, the surroundings, and the location. Also, the profitability is important when choosing what system to build.

The objective of this study is to analyze of the performance of two wall attached systems at Kjeller in Norway, and how they are affected in the Nordic climate. The first system is a 1.30 $kW_p$ Poly crystalline silicon (pc-Si) PV system and the second is a 1.32 $kW_p$ Copper indium gallium selenide (CIS) PV system. Output and weather data from the test location, between the 1st of February 2017 and the 31st of January 2018, are used for the analysis. The average annual final yield, reference yield, performance ratio, and system efficiency are calculated for both systems.

Over the assessment period considered it is found that the CIS system produced 14% more yield than the pc-Si system. This is unexpected since the difference in installed power of the two systems is small. The losses of the systems are analyzed in a quantitative investigation to uncover the mechanisms that are affecting the systems' performance and to find out why the CIS system performed better than the pc-Si system. The system and array capture losses were estimated, in addition to the losses due to soiling, irradiance, temperature and the inverter. A pulsed solar simulator is also used to study the performance changes of the modules due to degradation and the light soaking effect.

During the assessment period, the average annual reference yield was 811.7 h/year, and the final yield of the pc-Si and CIS systems were 623.1 h/year and 697.6 h/year respectively. The measurements conducted with the solar simulator showed that the performance of the CIS modules had improved due to the light soaking effect. The measured installed power of the pc-Si system was 1.28 $kW_p$, and the measured installed power of the CIS system was 1.39 $kW_p$.

It was uncovered that the CIS system performed worse than the pc-Si system in the local climate. This was discovered through the estimation of the temperature and irradiance losses, as well as the array capture losses. The system losses were larger for the pc-Si system than the CIS system, with a loss in final yield of 84.2 h/year and 35.8 h/year respectively. This is probably due to the oversized inverter.

The results show that the CIS system produced more electricity per $kW_p$ than the pc-Si system. From the analysis, it looks like this is partly a consequence of the light soaking effect and the inverter.

# Nomenclature

**Symbols**

| | | |
|---|---|---|
| $A$ | Area | $m^2$ |
| $c$ | Speed of light | m/s |
| $E$ | Energy | eV |
| FF | Fill factor | |
| $G_I$ | Reference in-plane irradiance | $W/m^2$ |
| $G_t$ | Irradiance on a tilted surface | $W/m^2$ |
| $h$ | Planch's constant | Js |
| $H_{constant}$ | The solar constant | $W/m^2$ |
| $H_I$ | In-plane irradiation | $kWh/m^2$ per year |
| $H_{sun}$ | Power density from the sun | $W/m^2$ |
| $I$ | Current | A |
| $k_B$ | The Boltzmann constant | $JK^{-1}$ |
| $L_C$ | Array capture losses | h/year or h/d(day) |
| $L_S$ | System losses | h/year or h/d(day) |
| $n$ | Ideality factor | |
| p-rate | Power rate | % |
| $P$ | Power | W |
| $P_o$ | Nominal power | $W_p$ |
| $PR$ | Performance ratio | % |
| $q$ | The elementary charge | C |
| $R$ | Resistance | Ω |
| $T$ | Temperature | °C |
| $V$ | Voltage | V |
| $Y_A$ | Array yield | h/year or h/d(day) |
| $Y_F$ | Final yield | h/year or h/d(day) |
| $Y_R$ | Reference yield | h/year or h/d(day) |
| $\eta$ | Efficiency | % |
| $\lambda$ | Wavelength | μm |
| $\Theta_z$ | Zenith position | ° |

| | | |
|---|---|---|
| $\Theta_A$ | Azimuth position | ° |

**Abbreviations**

| | |
|---|---|
| AM | Air Mass |
| AOI | Angle of incidence |
| AC | Alternating current |
| BAPV | Building applied photovoltaics |
| BIPV | Building integrated photovoltaics |
| CIS | Copper Indium Selenide |
| DC | Direct current |
| DNI | Direct normal irradiance |
| GHI | Global horizontal irradiance |
| MPP | Max power point |
| MPPT | Max power point tracker |
| mc-Si | Mono crystalline Silicon |
| pc-Si | Poly crystalline Silicon |
| POA | Plane of array |
| PV | Photovoltaic |
| STC | Standard test conditions |

**Subscripts**

| | |
|---|---|
| *0* | Saturation |
| *d* | Diode |
| *diff* | Diffuse |
| *dir* | Direct |
| *F* | Final |
| *G* | Gap |
| *in* | Incident |
| *max* | Maximum |
| *mpp* | Maximum power point |
| *oc* | Open circuit |
| *p* | Shunt |

| | |
|---|---|
| *ph* | Photon |
| *R* | Reference |
| *ref* | Reflected |
| *s* | Series |
| *sc* | Short circuit |
| *sys* | System |

# Contents

# 1 Introduction

During the last decades, the world has seen a vast growth in renewables. With this growth, the global photovoltaic market has grown rapidly. The installed capacity has increased from 6 GW in 2006 to 291 GW in 2016. Also, the price of both the manufacturing and installation of PV has decreased. From Q1 2010 to Q1 2017 the PV Watt price in Europe decreased by 83%. Good quality modules from China could in 2017 be produced for USD 0.4/W. Crystalline silicon-based PV currently dominate the market. In 2016 it accounted for about 94% of the total PV production. The total installation costs of PV vary for different domestic markets, due to reasons including labor costs and the experience of the developers. Globally, the PV manufacturing costs have decreased more rapidly than the installation costs (International Renewable Energy Agency, 2018).

In Norway, about 96% of the electricity come from hydropower (Statistics Norway, 2017). The power grid is connected to Europe, and yearly the country exports more electricity than it imports. The power prices are low compared to the rest of Europe. This makes it less profitable to install solar power in Norway compared to in other European countries. Still, the demand for solar power is increasing. The environmental awareness of the population has increased the last years, and environmentally friendly buildings have grown in popularity. Concepts like energy-plus-houses or zero emission buildings, in addition to stricter energy demands for new buildings, provides entry for solar energy in the energy market. Progress has also been made among the suppliers, and new companies have emerged in the market.

The last two years the installed PV capacity in Norway has increased rapidly, from 15.3 $MW_p$ in 2015 to 44.9 $MW_p$ in 2017 according to estimates from the consulting firm Multiconsult (Multiconsult & Viak, 2018). The larges growth and profitability are in installations on commercial buildings. This has occurred due to decreasing prices, green certificates, environmental awareness and clarifications on how much power that can be fed into the grid.

Profitability analysis has earlier been performed for PV installed in residential and commercial buildings. It is estimated that an internal rate of return of 5% can be achieved, based on today's price level, tariffs, and the expected increase in the power price. The energy price in Norway is predicted to increase towards 2030 (Jonas Skaare Amundsen, 2017).

PV on commercial buildings can either be building applied, BAPV, or building integrated, BIPV. BAPV is installed on top of the exterior surface of the building. Oppositely, BIPV replaces conventional building materials such as the façade material. The advantage of BIPV is that it saves the additional cost of the material that is replaced. Today solar modules are almost in the same price range as some types of frequently used brick facades (Bjørn Thorud, 2017). The advantage of BAPV is that it can be easier installed at an optimal tilt on a building, and it is less complicated to incorporate onto old buildings than BIPV.

Before installing PV systems on buildings, it is important to know the energy demand of the building, and what time of day the building is consuming the most energy. In commercial buildings, the highest energy demand is in the middle of the day, which makes the consumption

fit the production of PV systems on clear days. The architecture and surroundings of the building are also relevant when installing PV systems. Flat roofs or large south facing walls are the most suitable areas for solar energy, and it needs to be small amounts of shading due to surrounding objects.

There are several PV technologies on the market today. What technology to install on a building depends on the desired energy production and the desired design. Some PV modules now look like normal black façade panels. Other modules can come in different colors. There are PV technologies that produce more energy per installed area than others. Also, there are variations in how different technologies respond to local climate conditions.

The purpose of this thesis is to analyze the performance of a wall attached 1.30 $kW_p$ Poly crystalline silicon PV system, and a wall attached 1.32 $kW_p$ Copper indium gallium selenide PV system in Norway, and see how they are affected in a Nordic climate. It is also investigated why the CIS system is producing more electricity than the pc-Si system. Measured data between the 1$^{st}$ of February 2017 and the 31$^{st}$ of January 2018 were analyzed to evaluate the suitability of the two technologies as wall attached systems in a Nordic climate. This analysis is performed looking at the climate and system impact, as well as the degradation and light soaking effect. The latter is measured using a pulsed solar simulator. The results will give an indication of the system performance and which technology that is best suited as wall attached systems in a Nordic climate.

# 2 Theoretical prerequisites

The theory of chapter 2 is heavily based on PVeducation.org (Honsberg & Bowden, 2014) and the book: *Solar Energy – The physics and engineering of photovoltaic conversion technologies and systems* (Smets et al., 2016).

## 2.1 Irradiation

### 2.1.1 Energy from the sun

Photovoltaic technology directly converts electromagnetic radiation from the sun to electricity. The sun is perceived as a constant source of energy. Fusion reactions in the center of the Sun create photon radiation in a wide spectrum of wavelengths. In each photon energy is stored and the amount of energy is given as:

$$E_{ph} = h \times c/\lambda \tag{1}$$

Where $h$ is Planch's constant, $c$ is the speed of light, and $\lambda$ is the wavelength of the photon. The power density radiated from the surface of the sun, $H_{sun}$, is 5.961 * $10^7$ W/m$^2$ (Honsberg & Bowden, 2014). Only a small part of this energy reaches the earth. Still, it is the source of all life on our planet. Energy can neither be created or destroyed and appears in numerous forms. Both living organisms and the nonliving is dependent on energy in the form of radiation. Photovoltaic technology has broadened our understanding of the utilization possibilities that lie in electromagnetic radiation.

### 2.1.2 The solar spectrum

The power density of the irradiance reaching the atmosphere of the earth is also called the solar constant. The value of the solar constant, $H_{constant}$, is 1353 W/m$^2$ (Honsberg & Bowden, 2014). The solar constant and the spectrum distribution of the incoming radiation are the basis for what we call the Air Mass zero, AM0. In the atmosphere particles of different sizes absorb, reflect and scatter the irradiation in different directions, resulting in; a reduction of the incoming power density, path changes for parts of the irradiation and an alteration of the spectrum distribution reaching the ground. The absorbance of the radiation is separated into different AM levels, depending on how far the radiation has travelled through the atmosphere. Where the Sun is directly overhead, AM1, the rays have the shortest path to the surface of the earth. With an increasing angle of incidence from the shortest path length, the AM increases because the rays must pass more of

the atmosphere. The AM level AM1.5 is widely used, though it belongs to an angle of incidence of 48.2° (Honsberg & Bowden, 2014).

The amount of scattering and absorption affecting the radiation depends on the state of the atmosphere. The varying atmospheric factors include cloud coverage, the water vapor and dust particle contents, and the thickness and composition of the ozone layer. The AM0 spectrum is illustrated in Figure 2.1, together with the reduced AM1.5 spectrum. The solar constant is calculated by integrating the power density over the range of wavelengths. In the AM1.5 spectrum, there are clear power reductions at the wavelengths that normally are absorbed by $H_2O$, $O_2$, and $CO_2$, which are some of the molecules dominating the atmospheric content.

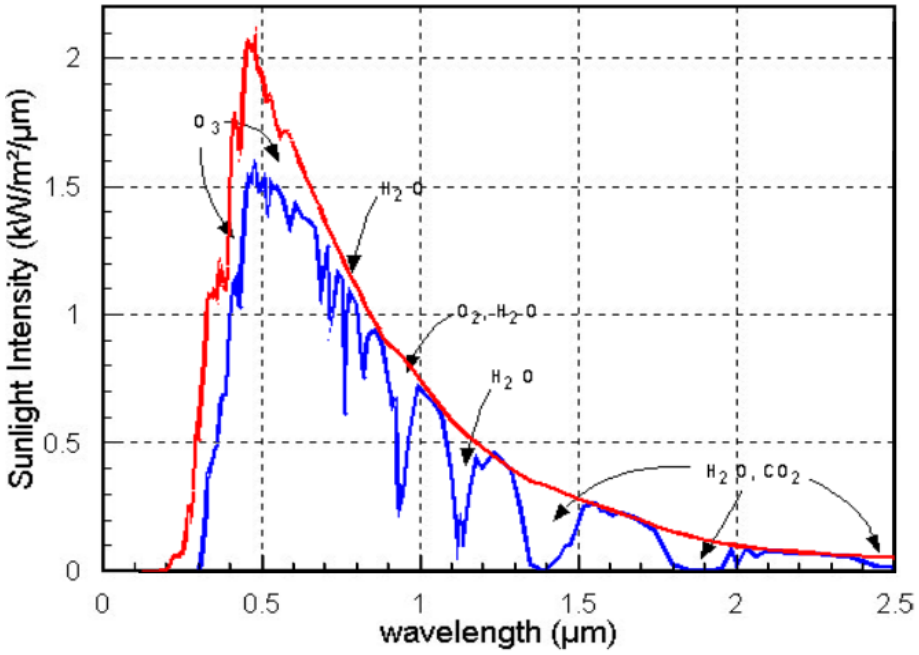


*Figure 2.1: This is a plot of the spectral distribution of the solar spectrum. The red curve is the AM0 spectrum, and the blue curve is the AM1.5 spectrum. In the AM1.5 spectrum, the intensity of some wavelengths are greatly reduced. Some of the particles that cause this reduction are noted the figure. (Honsberg & Bowden, 2014)*

### 2.1.3 Scattering

When the radiation passes the atmosphere, the spectrum is not only reduced, it is altered too. So is the pathway for a large amount of the photons. The scattering effect creates path changes and creates what is called diffuse radiation.

The best-known mechanisms for scattering are Rayleigh scattering and Mie scattering. Rayleigh scattering is dependent on the energy of the incoming photon. The blue short waved photons have a higher probability of being scattered in this manner. By Rayleigh scattering, the molecules absorbes the photon and releases it in any direction. This scattering mechanism is not changing the energy of the photon, only its direction, and that is why the sky appears blue.

Mie scattering, on the other hand, happens when photons collide with large molecules in the atmosphere such as water drops, aerosols or dust, with a particle size lager than the photon wavelength. A large number of wavelengths can be affected by Mie scattering. This scattering effect only affects the direction of the radiation small amounts, so mostly the radiation continues in the same direction as before. Mie scattering increases with large amounts of water vapor in the sky, and that causes the light intensity to decrease in cloudy conditions (Nave, 2016).

### 2.1.4 The components of irradiation

The irradiance on a horizontal surface consists of the direct radiation from the sun and the diffuse radiation. The sum of these two is often called global horizontal irradiance, GHI. On a tilted surface the irradiation also includes the reflected radiation from surrounding surfaces. The total irradiance on the plane of array, POA, of a tilted surface is given by:

$$G_t = G_{dir,\,t} + G_{diff,\,t} + G_{ref,\,t} \tag{2}$$

Where $G_t$ is the irradiance on a tilted surface, $G_{dir,t}$ is the direct component, $G_{diff,t}$ is the diffuse component, and $G_{ref,t}$ is the reflected component.

$G_t$ is important in any modelling or efficiency calculation of a PV system because the PV power production depends on the irradiation incident on the cell surface. When calculations of $G_t$ is needed, the direct, diffuse and the reflected component is calculated separately and summed together. The direct normal irradiance, DNI, and the angle of incidence, AOI, are used to calculate $G_{dir,t}$. This component is derived in the following way:

$$G_{dir,\,t} = \mathrm{DNI} * \cos(\mathrm{AOI}) \tag{3}$$

$G_{diff,t}$ is more complicated to calculate, and several models exist aimed at estimating it. The simplest model is the isotropic sky model that uses the direct horizontal irradiance, DHI, to calculate the diffuse component. This model assumes that the whole sky contributes equally to the diffuse radiation.

The ground reflected component is dependent on both the GHI and the albedo conditions. The albedo value is the reflected fraction of the total irradiance incident on a surface. This value increases with brighter surfaces.

Alternatively, to deriving the total irradiance from calculations, it is possible to measure $G_t$ directly. This can be done using a Pyranometer that measures the irradiance on a 180˚ sphere around the POA. The measured irradiance will then include all the components of the incident radiation. When using such a technique, one also disregards some of the reflection losses, because similar reflection losses often occur at the surface of the measuring devise (Sandia National Laboratories).

### 2.1.5 Relevant angles

In PV applications the positioning of the POA is crucial to optimise the amount of incoming irradiation. Due to the location and time dependent position of the Sun, the AOI of the direct radiation varies. The position of the POA and the Sun is often given relative to the horizontal coordinate system, where two angles describe the relative position. The zenith position, $\Theta_z$, is the angle, between the normal angle to the horizon and the normal to the POA. This angle is the same size as the tilt angle of a PV module. The azimuth position, $\Theta_A$, is the angle between the normal of the POA and the direction towards the North. The angles are illustrated in Figure 2.2, picturing the celestial sphere.

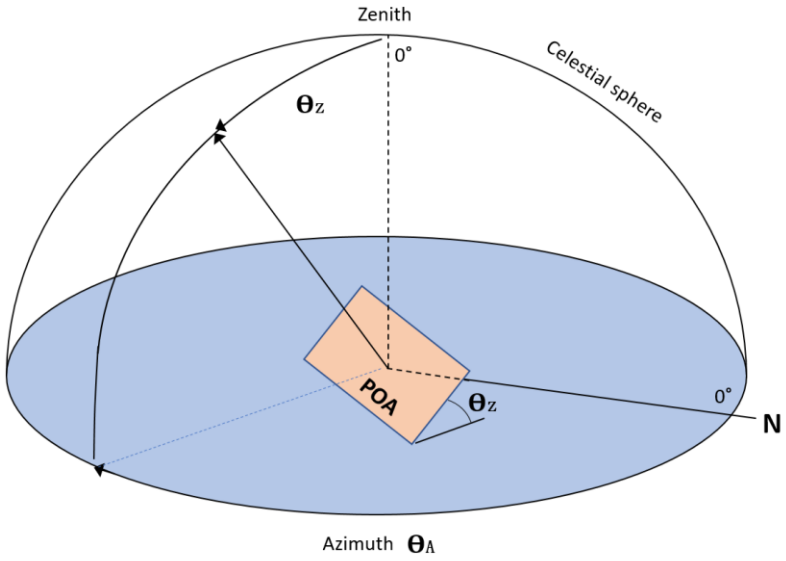


*Figure 2.2: Illustration of the celestial sphere with a tilted module. The tilt angle, zenith angle, and azimuth angle are marked. These angles are used to describe the position of the POA.*

### 2.1.6 Standard test conditions

Standard test conditions, STC, is a reference frame when comparing the performance of solar cells. At STC the irradiance is 1000 W/m2, the solar cell temperature is 25˚C, and the solar spectrum is equal to that of AM1.5.

The irradiation, temperature and AM changes due to weather, season and the position of the sun in the sky. Thus, it is not possible to obtain continuous STC outside. That is why local climate conditions and weather is highly relevant in the placement of a PV system.

## 2.2 The photovoltaic effect

### 2.2.1 Photon energy and the bandgap

The difference between a conductor and an isolator is that in a conductor the valence electrons are free to move in the crystal structure, but in an isolator they rarely move away from its original atom. The location of valence electrons in material structures can be pictured as two energy bands in which the valence electrons can exist. This is called the bandgap theory. The energy bands are called the valence band and the conduction band, and they consist of all the legal electron energy levels that the atoms of the structure posesses. See Figure 2.3. The energy gap is the space separating the two bands. This region is the energy states the valence electrons can never possess while being in the structure. $E_G$, the gap energy, is the energy the valence electrons lack in order to excite to the conduction band where they can move freely in the structure of the crystal. In a conductor there is no such gap, all energy states are legal. In an isolator the gap is large. The solar cells are made out of semiconductor materials. Semiconductors have a bandgap, but it is smaller than the bandgap of an isolator.

The bandgap is essential for the photovotalic effect in the solar cell to work, but it is also useful that the gap is not too large so that charge barriers can jump from one band to the other and move in the crystal stucture. Photons allow the electrons to borrow the energy necessary to climb to the conduction band. This is called photogeneration. When the temperature of the material is over 0 K or the material is absorbing electromagnetic radiation there will be a random motion of charged particles in the material. These are called thermally excited electrons.

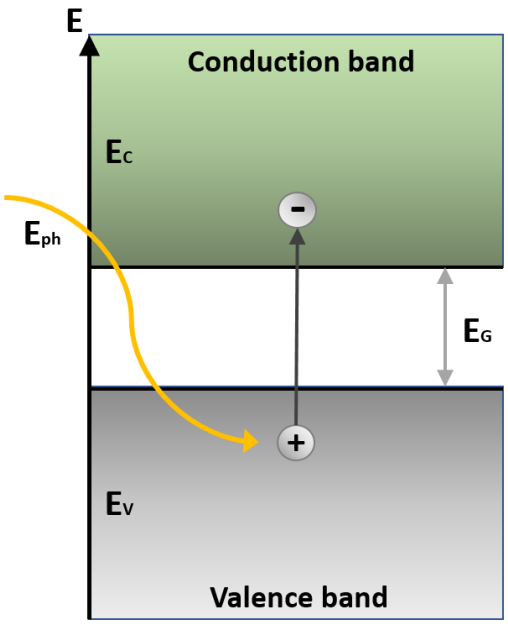


*Figure 2.3: Illustration of the bandgap model. The valence and the conduction bands are separated by a bandgap of $E_G$. When valence electrons are absorbing photons, they can move from the valence band to the conduction band.*

### 2.2.2 The photovoltaic effect

The bandgap theory applies to the physics behind the photovoltaic effect because it can explain the behavior of the charged particles, in a semiconductor. In a solar cell, a p-n junction is created through doping of two semiconductors with opposite polarity and placing them together. One of the materials has an excess of positively charged carriers, "holes", the other an excess of negatively charged carriers, electrons. Apart the charge neutrality of the materials is maintained. When they are placed together some of the surpluss electrons from the n-type material will cross over to acceptor atoms in the p-type material, and holes will replace them. A space charge develops around the junction, due to the charge of the ionized donor and acceptor atoms. The space charge creates a force affecting the electrons in the oposite direction of the flow. This force will, in the end, stop the electron flow and an equilibrium will rise. The electric field that establishes across the junction is called the depletion or space charge region of the solar cell. When the material is in a state of equilibrium, no free charge carriers can cross the depletion region because of the electrostatic potential difference between the two materials.

The region outside of the depletion region is called the quasi-neutral regions. The p-type area is usually called the Base, and the n-type area is called the Emitter. Outside of the junction, the majority charge carriers can behave normally and be thermally excited. In darkness, free electrons are generated and recombine with atoms at an equal rate, and the free particles can move in the material. The name of the charge carriers when the cell is in darkness is the intrinsic carrier concentration.

The movement of the charge carriers is due to diffusion and drift. Diffusion is caused by the random thermal motion of the charge carriers. These particles will move to the areas with the most space. Drift is due to charge barriers movement in the proximity of an electric field.

When light is directed towards a solar cell, the number of free charge carriers in the material will increase. Then, some of the photogenerated electrons in the Base will drift across the junction to the Emitter before they manage to recombine with an acceptor atom. The electrons will only be able to flow in this direction. In the Emitter the number of negative charge carriers will increase while the Base becomes positively charged. This results in a new voltage settling across the cell in the opposite direction of the voltage across the junction, and a new equilibrium is reached. The new voltage over the cell is called the open circuit voltage, $V_{oc}$.

If an external circuit is connected between the Emitter and the Base, a pathway for the electrons from the Emitter to the Base will arise. This will decrease the voltage across the cell, and electrons will continue to drift across the junction. Are no load connected to the external circuit the current through it will be high, and the cell voltage will become zero. The maximum current through the curcuit is called the short circuit current, $I_{sc}$. The basic composition of a solar cell is illustrated in Figure 2.4.

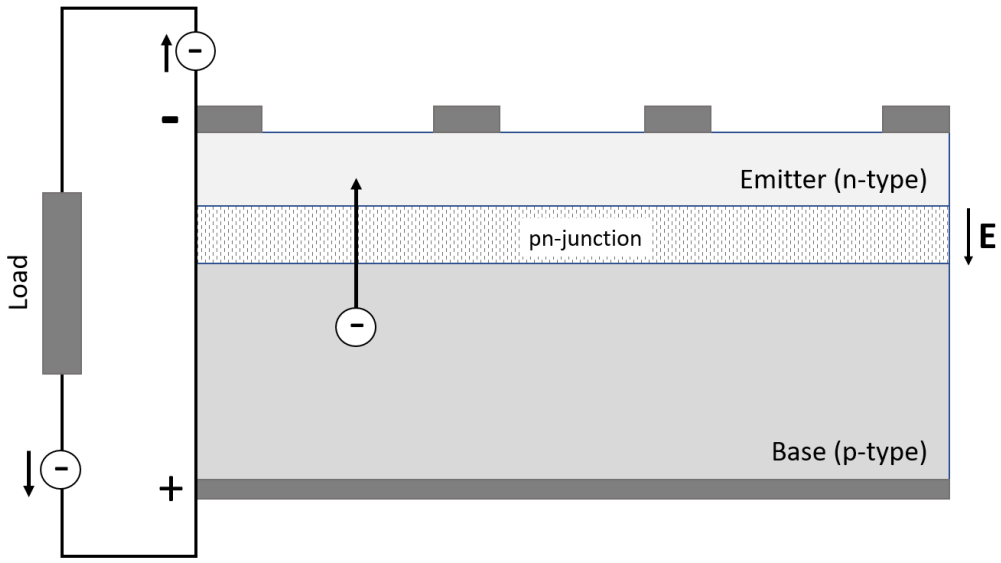


*Figure 2.4: Drawing of the standard solar cell. The Base is placed on the rear side and the Emitter on top of it. The depletion region is the area between them. When the cell is illuminated electrons from the Base can move across the depletion region, some electrons will then pass through the external circuit back to the Base.*

## 2.3 PV cell parameters and basic definitions

### 2.3.1 Short circuit current and open circuit voltage

The performance of a solar cell is characterized by certain parameters. The $I_{sc}$ and $V_{oc}$ are important parameters defining the possible power production of a solar cell. The short circuit current is dependent on the incident light, and the photogenerated current. It is also affected by the optical properties of the cell and recombination. The open circuit voltage depends on the doping of the cell material and the light generated current.

### 2.3.2 I-V characteristics and MPP

The relation between the circuit current and the voltage of a solar cell is called the I-V characteristic, where the limits for the current and voltage is $I_{sc}$ and $V_{oc}$. For a module consisting of several cells, the I-V characteristic is the representation of the current and voltage all the cells can produce together. An example of this is illustrated in Figure 2.5. Important parameters on the I-V curve except for the $I_{sc}$ and the $V_{oc}$ is the current, $I_{mpp}$, and the voltage, $V_{mpp,}$ at the maximum power point, MPP. At this current and voltage, the cell operates at its maximum efficiency and with a maximum power output $P_{max}$. With a maximum power point tracker, it is possible to make the modules operate at the highest possible power output at all times, although it is dependent on the situational I-V curve. The I-V characteristic of PV modules changes continually with factors such as the light intensity, spectrum, and temperature. That is why the characteristics of a PV module often is given at STC.

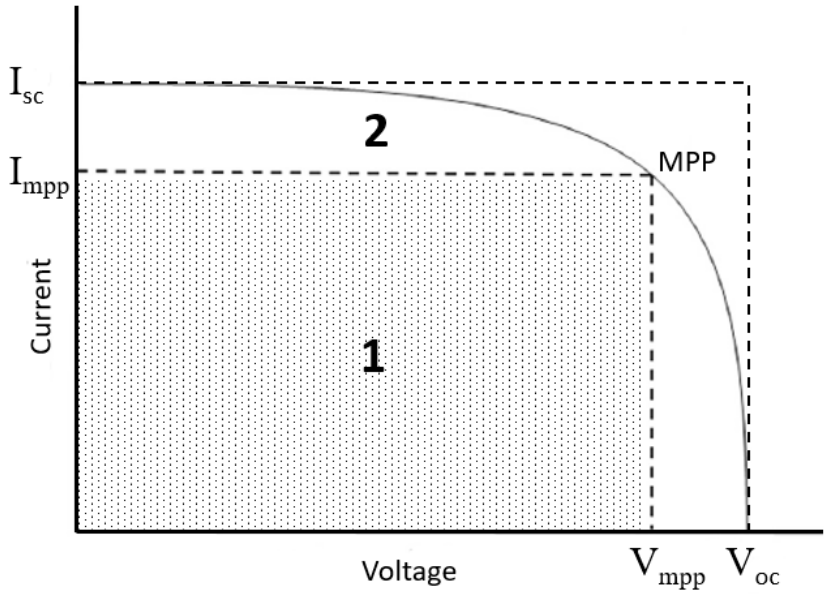


*Figure 2.5: Drawing of the I-V characteristics with important parameters as the $I_{mpp}$, $V_{mpp}$, $I_{sc}$, $V_{oc}$ and MPP.*

### 2.3.3 Fill Factor and efficiency

The fill factor, *FF*, is the ratio between $I_{sc}$ multiplied with the $V_{oc}$ and the maximum power, or the ratio between area 1 and area 2 in Figure 2.5. A low *FF* indicates that the I-V curve is pulled close to the center of area 1, a high *FF* indicates an I-V curve that instead covers most of of area 1. The efficiency will increase if *FF* is high, and an *FF* equal to 1 is not possible to achieve. *FF* is given as:

$$FF = \frac{P_{max}}{I_{sc}V_{oc}} = \frac{I_{mpp}V_{mpp}}{I_{sc}V_{oc}} \tag{4}$$

### 2.3.4 Conversion efficiency

The following formula gives the efficiency, $\eta$, of a solar cell.

$$\eta = \frac{P_{max}}{P_{in}} = \frac{I_{mpp}V_{mpp}}{P_{in}} = \frac{I_{sc}V_{oc}FF}{P_{in}} \tag{5}$$

Where the irradiance incident on the cell is given as $P_{in}$. This equation also applies to the calculation of the PV module efficiency.

### 2.3.5 The equivalent circuit – two diode model

When the solar cell is in darkness, it behaves similarly to a diode. The physics behind the solar cell can therfore be represented with an equivalent diode circuit. There are two different ways of modelling it; the one diode model with the equivalent circuit of an ideal diode, and the two diode model that also takes into account the non-ideality of the cell. The I-V characteristic of the two diode model is given by Equation 6, and the circuit is illustrated in Figure 2.6.

$$I = I_{ph} - I_{d1} - I_{d2} - I_p = I_{ph} - I_{01}\left\{exp\left[\frac{q(V-IR_S)}{n_1 k_B T}\right] - 1\right\} - I_{02}\left\{exp\left[\frac{q(V-IR_S)}{n_2 k_B T}\right] - 1\right\} - \frac{V-IR_S}{R_p} \quad (6)$$

$I_{d1}$ and $I_{d2}$ is the current through the ideal and non-ideal diode, $I_{01}$ and $I_{02}$ represent the saturation currents, $I_{ph}$ is the photogenerated current, $I_p$ is the current through the shunt resistance $R_p$ and $I$ is the output current. The remaining factors are the series resistance $R_s$, the elementary charge $q$, the Boltzmann constant $k_B$, the cell temperature $T$, and the output voltage $V$. The ideality factors of the ideal and non-ideal diodes is $n_1$=1 and $n_2$>1.

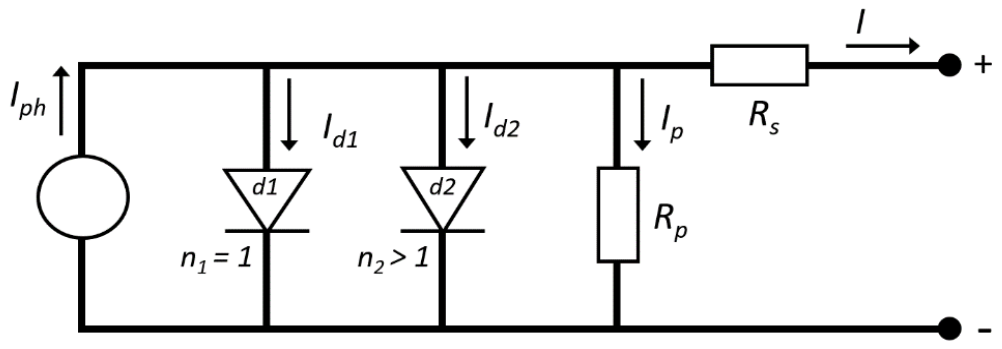


*Figure 2.6: The two-diode model equivalent circuit.*

### 2.3.6 Serie and shunt resistance

$R_s$ is a term for the current resistance through the material of the cell. It also includes the transmission resistance to the metal contacts, and between the rear and top contacts. The *FF* decreases when the $R_s$ increases. Thus, the series resistance should be as small as possible, and optimization of the cell design does this.

$R_p$ is caused by manufacturing defects such as impurities, that increases the recombination and gives the light generated charge carriers an alternative path. Opposite to the series resistance, the *FF* of a solar cell decreases with a low $R_p$. Thus, it is desired to have a high shunt resistance. At low light intensities, this factor has a big effect on the performance of the solar cell. Since there is a smaller light generated current and the proportion of the generated current that recombines increases. At high light intensities and high currents the effect of the series resistance increases instead. This makes the irradiance conditions at the location of the PV system relevant when choosing what type of solar cell to install.

## 2.4 The photovoltaic system

### 2.4.1 The pc-Si solar cell

Silicon is the most extensively used semiconductor material in solar cells. The silicon is made into doped wafers that typically has a thickness between 100 and 300 µm. The wafers can be manufactured in different ways, but are categorized into two groups; the monocrystalline silicon cells, mc-Si, and the polycrystalline silicon cells, pc-Si. The mc-Si crystal lattice is whole, and without any grain boundaries, the pc-Si lattice is discontinuous with many crystal grains grown together. Both types are heavily used. The mc-Si has the advantage of often having a higher efficiency than the pc-Si, but the pc-Si is easier and cheaper to manufacture.

Despite the different wafers, the mc-Si and pc-Si cells can be assembled in the same way. The typical composition of a crystalline silicon cell is to have a thick p-type Base wafer and a thinner n-type Emitter layer on top of it. The back side of the p-type wafer is connected to a back contact covering the whole surface area. On top of the n-type layer, there is always a thin layer of antireflective and passivating coating. At the front of the cell, there is a metal grid of front contacts, which transfers the current to the back contact of the next cell. The pc-Si cells are made into squares. A drawing of the typical pc-Si cell and a typical CIS cell can be seen in Figure 2.7.

### 2.4.2 The CIS solar cell

Copper indium gallium selenide, CIGS or CIS, solar cells is a thin film technology, also classified under the second-generation PV technologies. As the name indicates, these solar cells are much thinner than the mc-Si and pc-Si cells, and they are often less efficient. Thin-film solar cells are in need of a carrier that gives them mechanical stability. This design gives them the ability to be shaped and even made flexible. The CIS cell consists of several layers with varying bandgap energies, the layer with the highest bandgap on top. Their main absorption layer is a p-type CIS layer, and on top of it, there is a smaller n-type CIS layer. Over the n-CIGS layer, there is often a buffer layer with CdS. The n-type layer is extended with n-type ZnO layers, that acts as the front surface contact of the cell. On the back side of the p-type CIS layer, there is a back-surface contact. The whole cell is then usually deposited on a glass surface.

The difference in the cellular structure of the CIS cells and the pc-Si cells also changes the composition of the cells into modules. The CIS cells are made long and narrow, and they are connected in series. Differently, the crystalline silicon cells are made into squares. The modules are constructed connecting three strings in parallel, where the strings consist of 20 series connected cells. On the other hand, the module to module connection methods is similar for both technologies.

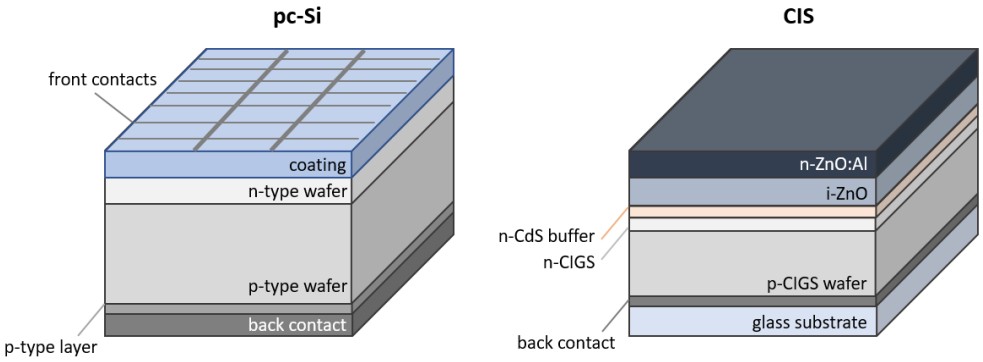


*Figure 2.7: Scheme of a pc-Si cell to the left and a CIS cell to the right.*

### 2.4.3 The PV array

A PV array is the collection of interconnected PV modules. There are two methods for connecting PV modules: series and parallel connections. With a series connection, the positive outlet of one module is connected to the negative outlet on the next module. Oppositely, with a parallel connection, the positive outlets of the modules are connected, and the negative outlets are too. A whole array can consist of both parallel and series connections. The modules that are connected in parallel will have a voltage equal to one module, and the individual modules' currents will be summed together. Are the modules connected in series, on the other hand, the voltage will be summed, and the current will not be. The chosen connection of the PV modules will thus decide the look of the array's I-V characteristic and can influence the system performance due to mismatch losses.

### 2.4.4 Mismatch losses

Mismatch losses are the losses that occur due to the parameter variation between the modules in an array. As pointed out, the array I-V characteristic depends on the connections between the modules. The modules do not have the same properties and are experiencing slightly different conditions from one another. Therefore, the current of a series connected array is limited by the lowest $I_{sc}$ in the circuit, and the voltage of a parallel connected array is instead limited by the lowest $V_{oc}$ in the circuit. The mismatch loss is the difference between the true $P_{max}$ of the array, and the assumed $P_{max}$ of the array, which is the summed maximum power of all the modules. The right composition of the PV array is also important regarding the rest of the components of the PV system.

### 2.4.5 The components of the photovoltaic system

In addition to the PV array, the PV system consists of additional components. The components include a mounting structure for the modules, cables, DC-DC converters, and inverters. It also includes the load, batteries or connections to the grid, depending on the system being stand-alone or grid connected. A DC-DC converter, or a charge controller as it is also called, adjust the output of the array, so it is stable and converts it to a compatible input for the inverter. The DC-DC converter controls the adjustment with a maximum power point tracker, MPPT, that can track the voltage at the maximum power output. In a grid-connected system, the DC-DC converter is often integrated with the inverter. The other function of the inverter is to convert the direct current, DC, output from the modules to grid compatible alternating current, AC, electricity.

In all the transfer and conversion components of the system, there is electricity loss. These losses are often referred to as system loss. For example, the inverter cannot convert all the power into AC. The conversion efficiency depends on the type of inverter and how it is fitted to the PV array. If the voltage of the array in under- or oversized compared to the intake of the inverter, the efficiency will decrease. The startup voltage is the voltage that the array must deliver for the inverter to start functioning. The inverter efficiency varies with the power input into the inverter. For string inverters, the efficiency is usually quite stable around 90-97%, but when the power gets close to zero, the efficiency drops rapidly. The inverter will not function at all if the power input is too low. The inverter uses power from the grid to operate, and this also counts as system losses.

Cable resistance is another cause of power losses. The power loss in the cables depends on the resistance and the current to the second power. These losses increase with the length of the cables and the size of the current. Cable losses, thus, depends on the system arrangement. In addition to the system loss, there is additional loss related to the inability of the array to fully utilize the available irradiance. This loss is often referred to as the array capture loss of a PV system. Most of the mechanisms that cause these losses are external factors (Jahn et al., 2000).

## 2.5 PV system loss mechanisms

The efficiency and power output of a solar cell depends on the I-V characteristic, and are thus sensitive to factors that alter the parameters: $I_{sc}$, $V_{oc,}$ and $FF$. The performance of PV modules is usually measured at STC. These conditions rarely apply, and the power reductions due to the real climate conditions are counted as losses. In addition to climate conditions, factors like degradation and light soaking also affect the performance of the modules.

### 2.5.1 The cell temperature dependence

The cell temperature is one factor that affects the I-V characteristic parameters, because increasing the cell temperature lowers the band gap energy of the semiconductor. With a reduced bandgap, additional electrons are thermally excited, increasing the intrinsic carrier concentration and the

diffusion current in the material. The electrical properties of the cell consequently change. The $I_0$ changes with the number of intrinsic carriers, and $V_{oc}$ is reduced due to its dependence on $I_0$. The effect of increased temperature is a reduction in the $V_{oc}$ and an increase in the $I_{sc}$, the voltage being more sensitive to the change.

How the output power changes with the cell temperature are modelled extensively, as the relationship is not only dependent on material properties but also system and environmental variables. Nevertheless, most models are assuming a linear relationship between the temperature and the power output of the cell. That is why the relation repeatedly is represented by a temperature coefficient given in %/˚C (Skoplaki & Palyvos, 2009). The temperature coefficient varies among PV modules. The c-Si modules have a greater cell temperature dependence than thin film modules. The temperature dependence of pc-Si and CIS solar modules is illustrated in Figure 2.8.

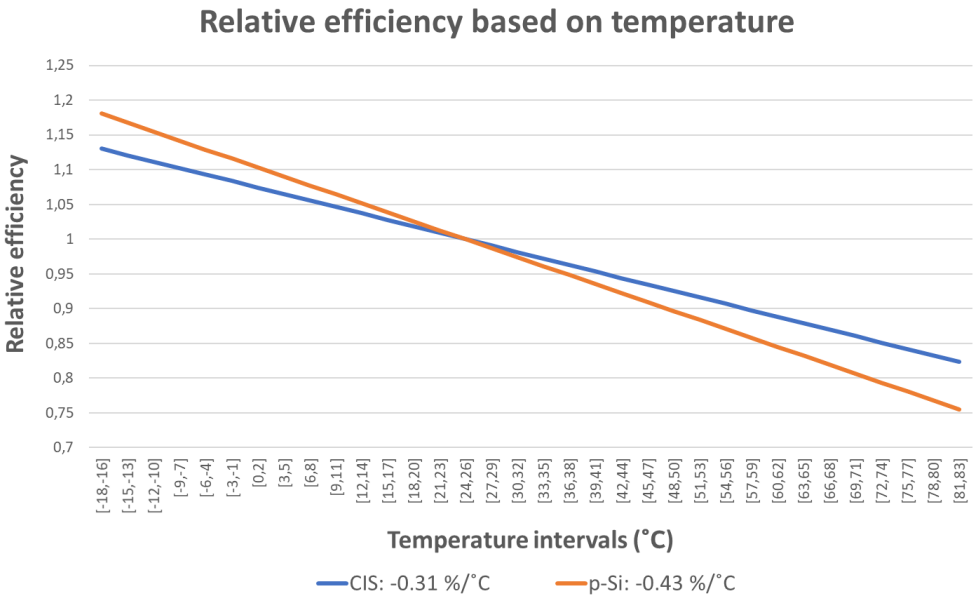


*Figure 2.8: Illustration of the linear temperature dependence of pc-Si and CIS solar modules.*

### 2.5.2 The impact of the light intensity on the PV performance

Outdoors the light intensity varies, and the efficiency of the solar module is affected by this. The intensity of the light at STC and AM1.5 is 1000 W/m$^2$. Unfortunately, real climate conditions very rarely hold this intensity level. Local atmospheric conditions and the position of the sun are factors that greatly affect the irradiation incident on the module surface. Between sunset and sunrise, the irradiation is approximately zero, and there is no power production. It is the efficiency variation caused by the varying intensity level during the day, that can be counted as losses. All PV modules have a unique response to different light intensities because the incident intensity changes all cell parameters. The intensity correlates to the number of photogenerated electrons in the cell. This affects $I_{sc}$, $V_{oc}$, $FF$, the efficiency, and even the series and shunt resistance as described in section 2.3.6.

*Optical losses*

The irradiation absorbed by the solar cell is dependent on the optical losses of the cell. Some portion of the light reaching a surface is reflected away. The amount of the light that is reflected depends on the area and texture of the surface, the light intensity, and on the angle of incidence. When the angle of incidence increases, the reflected portion of the light also increases. There is also some light that passes the cell without being absorbed. This is the transmitted radiance, and it can be reduced by increasing the absorbance of the cell or making it thicker. It is also possible to change the properties of the module surface to decrease the reflection losses. This can be done with surface texturing or antireflective coating. Optical losses can be reduced with optimization of solar cell design. Other light intensity related losses require considerations of the surrounding area.

*Effect of shading*

The shading of a PV module decreases the irradiation incident on its surface. Consequently, the power production is reduced and the I-V characteristic of the cell is changed. Shading affects the pc-Si and CIS modules differently due to their composition. The CIS modules with its long and narrow series connected cells have a linear response to shade (Frontier, 2016). The assembly of the pc-Si modules makes them behave differently to shading than the CIS. In a series connected string, the current is limited by the cell with the lowest current. When one or more cells in a string are shaded, the current is reduced proportionally, and that affects the current in the whole string. When a cell is fully shaded, it will work as a diode, and it will not let any current pass it. To reduce the losses due to shading bypass diodes are placed over each string.

Hot-spot heating happens as a result of the shading of one string connected cell that still has a small current through it. In this situation the other cells in the string will be forced to carry the same current as the shaded one, requiring them to produce a higher voltage. The voltage of all the other cells will then cause a reverse voltage to fall over the shaded cell. Power may then dissipate into the cell, and damage it. This will reduce the performance of the cell, and the entire module for its reminding lifetime.

*Effect of soiling*

Light absorbance in the cell can be reduced by the amount of dirt that accumulates on the surface of the module. Small dust particles, soil or larger coverage like bird droppings will gather on the surface of the modules when they are placed outside. The soiling, as it is called, will both absorb some of the incoming radiation and increase the portion of it that is reflected away. Cells with soil will act as if they are shaded. That is why soiling both can cause losses due to lower light intensities, and losses due to damages to the cells and mismatch losses.

*The albedo effect*

The albedo is the fraction of the solar radiation hitting a surface that is reflected. As described in section 2.1.4, the total irradiation consists of direct, diffuse and reflected light. The albedo of the local surroundings of the PV system affects the total amount of irradiation reaching the surface of the modules. With a high albedo the reflected portion of the radiation increases, and so is the intensity of the light that reaches the modules. The difference in albedo between surfaces with asphalt and surfaces covered by grass or soil is minor. The albedo of snow is high in comparison with the albedo of asphalt, the albedo of dry asphalt being between 0.09-0.15 and the albedo of fresh snow being around 0.82 (Sandia National Laboratories). In Nordic environments with a high occurrence of snowfall, the albedo can significantly affect the seasonal variations in the reflected part of the irradiance on a PV system.

### 2.5.3 Spectral mismatch losses

The solar radiation reaching the module surface has two important features. The effect of the first feature, light intensity, has already been deliberated. The other feature is the spectral distribution of the irradiance, which also affects the PV-system performance. The solar cell's ability to turn the photon energy into electricity varies with the wavelength of the photons. The spectral mismatch losses are sometimes defined by the spectral response of a solar cell. The spectral response is the ratio between the light generated current and the power incident light on the solar cell. This ratio takes the decreasing power at longer wavelengths into account. An example of a spectral response curve is shown in Figure 2.9.

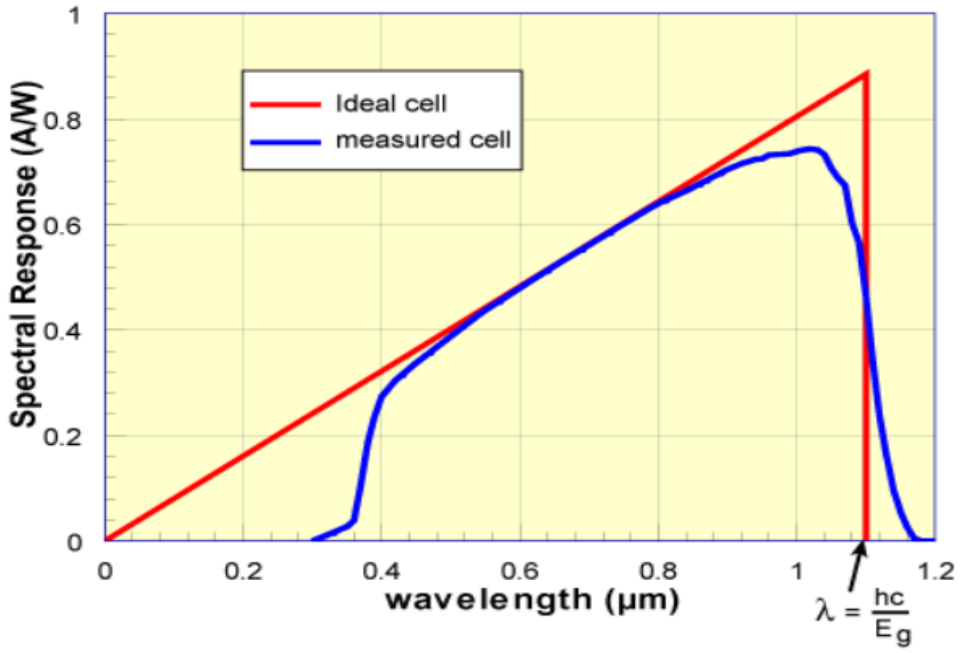


*Figure 2.9: The ideal and measured response curve of a silicon solar cell. (Honsberg & Bowden, 2014)*

Every material has in ideal response curve, but the measured spectral response deviates from this. The solar cell response to short wavelengths is often low because they are often absorbed in the front surface of the cell where they recombine fast. The response to long wavelengths is also usually low, as much of it is not absorbed due to the bandgap energy of the material, or because they are absorbed in the lower region of the cell where there also is unwanted recombination. This follows as a result of the decreasing collection probability with distance from the p-n junction. The spectral response of a solar cell is dependent on the bandgap of the semiconductor material, the level of recombination, and the thickness of the cell.

*Bandgap and efficiency*

The Shockley-Queisser limit limits the spectral utility of a single junction cell. In 1961 Shockley and Queisser discovered that there is an optimal bandgap for different solar spectrums. For a single junction cell, a solar cell with one p-n junction. The optimal bandgap is 1.1 eV, where eV is the electron voltage. With this bandgap, the maximum efficiency would be around 30%. (Shockley & Queisser, 1961) The optimal bandgap is derived based on the knowledge about the portion of the photons that is below the bandgap energy, and the portion of the photons that recombine before the cell can utilize it. In later studies, it has been found that the optimal bandgap in an AM1.5 spectrum is 1.4 eV. If the bandgap energy is too small, it reduces the voltage possible for the cell to produce. Different semiconductors have different bandgap energies, and Silicon has a bandgap of 1.1 eV with maximum efficiency at 29% (Nelson, 2003). Multi-junction cells are built with several semiconductor materials and thus have the possibility of exploiting a broader part of the spectrum. The bandgap of the CIS solar cells is between 1.0 eV to 1.7 eV (Smets et al., 2016). Even though there are other semiconductors with more optimal bandgaps, Silicon is heavily used because it is cheap and easily obtainable. The operational lifetime is one feature that does not separate the different PV types too much. The performance reduction due to wear over time is called degradation.

### 2.5.4 Degradation and illumination induced changes

Degradation happens to all PV modules. Wear and tear causes increased recombination in the cell, decreasing the $I_{sc}$ and $V_{oc}$. In locations with a lot of wind and soil, the surface of the module can be worn down over time. Earlier research has proven that degradation affects both pc-Si and CIS solar cells. Researchers in Golden, USA, have tested the stability of CIS modules at an outdoor test facility. They found that the degradation rate per year was between 1-4%. (Del Cueto et al., 2008)

Changes in module performance can in some PV technologies be caused by light exposure and can influence the determination of the performance of the modules. Illumination effects can make fast changes in the electrical properties of the cells, and cast uncertainty upon the accuracy of the initial performance measurements upon fabrication. The phenomenon is sometimes called light soaking. Light exposure can both have ha positive or negative impact on the performance, depending on

the technology. Some of the changes are long term, and some are reversible. The reversible changes are called metastable effects and will disappear when the modules no longer are exposed to light. Illumination induced degradation is a big problem in some thin-film technologies, like amorphous silicon thin-film cells. The CIS technology is affected by beneficial reversible metastability. Earlier researchers have found that the performance of CIS modules improves in order of minutes when exposed to light. In California, cells have been found to achieve between 7% and 14% improvement. In the same tests, approximately 75% of the gain was due to the *FF*, the reminder was in $V_{oc}$, and the $I_{sc}$ somewhat increased (Willett & Kuriyagawa, 1993). Other research also shows that light soaking primarily improved the *FF*, but also the $V_{oc}$. The metastable changes are also found to be wavelength dependent. Still, the performance of CIS solar cells is not fully understood and needs to be further studied.

Since degradation and light soaking impact the true performance of the CIS modules under real conditions, the modules should be tested under constant illumination, or soon after. The condition under light soaking can be prolonged supplying the module with DC electricity between the measurement and light soaking. When the modules are tested in such a manner, it will improve the system simulations and output determination (Gostein & Dunn, 2011).

# 3 Experimental and analytical methodology

In this study, a PV system consisting of pc-Si modules from IBC solar, and one consisting of CIS modules from Solar Frontier are studied. The systems are located at Kjeller in Norway. Data from the two grid connected PV systems is collected together with weather data from the test site and used to conduct a performance analysis. Production data covering over a year is collected and analyzed for both systems, so is irradiation and temperature data from the same experimental test site. Module tests and soiling tests are conducted with a Solar simulator. The simulation software PVsyst is applied to perform a performance prediciton for the two systems. A quantitative analysis of the performance and losses of the two systems is performed. This is done with the use of MATLAB and Excel.

## 3.1 Test station

### 3.1.1 Surroundings

The two PV systems studied in this research are placed next to each other on a wall with a 90˚ tilt. The test site is located at IFE in Kjeller, Norway. The latitude is 59.973˚, the longitude is 11.051˚, and the elevation is approximately 100 m (Google maps). The azimuth angle of the wall is 13˚. The modules are attached slightly more one centimeter from the wall. Some traffic is in the proximity of the location. It is a suburban area, with some vegetation. The topography is flat, and it is an inland alike climate. There is one building on the left-hand side of the wall that can cause some shading on the modules in the evening. On the left side of the wall, there is a staircase. The staircase and the wall may cause some shading in the morning and evening time. Less than a meter under the setup of the modules there is a roof covering some equipment. The roof has a small tilt. If snow has fallen, there is an accumulation of snow on the roof similar to that on the ground. By the modules, close to one of the top pc-Si modules, there is a ventilation outlet. The test site can be seen in Figure 3.1.


*Figure 3.1: A picture of the test site, explaining where the two systems is mounted and where the pyranometer and temperature sensor is positioned.*

### 3.1.2 System

The pc-Si system consists of five IBC Polysol 260 W modules from IBC solar, with a total nominal power of 1.30 $kW_p$. The second system consists of eight CIS thin film 165 W modules from Solar Frontier, that has a nominal power of 1.32 $kW_p$. The installed nominal power of the CIS system is thus approximately 1.5% higher than for the pc-Si system. The CIS modules cover an area that is 20% larger than that of the pc-Si modules, and the module efficiency is 13.44% for the CIS and 15.88% for the pc-Si modules. Some of the module specifications are listed in Table 3.1. The pc-Si modules are connected in series, while the system configuration of the CIS is four modules in series, and two strings connected in parallel. In Figure 3.2 the configuration of the systems can be seen. Each system is connected to a string inverter from Delta. The two inverters are placed indors and connected to the power grid. A few meters of cables are used to connect the modules, inverter and the grid.

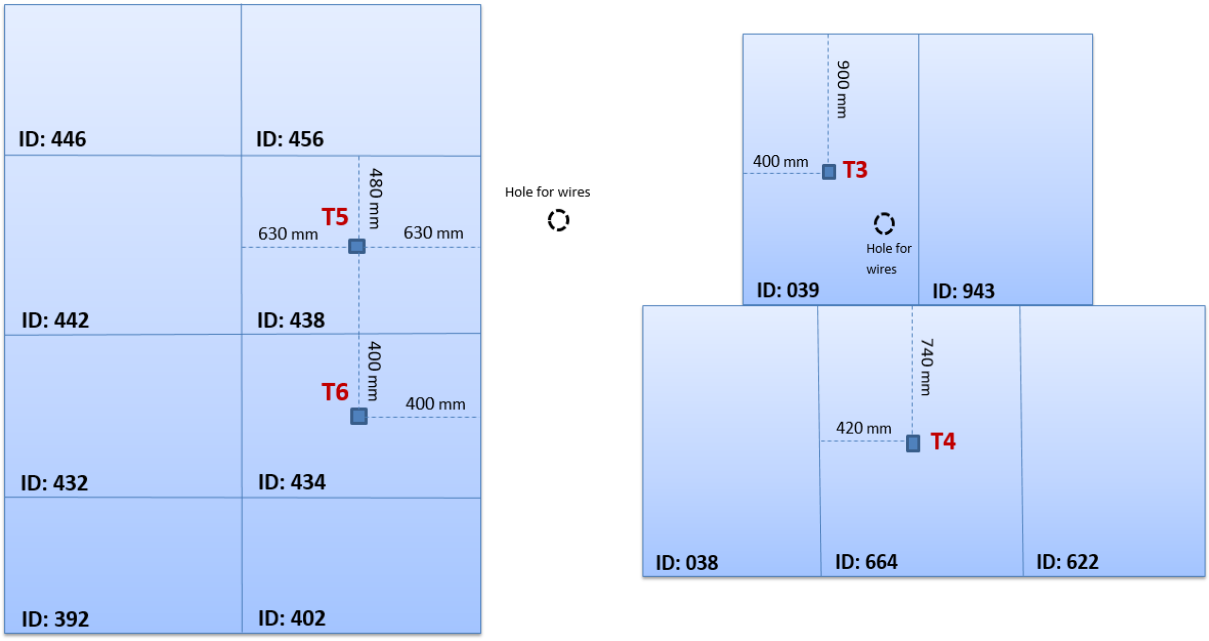


*Figure 3.2: The layout of the CIS system to the left and the pc-Si system to the right. The positions of the temperature sensors fastened on the back of four modules are also given.*

*Table 3.1: This table lists the module specifications for the Polysol 260 CS modules (pc-Si) and the Solar frontier 165-S modules (CIS). All the values are collected from the module datasheets, except the total nominal power of the modules, measured at the manufacturer.*

| | **PolySol 260 CS (pc-Si)** | **SF 165-S (CIS)** |
|---|---|---|
| **Number of modules** | 5 | 8 |
| **Peak power ($P_{MAX}$)** | 260 W | 165 W |
| **Open circuit voltage ($V_{OC}$)** | 38.1 V | 110.0 V |
| **Short circuit current ($I_{sc}$)** | 8.98 A | 2.20 A |
| **Module efficiency (@STC)** | 15.88 % | 13.44 % |
| **Temperature coefficient $P_{MAX}$** | -0.43 %/K | -0.31 %/K |
| **Total Area (A)** | 8.184 $m^2$ | 9.8248 $m^2$ |
| **Total nominal power ($P_O$)** | 1.30 $kW_p$ | 1.32 $kW_p$ |
| **Total nominal power of the modules, measured at the manufacturer** | 1.31 $kW_p$ | 1.35 $kW_p$ |

Datasheets are given in the appendix.

### 3.1.3 Local weather measurements at the test site

The local irradiance at a 90˚ tilt is measured with a pyranometer. The pyranometer is attached to the staircase a few meters from the modules. There are small differences between the irradiation measured by the pyranometer and the irradiance on the modules. This difference is neglected in this study, due to the insignificant impact on the results. The ambient temperature at the site is measured by an air temperature sensor, placed on the wall close to the modules. The position of both the pyranometer and the ambient temperature sensor can be seen in Figure 3.1. Temperature sensors are connected to the back surface of two pc-Si and two CIS modules.

## 3.2 Measurement equipment

### 3.2.1 System output

Two RPI H3 string inverters from Delta Energy Systems is used to control and convert the output of the systems. This inverter is designed for residential PV applications. An MPP tracker is integrated into the inverter. Relative to the two systems the inverter is slightly over dimensioned. It has a nominal DC power intake of 3.15 kW. The installed nominal power is around 1.3 kW for both systems. The input voltage range of the inverter is 125-600 V, and the startup voltage is 150 V. The voltage at nominal power at STC is 342 V for the CIS system, and 155.5 V for the pc-Si system. The pc-Si system voltage at nominal power is very close to the startup voltage and very close to the limit for the inverter.

See the appendix for more information about the inverter.


*Figure 3.3: The Delta RPI H3 inverter. The picture is borrowed from the datasheet.*

*Modelling of the inverter efficiency curve*

The datasheet of the inverter informs that it has a peak efficiency of 97% and an EU efficiency of 96.2%. The EU efficiency is a yearly average efficiency during operation in central Europe. The manufacturers rarely provide the efficiency curve. In this study, the inverter losses are estimated using the inverter efficiency curve modelled by the PV simulation software PVsyst. The efficiency of an inverter is non-linear and has a threshold power because of the inverters own power consumtion. For the RPI H3 Delta inverter, PVsyst has used the efficiency information from the manufacturer to construct three sets of efficiency profiles. These profiles are based on three different input voltages, 500 V, 350 V and 320 V. The eight final points are the results of quadratic interpolation between the three lines. The efficiency profile is thus a function of the input power and the input voltage (PVsyst 6 Help, 2018b). A picture of the efficiency profile from PVsyst is given in Figure 3.4.

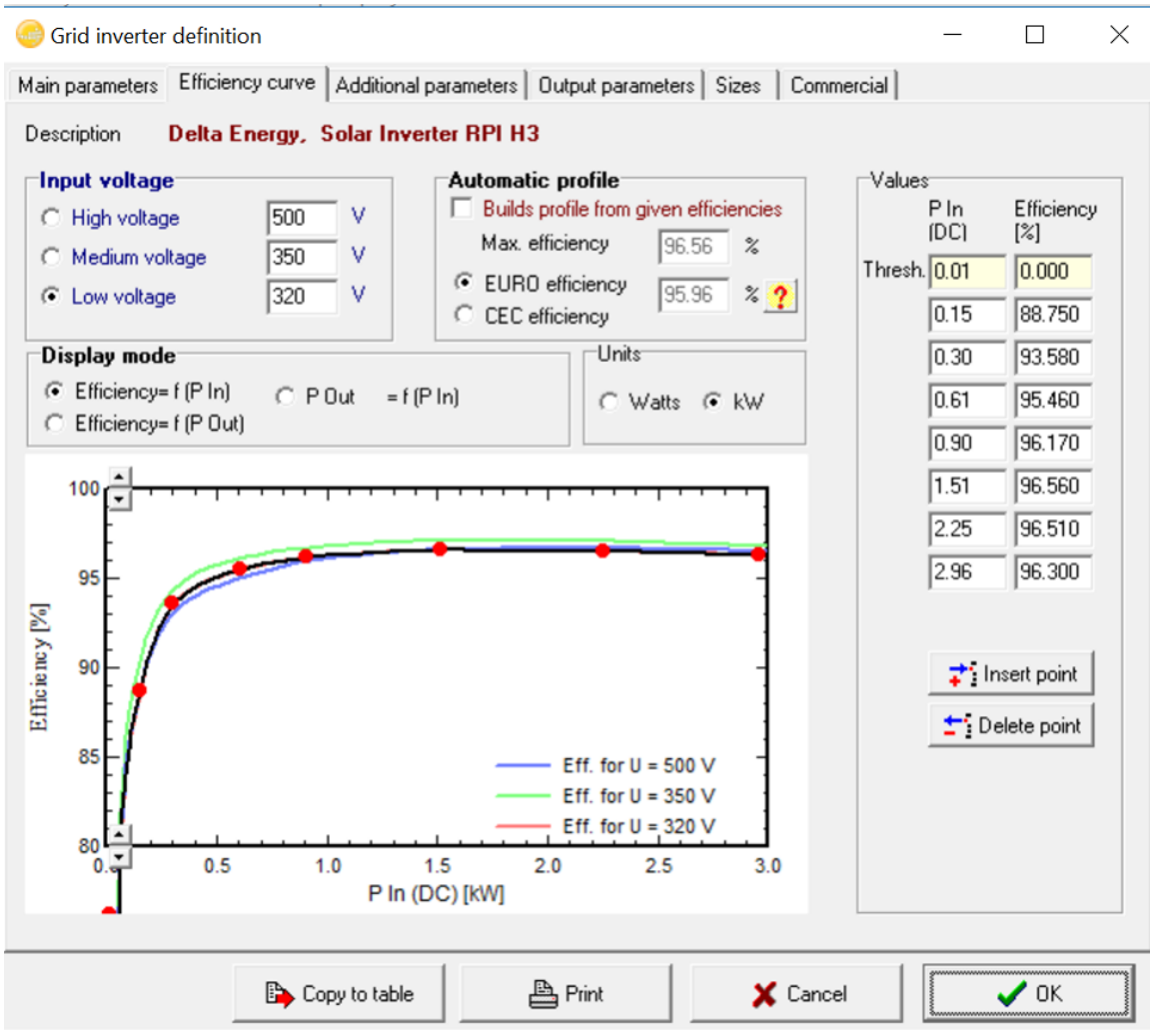


*Figure 3.4: The efficiency profile for the RPI H3 inverter, modelled by the PV simulation software PVsyst. The model estimates the relative efficiency of eight power inputs.*

*Inverter data logging*

The data from the inverter is sent to a gateway every few seconds. These data can be collected in the web-based portal. The inverter resets every night, and start the loggings in the morning when the production is sufficiently high. It has been on throw-out the period considered in this research.

The inverter registers the current and voltage input (DC side), the current and voltage output (AC side), the output power and yield. Since the power, current, and voltage is everchanging, average values are calculated by the equipment. The averages were calculated for 15-minute intervals until the 26$^{th}$ of June 2017, when the inverter was calibrated. That day, it was adjusted to calculate five-minute averages, which it continued to do for the rest of the assessment period. The AC yield value accumulates during the day, so the last value of the day is the total amount of energy generated.

The inverter runs on a clock, and the clock automatically adjusts to summer and winter time. The timestamp-time of the logged values is believed to be the midway point in the interval of which the averages are calculated. This assumption is made based on the observation that the logging appears in the web portal halfway through the time interval of the following logging.

### 3.2.2 Irradiance

The irradiance is measured by the pyranometer that is attached to the staircase next to the modules at the same angle and azimuth as the panels. With a 180˚ lens, it measures the intensity of the irradiance in the same POA as the modules. When it is measured in this way, the measurements include the direct, diffuse and reflected parts of the irradiance. The pyranometer is supplied by Kipp and Zonen. It has an uncertainty of ±1.41%.

The pyranometer is connected to the staircase, so it is possible to clean. It is important to clean the pyranometer lens regularly, so that soil will not disturb the measurements. During 2017 the pyranometer has been cleaned a few times, but the dates of the cleaning have not been written down. A picture of the pyranometer can be seen in Figure 3.5. Since the pyranometer is placed a few meters next to the modules, the pyranometer is not above the roof that is under the modules. This can cause some differences between the reflected irradiation that is measured by the pyranometer and what reaches the modules. This can cause some uncertainty in the measurements in the winter time when snow covers the roof. The pyranometer takes measurements every ten seconds. It is connected to the NILU web portal, that calculates the average irradiation over five-minute intervals.

*Figure 3.5: Photo of the pyranometer mounted at the test site.*

### 3.2.3 Ambient and back-surface temperatures

The ambient temperature is measured by a temperature sensor placed on the wall next to the modules. The position can be seen in Figure 3.1.

The back-surface temperature measurements are performed using two platinum resistance thermometers on each module type. The sensors are of the type PT1000. The sensors are sitting inside a small aluminium block that is glued to the back-suface of the moduels. Figure 3.2 shows the layout of the systems and the positioning of the temperature sensors. The sensors are placed in the center area of the modules. The temperature is assumed to be uniform over the whole area of the module.

The sensors are connected to a recorder that transfers the measurements to the NILU data logger. The measurements take place every ten seconds. The average value for the temperature is calculated in the same manner as for the irradiance.

The measured back-surface temperature is not the same as the temperature of the solar cells. The temperature coefficients in the datasheet refers to the cell temperature. Since the modules are attached to the wall, with a short distance between their rear side and the wall, the back-surface heat exchange is very low. The heat exchange decreases because of the small amount of wind and air that can pass behind the module. A report by Sandia (Kratochvil et al., 2004) provides empirical temperature-difference coefficients for the cell and the back-surface temperatures of different types of installations. The coefficients are representative for different types of flat-plate PV modules from different manufacturers. They report that the temperature difference will be lower than 1°C when the modules have a close roof mount. At an almost fully insulated back-surface, the temperature difference can be assumed to be zero. The cell temperature and the back-surface temperature is therefore estimated to be equal in this study.

*Variance between the back-surface temperature sensors*

Averages of each systems' two temperature measurements were calculated and used for the temperature analysis. The temperature sensors T3 and T4 are attached to the CIS modules, and the temperature sensors T5 and T6 are attached to the pc-Si modules. Temperature sensors T3 and T4 have a greater difference than sensors T5 and T6. The difference is greatest at high temperature measurements. The difference can be seen in Figure 3.6, where the temperatures measured between the 11th and 20th of August 2017 are plotted.

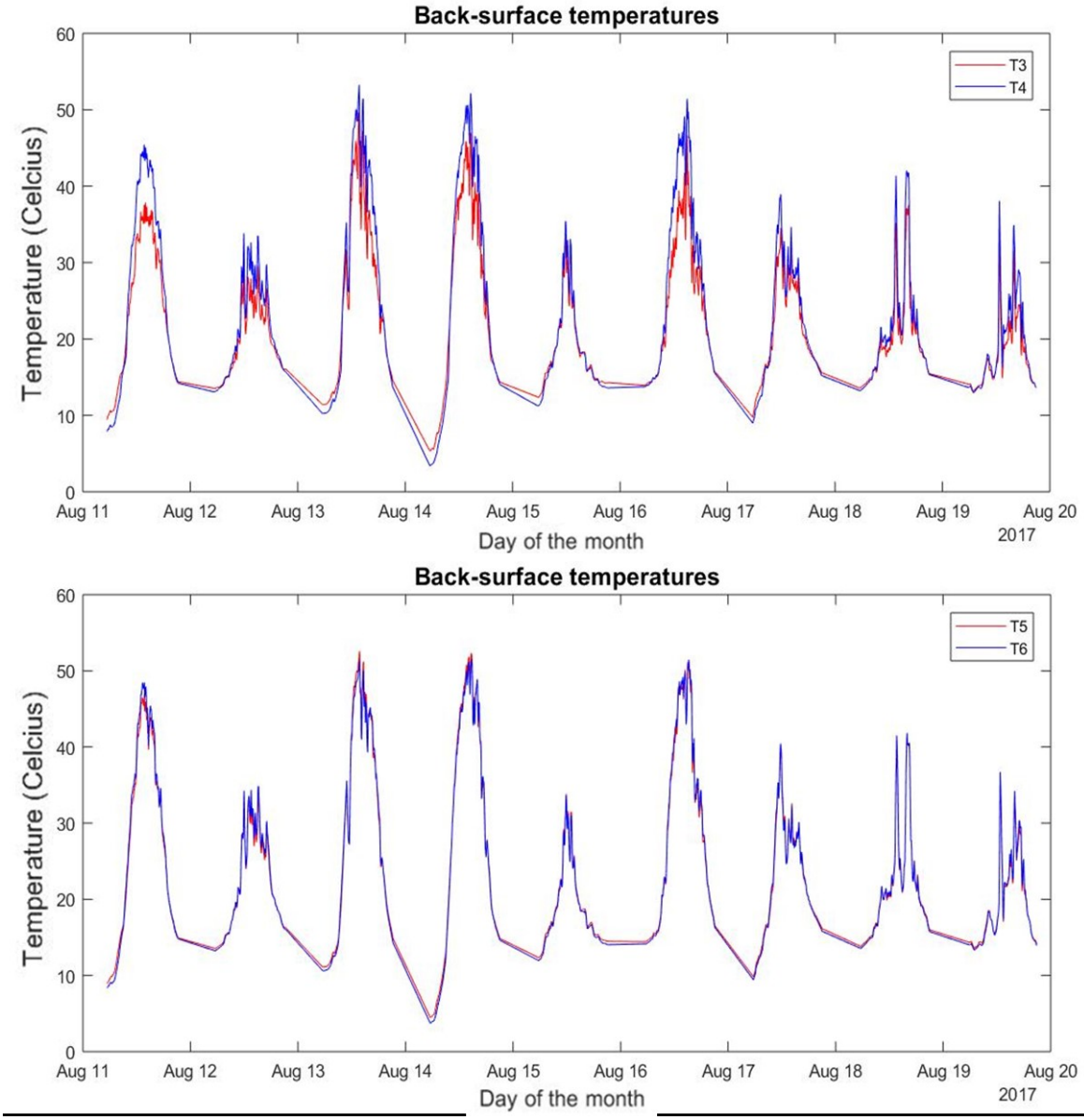


*Figure 3.6: Back-surface temperatures plotted from 11.09.17 – 20.09.17. The sensors T3 and T4 are plotted in the top graph and T5 and T6 in the bottom graph. The figures show that the difference between T3 and T4 is larger than the difference of T5 and T6.*

The highest measured temperature difference between T3 and T4 is 10°C. The average temperature difference during a year is 0.79°C with a standard deviation of 2.4°C. The datasheet for the temperature sensors is not found. Similar temperature sensors have an uncertainty of 0.015°C (Pico technology).

A paper on the measurement unsertainties in the traceability chain for the calibration of photovoltaic devices states that the regular outdoors temperature non-uniformity of PV modules is 3°C (Müllejans et al., 2009). The standard deviation between the temperature sensors and for the measuring device is lower than the temperature non-uniformity, from which we can assume that the uncertainty in the temperature measurements does not exceed ±3°C. The uncertainty in the temperature measurements will at most amount to an uncertainty of ±1.3% in the power estimates.

An infrared camera has been used to take a picture of the modules under operation, the picture can be seen in Figure 3.7. The picture is taken at midday on a clear day. The colors in the picture indicate what temperatures the objects have. Bright yellow is a few degrees Celsius higher than the dark yellow color. The pc-Si modules are the five modules to the right. Temperature sensor T3 is attached to the top left module, and sensor T4 is attached to the bottom center module. If the colors of the modules are studied, one can se that the lower module is warmer than the top one. Beside the top left module, there is a ventilation outlet. This ventilation outlet lets out cold air from the building which cools the surrounding objects. The ventilation outlet is probably the greatest contributor to the temperature difference between T3 and T4.

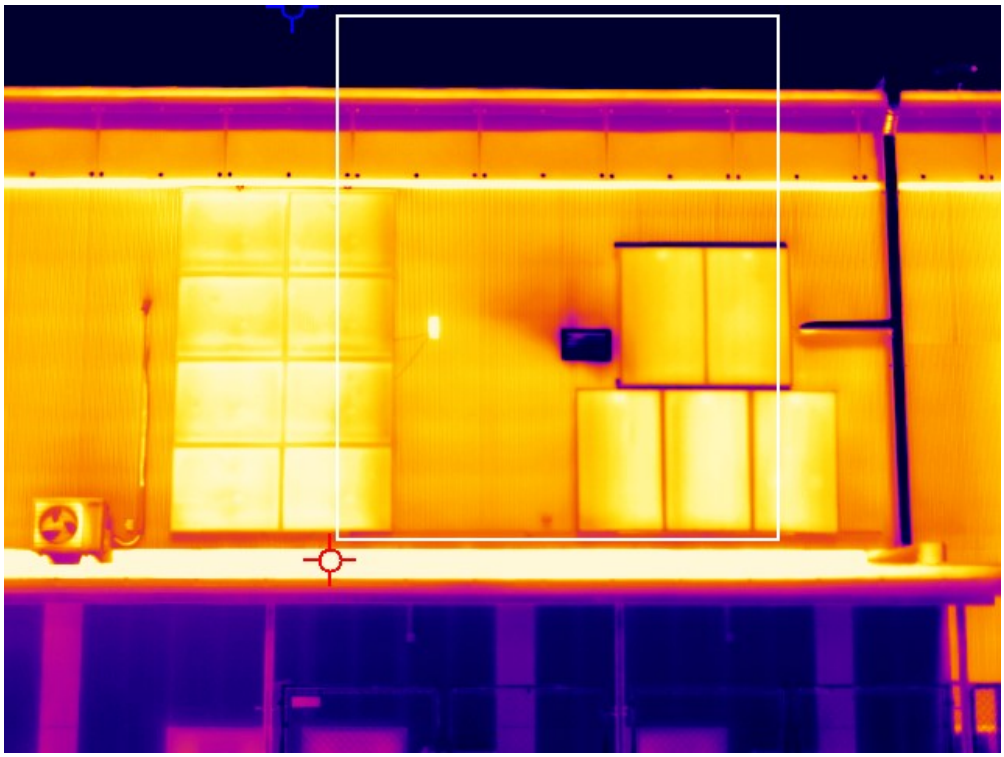

*Figure 3.7: Picture of the test side done with an infrared camera. The picture shows that the temperature of the modules is uneven. A ventilation outlet cools some of the modules. Photo by Bjørn Brevig Aarseth.*

## 3.3 Data analysis

### 3.3.1 Data selection

The pc-Si and CIS systems at IFE, Kjeller, had production data from 9th of December 2015. The data that was chosen for this study was measured from the 1st of February 2017 to the 31st of January 2018, containing 365 days of data. Weather data from the test site was available for the same period. The reason why January 2017 was taken out of the study and replaced with January 2018, was that some days in January 2017 were missing irradiation and temperature data. The inverter, irradiation and temperature data were studied to see if any other data were missing. No more data was found missing.

*Estimation of the losses*

In the previous chapter, it was explained how different external factors are affecting the performance of PV modules. Temperature, the intensity of the irradiance, spectral mismatch, reflection, shading and soiling coverage are all factors that make the production vary from the nominal performance. The losses that occur in the modules due to the locale climate is often called the array capture losses. Losses also occur in other parts of the system, such as the inverter and the cables. These are the system losses. They contribute to losses before the power is transmitted into the grid. Other aspects such as natural or light induced degradation or light soaking, change the electrical performance of PV modules. In this performance study, the system and array capture losses will be estimated. The loss mechanisms that will be analyzed in depth is the degradation, light soaking, soiling, inverter, temperature, and irradiance.

### 3.3.2 Simulations in PVsyst

Models of the two systems in this study were created in the PV simulation program PVsyst. Two models were simulated for each system. One with climatic data from the Meteonorm database and one with climatic data measured at the test site. Meteonorm is a database that is accessible through PVsyst. It offers climatic data for a typical year at a chosen position. The typical year is estimated with data from over 8000 weather stations. Interpolation is used to obtain data for all positions. (PVsyst6 Help, 2018). The Norwegian Meteonorm stations are located in Bergen, Bodø, Tromsø and Karasjok. Climatic data for the test site position was collected from the database. In the other simulations measured ambient temperature and irradiance in POA for the assessment year were imported into the model.

PVsyst contains information about 12500 modules and 4500 inverters. This information is collected from the manufacturers (PVsyst 6 Help, 2018a). If the information for the modelled system is not found in the database, it is possible to set the module specifications manually.

The factors that were manually adjusted in the models was; the position of the modules, if the modules were grid connected, the module type, the inverter type, and the arrangement of the array. The information for the pc-Si module had to be manually adjusted since the exact module type was not found in the database. Data for a similar module from the same manufacturer was edited to fit the specifications given in the datasheet of the pc-Si module.

The module specifications in PVsyst include the temperature coefficients and the efficiency at 200 W/m$^2$. The light soaking effect of the CIS modules is represented as a 2% gain in yield. The default albedo of 0.2 is used in the simulations. By default, PVsyst sets the absorption coefficient of incoming radiation to 0.9, and the wind speed is assumed constant at 1.5 m/s. With these factors and the ambient temperature, the cell temperature is estimated. The incident angle modifier, IAM, is also set to its default of 0.05. This is a factor that represents losses that occur due to additional reflection at large AOI.

The simulations created production estimates for both systems for a typical year and for the assessment period. The data was used to estimate the monthly yield and irradiation. These values were later used to calculate the system efficiency, the reference and final yield, and the performance ratio of the systems.

### 3.3.3 Data correction

*Time delay and timestamp corrections*

There are differences between the clock of the inverter and the clock of the recorder for weather measurements. The clock of the inverter automatically adjusts to summer and winter time. The timestamps of these measurements seemed to be correct and set in the middle of the time interval of the calculated averages. The clock of the weather measurements is not automatically adjusted to summer and wintertime. This clock is found to go a little too fast. Consequently, after a period, the timestamps start having an offset. This is undesirable, but the problem is not yet resolved. However, the clock has repeatedly been corrected to reduce the offsets.

The NILU data logger clock was manually adjusted to summertime and corrected for a ten-minute offset the 6$^{th}$ of May 2017. It was adjusted anew the 18$^{th}$ of January 2018. This time it was corrected for a 15-minute offset and set backward one hour to wintertime.

The consequence of the clock error is firstly that most of the data points have a time offset, except the few days right after the two adjustments of the clock. Secondly, the adjustments for the summer and wintertime were both done at a later date than they were supposed to. The outcome of this is that some days between the true date for the adjustments and the manual adjustments that were done, still had wrong timestamps. This implied that an accurate correlation between the inverter data and the irradiation and temperature data could not be made. Nevertheless, the data was not too displaced to achieve an overall performance analysis. This fact limits the precision achievable in parts of the analysis.

It was decided to decrease the offsets by finding the dates where the summer and wintertime were incorrect and adding or subtracting an hour from the timestamps of those logged values. The time-lapse for the second offset of 15 minutes was found to be approximately nine months. This information was used to calculate an average monthly offset of 1.7 minutes. Average offsets for each month was then estimated and corrected. Also, the timestamp was set in the middle of the five-minute intervals.

*Sunrise and sunset corrections*

The irradiation and temperature data is logged all through the day and night. It is well known that the pyranometer has a thermal offset, both during nighttime and during daytime. In order to remove negative values due to the nighttime offset, only data between sunrise and sunset is used. The sunrise and sunset data were collected from the "Time and date" webpage, which is the biggest provider of date and clock data in the world (Timeanddate, 2018). The procedure to remove the daytime offsets are complex and requires additional measurements of the pyranometer. Thus, no corrections for the day time thermal offsets have been made in this work.

*Inverter data*

The smallest power value that is measured by the inverter is zero. Since the inverter is consuming a small amount of energy from the grid at all times, one would expect it to log negative values during the night when there is no electricity production from the modules. The night data is irrelevant in this study as it focuses on the production between sunrise and sunset, but the inverter data needed an inspection to see if the energy usage of the inverter was subtracted from the production data. Hence, the power was calculated from the output current and voltage and compared to the logged power values. This analysis showed that the energy usage of the inverter was accounted for in the production data. The result also showed that the inverter uses more energy to convert the electricity when the power production is high than when the modules are producing less. It was then assumed that the inverter was logging the correct power, except in the periods with no production, where the power is set to zero. The energy usage of the inverter when it is not converting any electricity is small, and this error in the logging system will not affect the results to a great extent.

The PVsyst model is adding negative power values to its prediction output. To compare the PVsyst model directly to the dataset, the negative values were removed from the PVsyst model. All the hourly values of -1 Wh are changed to 0 Wh.

### 3.3.4 Presentation of results

The main performance parameters used to present the results of this study is the specific yield, the system array efficiency, and the performance ratio. This is done in accordance with the International Energy Agency Photovoltaic Power system (IEA PVPS) program task 2 (Jahn et al., 2000) and similar performance studies (Ayompe et al., 2011).

*Final and Array yield*

The final yield, $Y_F$, is the net energy output, $E_{tot,\ AC}$, on the AC side of the inverter per $P_o$. The array yield, $Y_A$, on the other hand is the energy output, $E_{tot,\ AC}$, on the DC side of the inverter per $P_o$. The yield is either presented as an average day in a month, h/day, or as the average for a whole year, h/year.

$$Y_F = \frac{E_{tot,\ AC}}{P_O} \tag{7}$$

$$Y_A = \frac{E_{tot,\ DC}}{P_O} \tag{8}$$

*Performance ratio*

The performance ratio, *PR*, is the ratio between the system output energy (AC side) and the theoretically possible energy output if the system had operated at its rated conditions at STC. This ratio indicates the overall effect of losses related to the incomplete utilization of the irradiance, temperature and other system inefficiencies.

$$PR = \frac{Y_F}{Y_R} \tag{9}$$

$$Y_R = \frac{H_I}{G_I} \tag{10}$$

The *PR* is defined at the ratio between $Y_F$ and the reference yield, $Y_R$. $Y_R$ is the ratio of the irradiation incident in the plane of the modules, $H_I$, to the reference irradiance, $G_I$. $G_I$ is 1 kW/m$^2$.

*System and array capture loss*

The system and array capture losses, $L_S$ and $L_C$, can be calculated from the $Y_F$, $Y_A$, and $Y_R$. The array capture losses are the losses that occur in the array due to the arrays inability to fully utilize the incident light. The system losses are the losses that occur in the rest of the system components. The system and array capture losses are calculated with the following equations.

$$L_S = Y_A - Y_F \tag{11}$$

$$L_C = Y_R - Y_A \tag{12}$$

*System efficiency*

The system efficiency, $\eta_{sys}$, is the ratio of $E_{tot,\ AC}$ to the product of the total module area, $A_{sys}$, and $H_I$

$$\eta_{sys} = \frac{E_{tot,\ AC}}{A_{sys} \times H_I} \tag{13}$$

### 3.3.5 Method used in the performance analysis

Calculations of the monthly and annual yield and system efficiency are done using measured data. To find how the temperature, irradiance and inverter affected the performance of the systems, the reduction or increase in efficiency were estimated relative to the measured average STC efficiency. The calculations and graphic presentations were either performed in MATLAB R2017 or Excel.

*Calculating the yield*

The yield is presented as total monthly values and a total for the year. It is calculated summing together the last yield value of every day of the month, since the last value of the day shows the total yield produced that day.

*Calculating the energy incident on the modules*

The total energy incident on the systems were calculated using the five-minute average irradiation values logged by the NILU data logger. For each five-minute interval, the monthly and yearly sums of energy was calculated. This was done according to Equation 14.

$$E_{tot,irr} = A_{sys} * H_I = A_{sys} * \sum_{i=1}^{n} (P_i * 10^{-3} * \Delta t) \quad (14)$$

$$\Delta t = \frac{5min}{60min/h}$$

Where the $E_{tot,irr}$ is the total energy incident on the module surface of each system, $P_i$ is the power data points in W/m$^2$, $\Delta t$ is the five-minute time interval for each data point given in hours, and n is the total number of data points.

The energy distribution of the incident light in the POA was calculated for a range of irradiance intervals using the irradiation measurements of the pyranometer. The energy was separated into eleven intensity intervals of 100 W/m$^2$. The monthly distribution is illustrated in Figure 3.8 and Figure 3.9. The distribution for the entire year is presented in Figure 3.10. The monthly distributions are colored according to the total amount of energy per m$^2$ received by the systems that month. The colors represent: Red > 90 kWh/m$^2$, Green > 70 kWh/m$^2$, Blue > 30 kWh/m$^2$, Light blue > 0 kWh/m$^2$.

The energy distribution over a range of cell temperature intervals was also found for the energy delivered at each intensity interval. An example of this is illustrated in Figure 3.11.

## Relative energy contribution by month

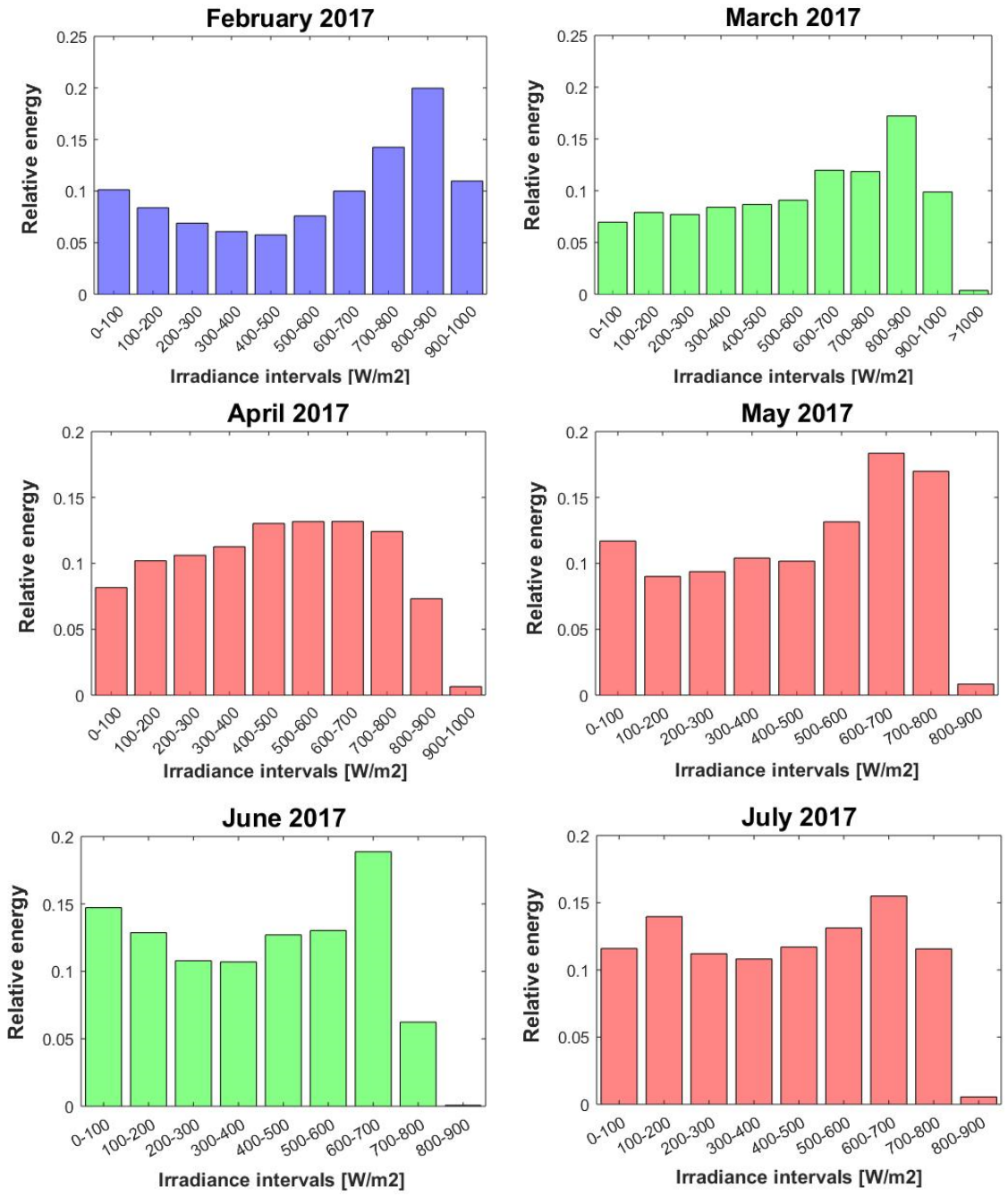


*Figure 3.8: This figure shows the monthly relative energy contribution in the POA, for irradiance intervals of 100 W/m$^2$. The months February 2017 to July 2017 is presented in this figure.*

## Relative energy contribution by month

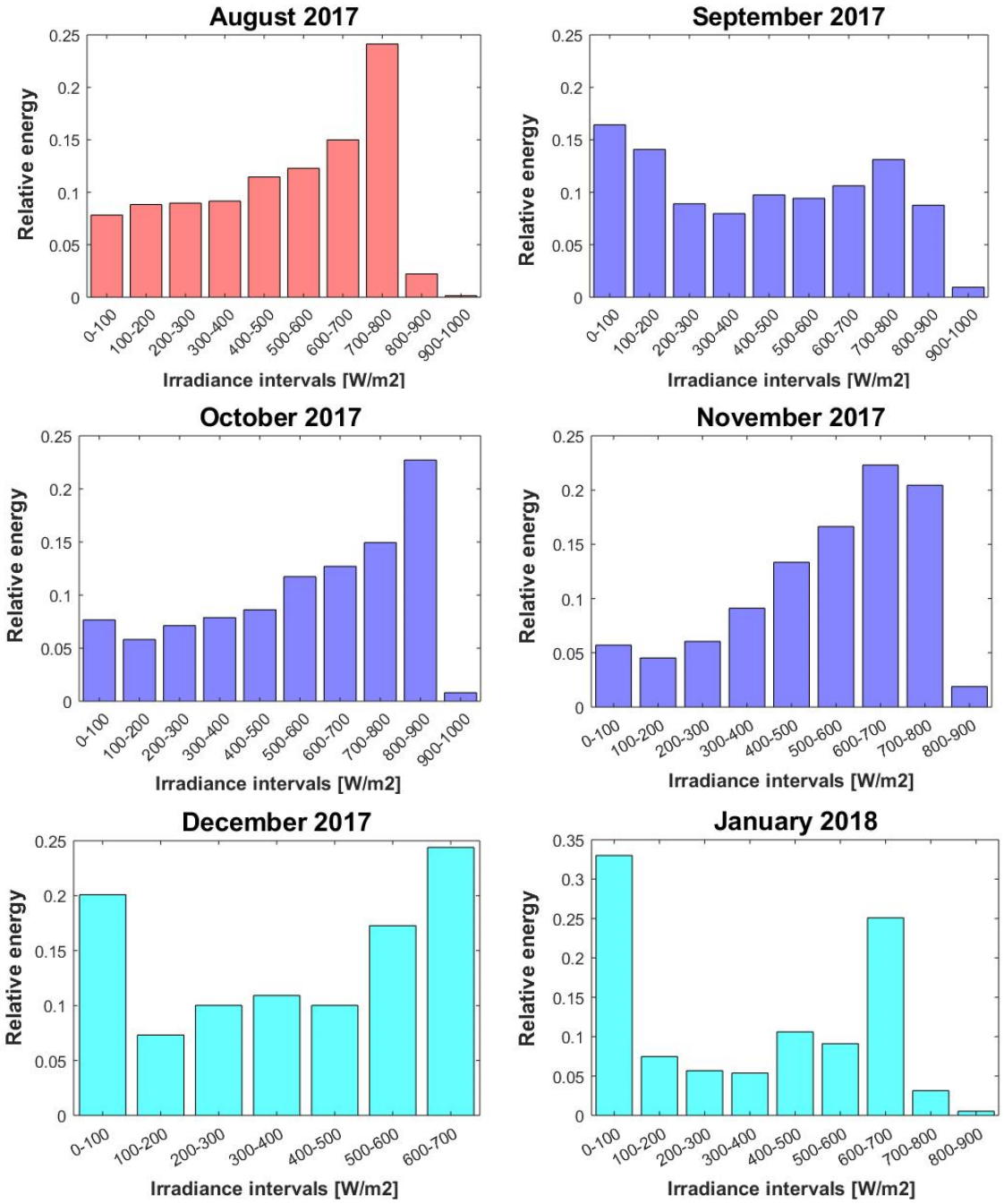


*Figure 3.9: This figure shows the monthly relative energy contribution in POA, for irradiance intervals of 100 W/m$^2$. The months February 2017 to July 2017 is presented in this figure.*

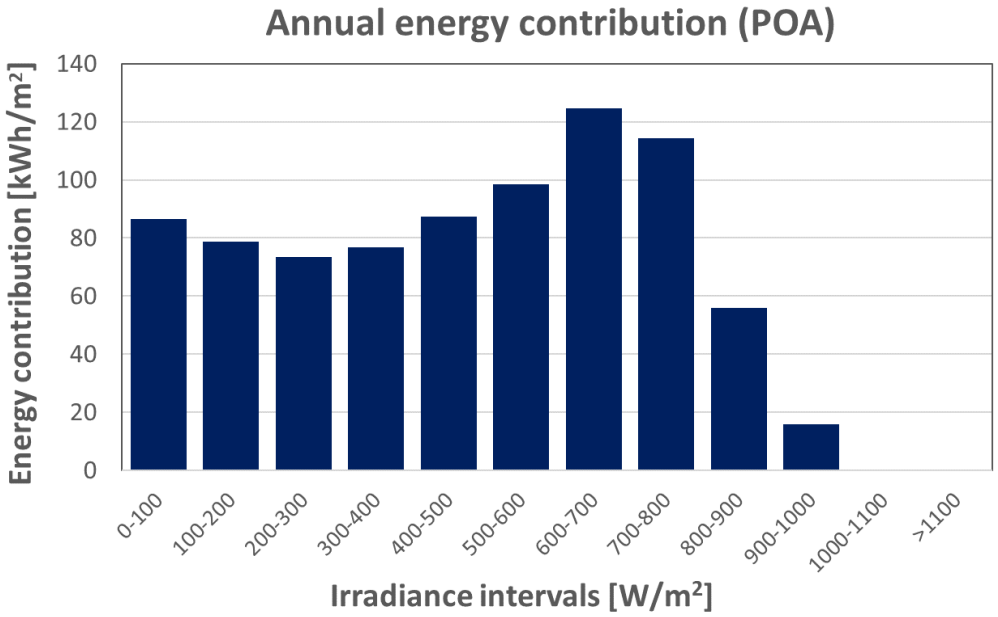


*Figure 3.10: This figure shows the annual relative energy contribution in POA, for irradiance intervals of 100 W/m$^2$.*

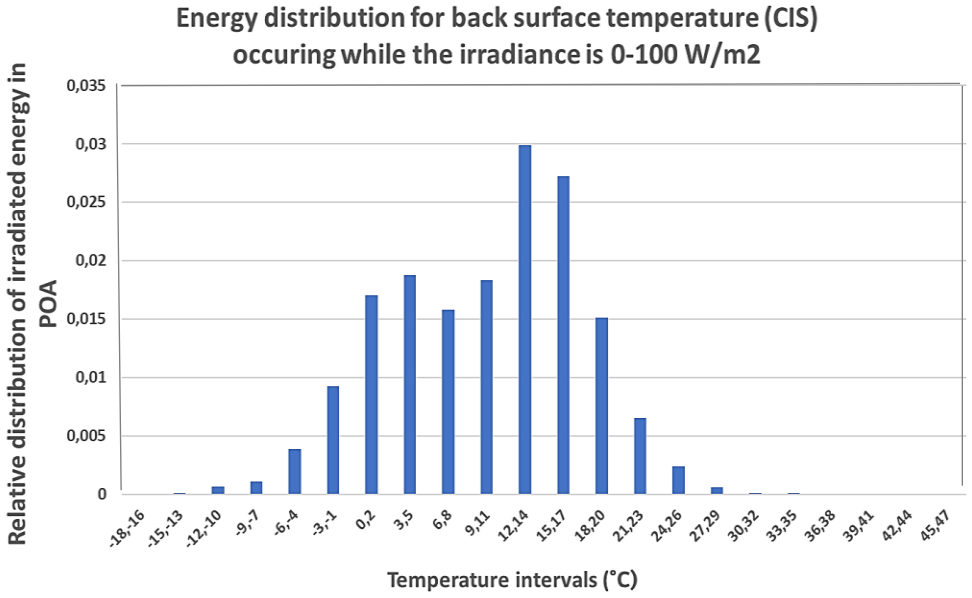


*Figure 3.11: This is the relative energy distribution in POA of the incident energy on the modules in the interval 0-100 W/m$^2$, distributed between the back-surface temperatures of the CIS modules.*

*Estimating the efficiency*

The efficiency of the systems could be estimated based on the AC power output or with the yield output from the inverter. It was decided that the most accurate estimates would be calculated using the measured yield produced and calculating the energy irradiated on the modules of the systems. The reason why the AC power was not used is that the value is continuously changing. Thus, the mean values would have a higher uncertainty. The calculation of the total yield and the total incident energy on the systems is described in the previous paragraphs. The system efficiency of each system was calculated with Equation 13.

*Measurement of the module performance under varying light intensities*

To gather information about the relationship between the intensity of the incident light and the module performance, also reffered to as the low light behaviour, all the modules were tested at different light intensities in a solar simulator. These measurements were adjusted so that all factors except for the light intensity hold STC. Measurements of the modules were done at ten different light intensities from 200-1100 W/m$^2$. A further description of the solar simulator procedure is given in section 3.4.1. The average relative module efficiency for each system for all the intensity levels could then be calculated. The average measured efficiency at STC was used as the reference efficiency. This is done seperatly for both the pc-Si and the CIS modules.

The Solar simulator could not measure the efficiency at 0 W/m$^2$ and 100 W/m$^2$, but the efficiency at these light intensities were estimated. The estimation was done with the assumption that there was a linear relation between the efficiencies and the intensity from 0 W/m$^2$ to 300 W/m$^2$. The slope of the line between 200 W/m$^2$ and 300 W/m$^2$ was then used to estimate the efficiencies that were lacking.

The results are plotted in separate graphs in Figure 3.12. The relative efficiency curve of each module is plotted along with the average curve. In addition to the results, the relative efficiency at 200 W/m$^2$ from the datasheet is added to the plots. The manufacturers of the CIS modules have also provided a standard deviation for the relative efficiency at 200 W/m$^2$.

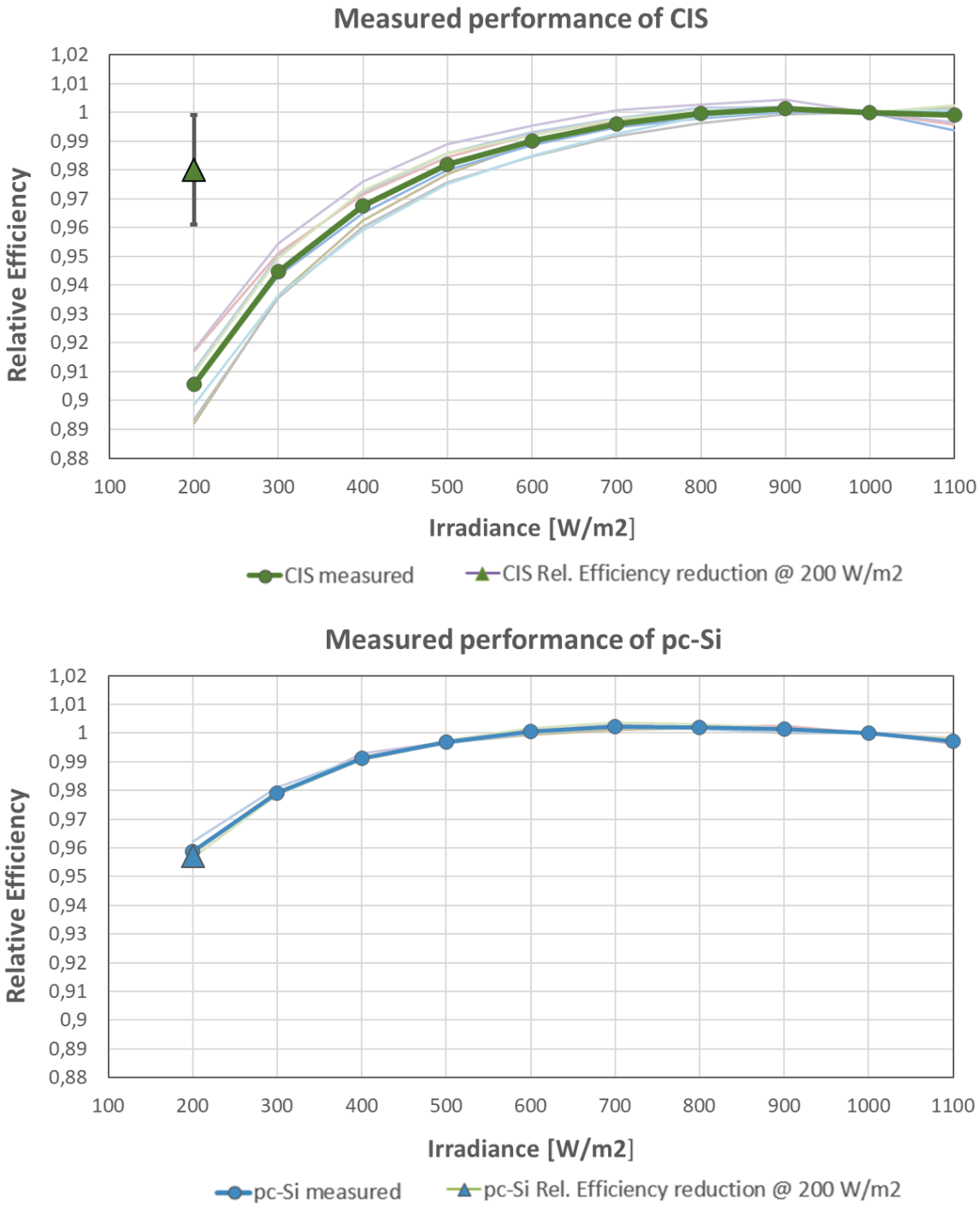


*Figure 3.12: Measures module efficiency at varying light intensities. The top graph shows the measured relative efficiency for the CIS modules, in addition to the calculated average relative efficiency cure. The relative efficiency at 200 W/m$^2$ specified in the datasheet, is also plotted along with its standard deviation. In the bottom graph, the measured relative efficiency of the pc-Si modules is plotted with the calculated average relative efficiency curve. The relative efficiency at 200 W/m$^2$ specified in the datasheet, is also given in this graph. The manufacturer of the pc-Si modules does not inform about the standard deviation.*

From the bottom graph, one can see that the measured efficiency of the pc-Si modules at 200 W/m$^2$ is close to the value specified by the manufacturer. The variance between the performance of the modules is also low. The performance of the modules decreases when the intensity is lower than 600 W/m$^2$. The measured relative efficiency at 200 W/m$^2$ is 95.9% of the measured efficiency at STC.

Looking at the curves of the CIS system, a clear difference is found between the measured and the specified relative efficiency at 200 W/m$^2$. The specified relative efficiency at 200 W/m$^2$ is higher than the one measured in this study. If the standard deviation is included, the difference between the measured and the specified relative efficiency is 5.5%. The variation between the performance of the different CIS modules is higher than for the pc-Si modules, but none of them is approaching the value specified by the manufacturer. The performance of the modules starts decreasing when the intensity is lower than 800 W/m$^2$. The measured relative efficiency at 200 W/m$^2$ was found to be 90.6% of the measured efficiency at STC.

Some uncertainty is connected to the measured results since there is uncertainty in the measurement equipment. This is explained further in section 3.4.1. Nonetheless, the results do not seem to deviate much between the modules of the same type, making our results more trustworthy. The measured relative efficiency at different light intensities was used in the estimation of the performance change due to the real irradiance conditions.

*Estimating the average efficiency change due to the irradiance conditions*

From the measured relative efficiency at different light intensities, efficiency scores were made for eleven intensity intervals from 0-1100 W/m$^2$. The efficiency scores were found by subtracting the measured efficiency at STC from the efficiency at each light intensity measured, attaining the change in efficiency at each of the measured intensities. Then the average efficiency change at each intensity interval was estimated.

The weighted average efficiency change for the period was in the end estimated using the relative energy distribution as weights. The average efficiency change was calculated for each month and the whole assessment year.

*Checking for correlation between the back-surface temperatures and the irradiance*

The light intensity and back-surface temperatures were checked for correlation. The correlation between two variables is to what extent the two variables are related. In this case, a significant correlation between the intensity and temperature means that the estimation of one factor's effect on the system performance will be affected by the other factor too. Scatter plots were made to see if there were any correlation between the average back-surface temperature and the intensity measurements. The dataset that was used included the measurements for the entire assessment period. The scatter plots with the regression lines can be seen in Figure 3.13. A significant correlation was found. Due to this finding, the performance change due to both the irradiance and the cell temperature was estimated in addition to the effect of the irradiance alone.

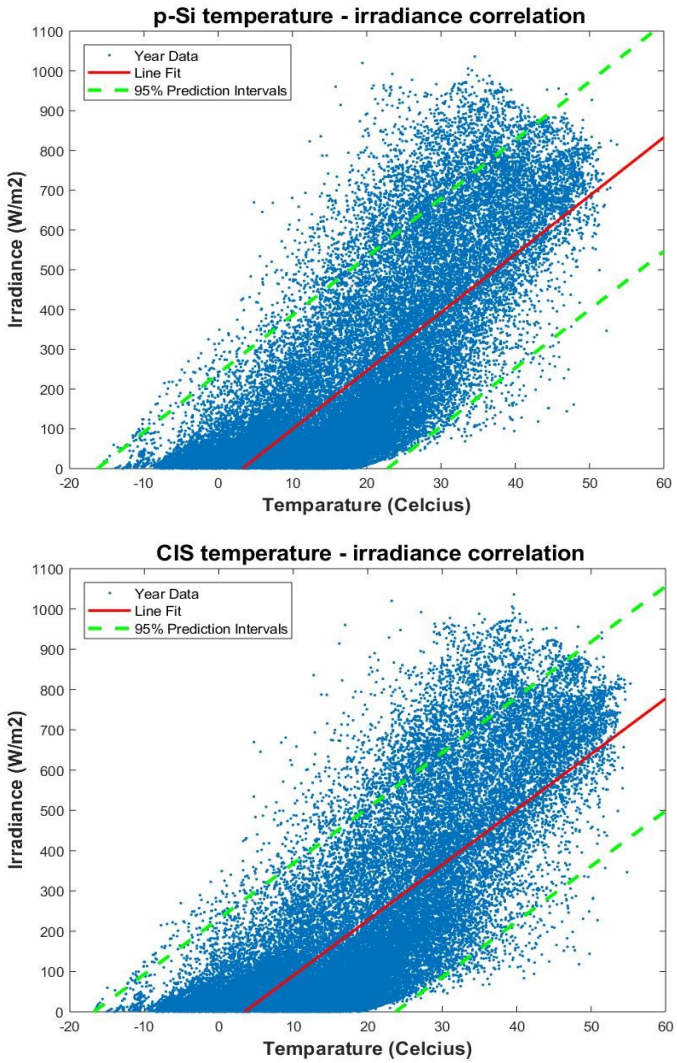


*Figure 3.13: The back-surface temperature plotted against the irradiance. The temperatures used in the upper plot is the average for the pc-Si modules, and the temperatures in the bottom plot are the average of the CIS modules. The red lines are the fitted regression lines, and the green dashed lines is the 95 % confidence interval.*

### *Estimating the average efficiency change due to the irradiance and temperature conditions*

To estimate the system efficiency loss due to both the cell temperature and the irradiance conditions, new efficiency scores needed to be found. The scores were based upon the temperature coefficients from the datasheet and the measured relative efficiency at different intensity intervals. Each score represented an interval of three temperatures, between -18°C and 56°C, in a certain intensity interval. This resulted in a total of 25×11 efficiency scores.

The weighted average efficiency change due to both the irradiance and the cell temperature was then estimated with the relative energy in each of the temperature/irradiance intervals. The average efficiency change was estimated for each month and the entire assessment year.

*Estimating the system efficiency loss due to the inverter*

Average values for the system efficiency loss due to the inverter has been calculated for every month and the average for the entire assessment year. The efficiency profile from PVsyst given in section 3.2.1 is used for this analysis. The linear relation between the power produced by the arrays (one the DC side) and the irradiance incident on the modules was then exploited to find the inverter efficiency at different light intensity levels. The array efficiency connects the power and the irradiance, so the average array efficiency at each intensity interval needed to be estimated.

The average array efficiency at each intensity interval could not be estimated from the measured production data since the dispositioned timestamps of the weather measurements made it impossible to correlate the weather data and the inverter data accurately. The average array efficiency of each intensity interval was instead estimated by using the measured efficiency at STC and both correcting it for the alterations due to the cell temperature and the irradiance.

Once the average efficiency of each intensity level was estimated, the average inverter efficiency for each intensity interval could be found. This was done with linear interpolation, Equation 15. The weighted average inverter efficiency could then be estimated, weighing the inverter efficiency at each intensity interval with the relative amount of energy.

$$\hat{y} = y_0 + \frac{y_1 - y_0}{x_1 - x_0} * (x - x_0) \qquad (15)$$

The MPPT effectiveness is not included in the inverter efficiency profile since this is hard to estimate correctly. The efficiency of the MPPT is usually high, around 98-100%.

## 3.4 Experimental methodology

### 3.4.1 Solar simulator measurements

A pulsed solar simulator can be used to simulate the desired test conditions so that exact PV module characteristics can be measured. Normally the simulator would be used to measure the module characteristics at STC. STC is heaily used as a reference condition according to the IEC 60904-3 standard (Commission, 1987). Solar simulators are used by the manufacturers of PV modules to measure the characteristics of each module before sale. The measured performance usually follows the purchased module.

In this study, the solar simulator would be used to detect degradation and possible improvements due to illumination induced changes. During flash tests with the solar simulator, measurements of the I-V characteristics and power output were taken at STC. The measured performance of the modules at STC could be compared to the module performance measured by the manufacturer. The simulator would also be used to take measurements of the low light behavior of the modules.

In this study, the SPI-SUN Solar simulator, 5100SLP BLUE from Spire was used to take measurements of the modules. The simulator has an adjustable frame for different sized modules. The simulator is equipped with a light source that that can flash the modules at a specified irradiance level. The lamp is in the bottom of the simulator, and the module is placed with its front down towards the lamp. An electrical load is connected to the module during the test to apply a changing voltage, and a temperature sensor is placed on top of the module. A measuring instrument records the I-V curve, module temperature, and irradiance. The irradiance stability at 1000 W/m$^2$ is ≤0.2%, and the spectrum is AM1.5 ≤ ±18%. The simulator specifications are given in the appendix. A picture of the simulator can be seen in Figure 3.14.


*Figure 3.14: The SPI-SUN simulator, 5100SLP BLUE from Spire.*

*Operation of the solar simulator*

The solar simulator tests were performed in a storage room where the solar simulator had been stored for less than a year. The machine had been of little use. The modules were stored in the same room before and during the measurements.

A temperature sensor is placed on the back side of one of the module cells to measure the temperature. To limit uncertainties in relation to the temperature, the laboratory area should be carefully temperature controlled and held close to the reference temperature of 25°C (Dirnberger, 2017). The temperature of the storage room used for the measurements was not controlled. This resluted in lower than optimal temperature values. Since the temperatures of the modules were lower than 25°C, the solar simulator corrected the I-V curve results with the temperature coefficients of the modules.

During measurements, the module is connected to the simulator using MC4-contacts. The simulator is connected to a computer with a measurement software from the same supplier. Specific module parameters and simulation parameters can be adjusted in the software. During a flash of the light source, the simulator takes many point measurements with different I-V combinations. For the test to be accurate, the number of point measurements should be around 3500. To get the right number of measurements the load voltage had to be adjusted. One flash of the lamp is enough to produce the I-V curve of the module at the specified conditions.

Before each new series of measurements, a repeatability test was performed. The repeatability test consisted of ten consecutive measurements. The test checked the uncertainty and repeatability of the measurements and found the standard deviation for the performance parameters. The standard deviation of the $P_{max}$ was less than 0.15% each time it was measured.

The solar simulator may have been affected by the temperature of the storage room. The solar simulator is recommended to operate at a temperature of 23±5°C. The temperature of the room was not measured. The modules that were tested were stored in the same room. They held temperatures between 19-22°C. How much the temperature of the room deviated from this is unknown. The measurements were performed in Feburary and March, and the ambient tempertaure during the night was lower then 0°C. If the temperature was lower than recommended, the uncertainty of the measurements would increase (Solar, 2016).

*Experimental procedure*

The 7th of February 2018 the pc-Si and the CIS modules were dismounted and brought to the simulator for individual testing. A lift was rented for the test period. The lift was used to reach the modules. Two people were in the lift at the same time to be able to take the modules down. Before dismounting them, the modules were disconnected from the inverters and the back-surface temperature sensors.

The 8th and 9th of February 2018 the solar simulator tests were performed on the pc-Si modules. All the solar simulator tests were originally planned last two days. The test period was extended because the testing and the dismounting lasted longer than expected and because there were unexpected problems with the simulator that needed repair. All the modules were therefore placed back on the test site and connected again after the pc-Si modules had been measured.

The CIS modules were dismounted and measured the 6th of March 2018. The measurement procedure of the CIS modules was different than for the pc-Si modules. To study the metastability of the CIS modules due to light soaking the CIS modules were measured four separate times. The first measurements of the CIS modules were done a few hours after they had been disconnected from the grid. The modules were also measured 24 h, 48 h and one week after the first measurement. Between the measurements, the modules were stored in a dark storage room so that the conceivable improvenet due to light soaking could decrease.

After the measurements, the module parameters were compared to the original performance parameters from the manufacturer. The P-rate is used in the presentation of the results. The P-rate is the difference between the measured and the original maximum power, divided by the original maximum power.

*Low light testing*

Along with the performance measurements at STC, measurements of the modules were taken at different light intensities. All the parameter specifications were unchanged except for the lamp intensity that was altered in increments of 100 W/m$^2$. This was done in the range of 200-1100 W/m$^2$. This test was done for every module in the study. The measurements resulted in I-V curves and the relative efficiency normalized to the efficiency at 1000 W/m$^2$.

When the simulator irradiance is adjusted, the nonuniformity and the spectral distribution can be affected. If the irradiance is adjusted with the power of the lamp, it can cause increasing shares of high wavelength irradiance. If grey filters are used this can affect the nonuniformity. If this happens it can lead to large systematic errors (Dirnberger, 2017). The module metastability may also have influenced the measurements of the CIS modules.

### 3.4.2 Soiling test

During the solar simulator tests, measurements of the accumulation of dust on the modules and the reduction in performance due to reduced transmission were conducted. Three modules of each type were randomly selected for soiling testes. These modules were measured in the solar simulator at STC before and after they were cleaned. This was done to see if there was any change between the measurements done with dust on the surface of the modules and the measurements without dust.

Dry rags were used to clean the surface of the modules. New rags were used for each module, and gloves were used during the handling of the rags. The rags were weighted before and after cleaning each module. A Mettler Toledo Excellence Plus scale was used during the on-site measurements of the dust accumulation. The measurement area of the scale is covered by glass, with movable glass walls, and has an accuracy of 0.1 mg. The rags were kept in a vessel before the cleaning and before the weighing so that the weight of the rags would be affected as little as possible by air moisture. Pictures of the rags, vessel, gloves, and scale used in the soiling tests can be seen in Figure 3.15.

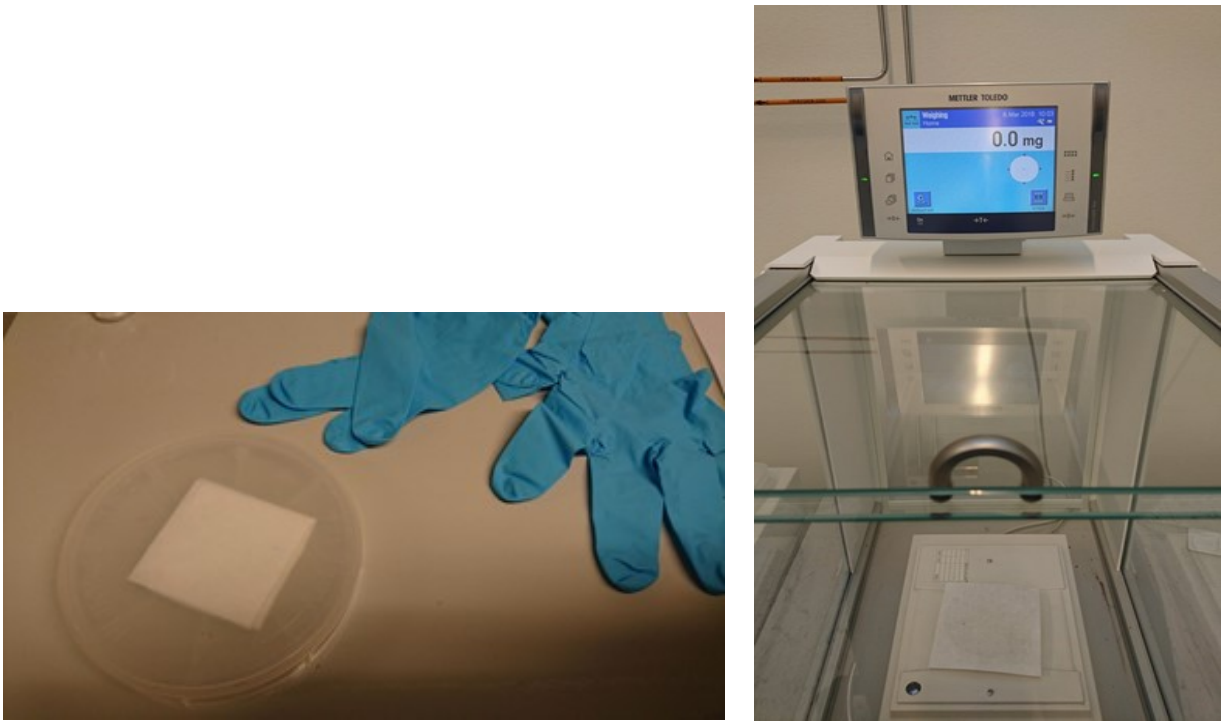


*Figure 3.15: The Mettler Toledo Excellence Plus scale in the right picture, and a folded rag inside a vessel and gloves in the picture to the left.*

# 4 Results and discussion

This study presents results from a 1.3 $kW_p$ pc-Si system and a 1.32 $kW_p$ CIS system installed on a 90˚ wall, with an azimuth of 13˚ on a building at Kjeller, Norway. The system has been monitored since the 9th of December 2015, and the electricity is fed into the grid. The assessment period of the performance study is twelve months from the 1st of February 2017 to the 31st of January 2018. The system and weather data collected from this period were processed using custom-made scripts in MATLAB. The parameters used to evaluate the performance of the two systems are the yield, the final yield, the performance ratio and the system efficiency. The degradation and light soaking effect have been estimated with the measurements of a solar simulator. System and array capture losses have been estimated, and a deeper study of the inverter, irradiation, and combined irradiation and temperature losses have been conducted. These losses are also presented through the performance parameters.

## 4.1 System performance

### 4.1.1 Yield

Figure 4.1 presents the monthly yield for both the CIS and the pc-Si systems from February 2017 until January 2018. The yield is the electricity production delivered on the AC side, presented in kWh. Beside the results for the pc-Si and the CIS systems, the ratio between the yield of the CIS and the yield of the pc-Si is shown on the right-hand axis. As described section 3.3.4 the output is a result of the total system efficiency and the incident irradiance on the modules. The annual yield is the production for a specific year and cannot be used as a representative estimate of the average yearly production.

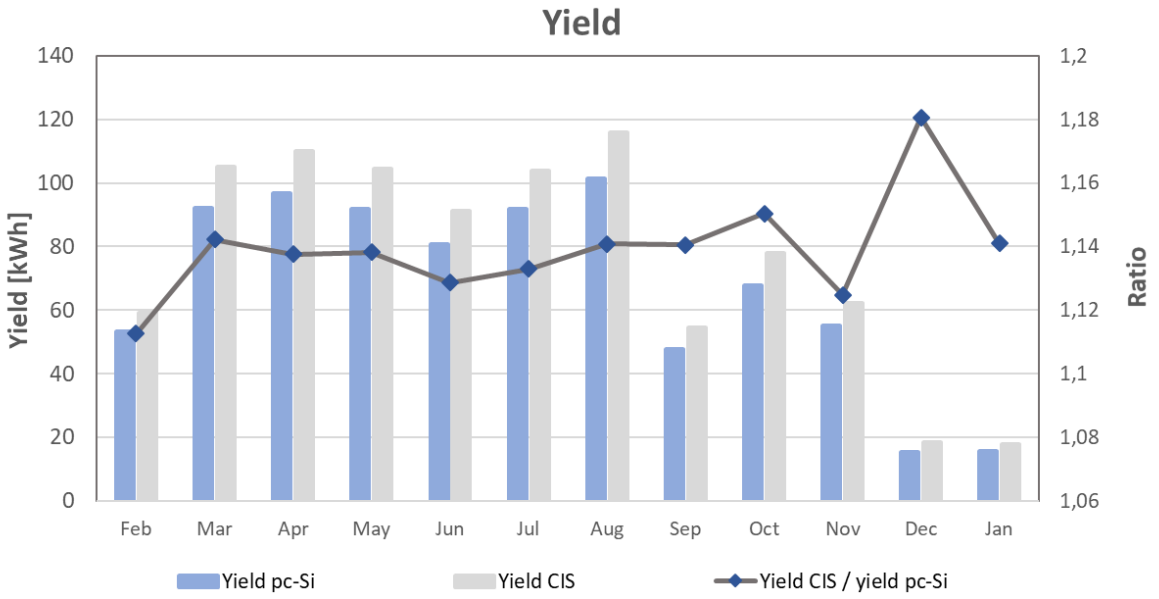


*Figure 4.1: The output yield for both the pc-Si and CIS systems from February 2017 to January 2018, presented as monthly values in kWh. Along with the yield is the yield ratio between the two systems plotted.*

The highest energy production takes place between March and May, as well as July and August. December and January are the months with the lowest energy production. The ratio between the yield of the two systems varies more during the months with the lowest production. It can be observed that during the studied year, the CIS system produced from 11% to 18% more energy per month than the pc-Si system. In average the ratio is approximately 1.14.

*Table 4.1: The total yield in kWh of the pc-Si and the CIS systems in 2016 and 2017, and the yield rate of the two systems.*

| Year | Yield CIS [kWh] | Yield pc-Si [kWh] | Yield CIS/Yield pc-Si |
|---|---|---|---|
| 2016 | 922.6 | 804.9 | 1.146 |
| 2017 | 938.5 | 824.7 | 1.138 |
| Total | 1861 | 1630 | 1.142 |

In Table 4.1, the annual yield for 2016 and 2017 is presented for both systems. The total yield from one year to the next is almost unchanged, with an increase of around 2%. In 2017 the pc-Si system produced 804.9 kWh energy, while the CIS system produced 922.6 kWh, 13.8% higher. In total the CIS system produced 14.2% more electricity. The nominal installed power of the two systems is 1.3 $kW_p$ for the pc-Si system and 1.32 $kW_p$ for the CIS system respectively. Hence, the

difference in yield between the two systems cannot be explained by the nominally installed power alone.

The yield and the yield ratio in June are shown exemplarily in Figure 4.2. The ratio is relatively constant through the month, while the difference in production naturally varies substantially. During this month the daily yield of CIS and pc-Si does not go beyond 6 kWh and 5 kWh respectively. In general, the ratio between the two systems varies more in the winter months than in the summer months.

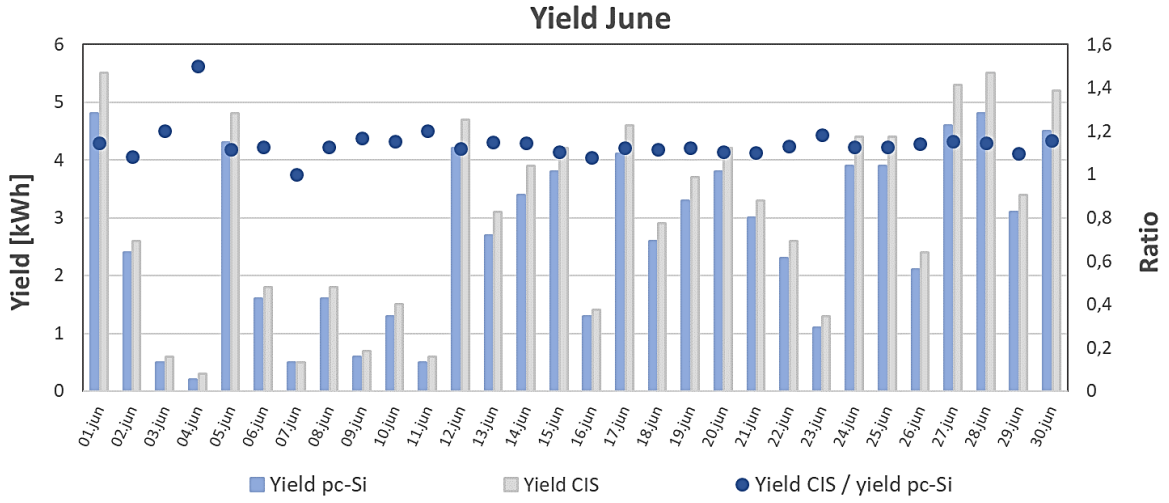


*Figure 4.2: The output yield for both the pc-Si and CIS systems for June 2017. The yield ratio between the two systems is also plotted.*

In the first graph in Figure 4.3 it is illustrated how the ratio changes with production, and the daily yield values are plotted for the entire year. For very low production the CIS system seems to have significantly better relative performance than the pc-Si system. However, some of the low production data points give a yield ratio of one. These results are only for outputs smaller than 1 kWh. Since the yield data has a resolution of 0.1, the yield data with low values have large relative rounding errors. In the bottom graph, the yield values that gave a yield ratio of one was changed. One more decimal was added to these yield values, so that they had two decimals. An example of the approach is that days when both systems produce a yield of 0.3 kWh, the yield of the CIS system is changed to 0.34 kWh, and the yield of the pc-Si system is changed to 0.25 kWh. Both numbers can be rounded to 0.3 kWh. With this correction, there is a clearer relationship between production and the yield ratio of the two systems. The days where the production of the pc-Si is 0 is removed from this data.

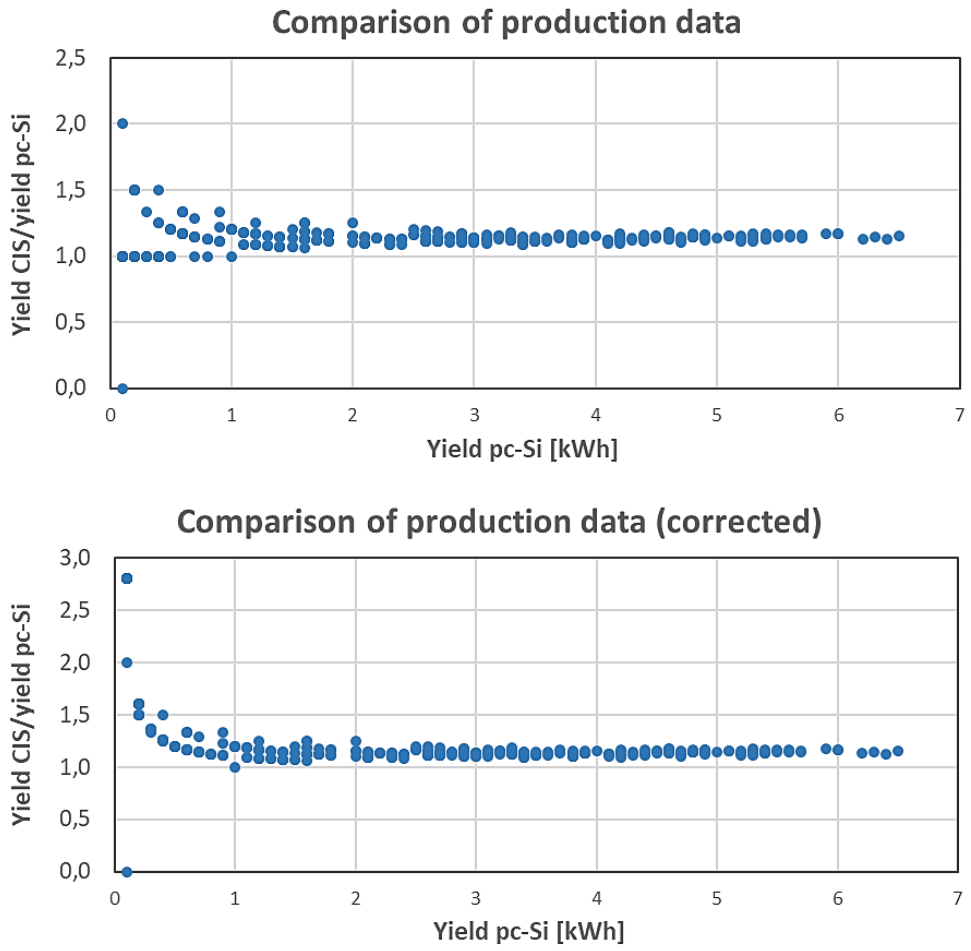


*Figure 4.3: The output yield for the pc-Si system is compared to the yield ratio between the systems. Data for every day in the period: 01.02.2017-31.01.2018. The left figure shows the uncorrected results and the right figure shows the results with corrections for possible rounding errors.*

### 4.1.2 Simulation

Both systems in this study were modelled in the PV system simulation program PVsyst. The systems have been modelled using two different raw data; the first model contains climatic data from the Meteonorm database and, the secound contains an imported weather file with measured weather data from the test site. Both the measurements of the ambient temperature and irradiance in POA is used. The models include specified factors for the array, the inverter, the system location and loss mechanisms. The factors included in the models are specified in section 3.3.2.

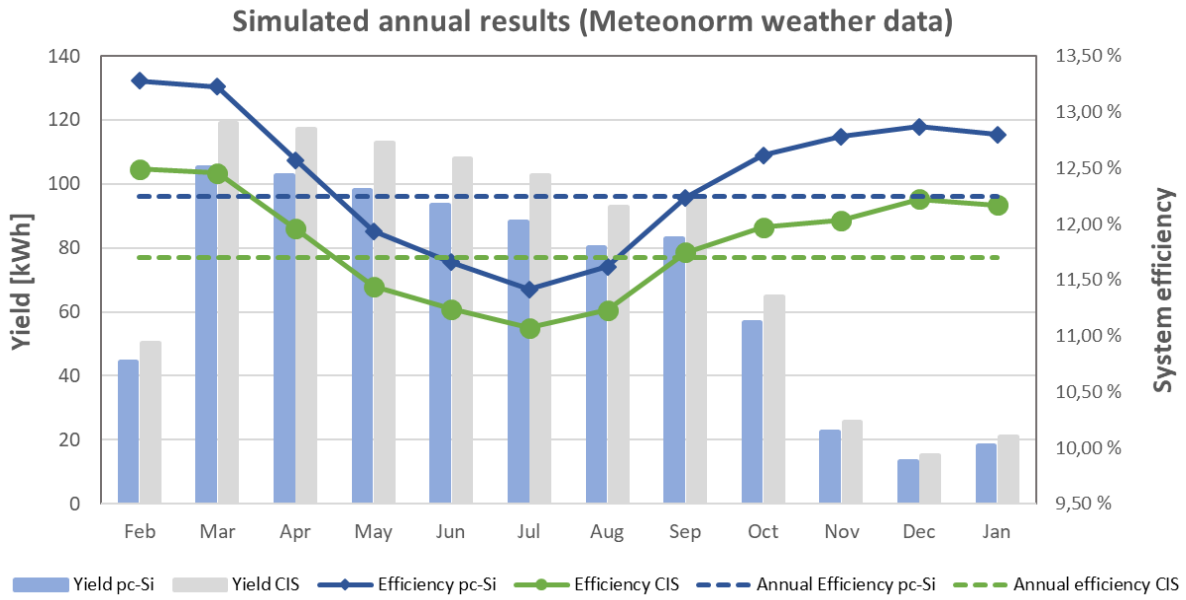


*Figure 4.4: The simulated yield for the pc-Si and the CIS systems from February 2017 until January 2018. In addition, the system efficiency for every month is plotted and the annual efficiency for both systems is added as a dashed line. Weather data from Meteonorm is used in the simulation.*

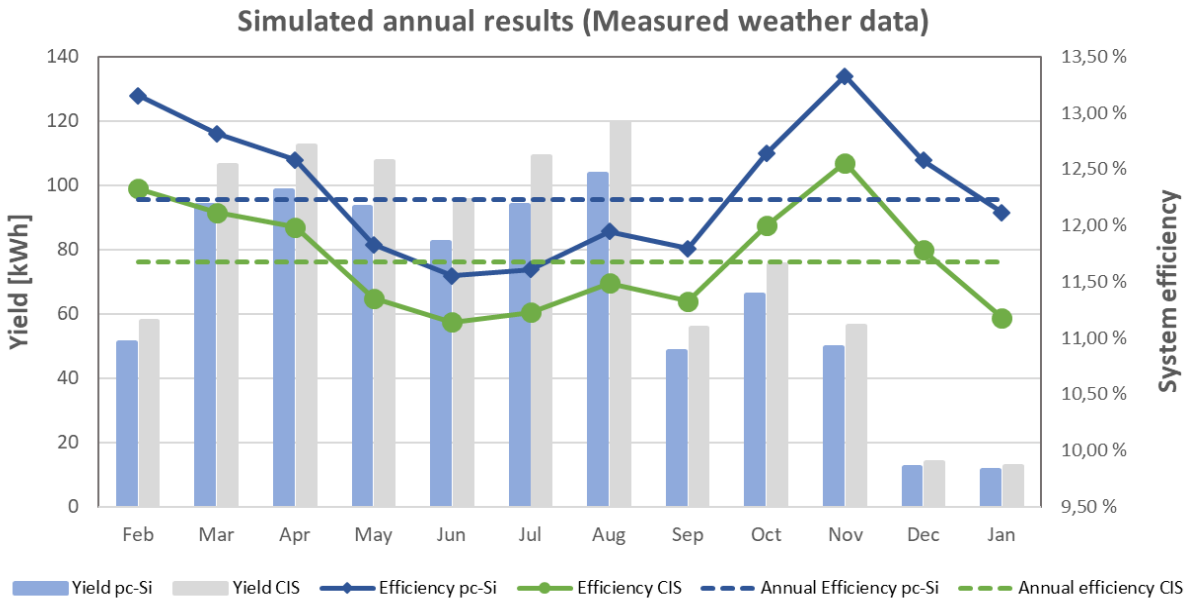


*Figure 4.5: The simulated yield for the pc-Si and the CIS systems from February 2017 until January 2018. In addition, the system efficiency for every month is plotted and the annual efficiency for both systems is added as a dashed line. Measured weather data at the test site is used in the simulation.*

The monthly yield and system efficiency of the two systems are illustrated in Figure 4.4 and Figure 4.5. The first figure shows the results from the simulation with the Meteonorm data. Meteonorm is a database that contains data from over 8000 weather stations. With this data, Meteonorm creates representative typical years for any place on earth. In the simulation, a typical climatic year for Kjeller in Norway is used. The second figure illustrates the result for the simulation with imported weather data. The imported data are measured by the pyranometer and the ambient temperature sensor at the test site. This data are also used for the analysis of the measured system output data. The monthly system efficiencies are calculated using the total incident energy on the systems and the output yield on the AC side of the inverter. The system efficiency for the assessment period is calculated for the systems and shown as dotted lines.

The figures show that the monthly produced energy and the monthly efficiency of the two different simulation methods exhibit some differences. Since the models contain different weather data, this variation was expected. Nevertheless, the total energy production for a year in the two simulations only differs by less than 0.05%. This is the case for both PV systems. Note also that the efficiencies of both the pc-Si and CIS systems are considerably lower in the summer months than in the winter months, with January in the last figure as an exception. The effect is greater for pc-Si than for CIS due to the difference in temperature coefficients between these two technologies. However, the cold Nordic climate reduces the net temperature losses compared to warmer climates. During winter time, the operating temperature of the pc-Si modules is often less than 25°C, leading to positive temperature correction.

### 4.1.3 Annual results

In addition to the simulations, the measured production data has been used to study the actual performance of the systems. The output yield on the AC side, collected from the inverters, and the irradiance data from the pyranometer has been used to calculate the average system efficiency every month from the 1st of February 2017 until the 31st of January 2018. The electricity production and the system efficiency of both systems are illustrated in Figure 4.6. A yearly average system efficiency has also been calculated for both systems.

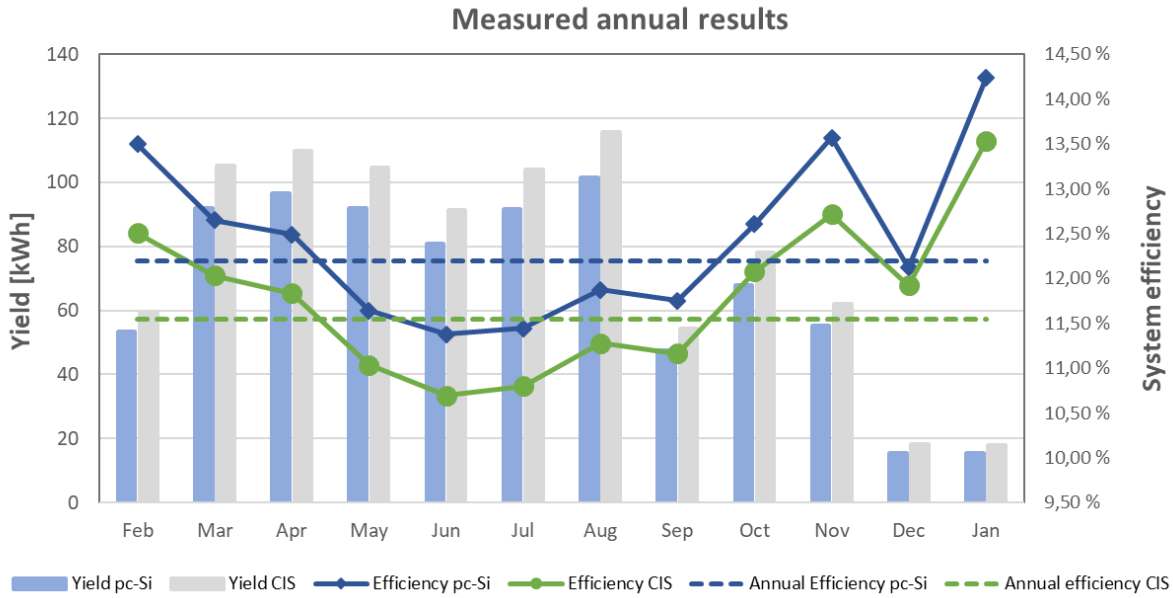


*Figure 4.6: The measured yield for the pc-Si and the CIS systems from February 2017 until January 2018. Also, the system efficiency for every month is plotted, and the annual efficiency for both systems is added as a dashed line. Measured weather data at the test site is used in the calculations.*

The total yield produced during the assessment period was 810.0 kWh for the pc-Si system and 920.8 kWh for the CIS system. The efficiency in the summer months is lower than in the winter months. This corresponds well with the results from the simulations and theory. The highest efficiency occurred in January. The efficiency in December is low compared to the other winter months. The performance parameters for the measured annual data are given in Table 4.2, together with the results from the two simulation approaches.

*Table 4.2: The simulated and actual results for the pc-Si and the CIS systems from February 2017 until January 2018. Stated is the annual yield, irradiance and efficiency.*

| | **Data** | | **PVsyst with actual weather data** | | **PVsyst with weather data from Meteonorm** | |
|---|---|---|---|---|---|---|
| | pc-Si | CIS | pc-Si | CIS | pc-Si | CIS |
| **Yield [kWh]** | 810.0 | 920.8 | 804.4 | 921.8 | 806.1 | 925.0 |
| **Irradiance [kWh]** | 6643 | 7975 | 6579 | 7898 | 6584 | 7904 |
| **Reference yield [h/year]** | 811.7 | 811.7 | 803.9 | 803.9 | 804.5 | 804.5 |
| **Final yield [h/year]** | 623.1 | 697.6 | 618.8 | 709.1 | 620.1 | 711.5 |
| **Performance ratio [%]** | 76.8 | 85.9 | 77.0 | 88.2 | 77.1 | 88.4 |
| **System efficiency [%]** | 12.19 | 11.55 | 12.24 | 11.70 | 12.23 | 11.67 |

The annual results show that the pc-Si system is more efficient than the CIS system, as expected since the pc-Si modules have a higher module efficiency than the CIS modules. The performance ratio of the CIS system is however higher than that of the pc-Si system. This could mean that the CIS system is producing more energy per installed $kW_p$ than the pc-Si system.

Since the results from the measured data and the PVsyst simulation uses the same weather data, they can be compared to evaluate the precision of the model. The irradiation incident on the modules should be the same for both methods. Despite a variation of less than 1%, which is probably a result of some import issues of the weather file, the irradiation is alike. The simulation gives a good estimate for the system production, with a difference of less than 1%. The system efficiencies estimated by the model is higher than that calculated with the real production data, and so are the performance ratio. Hence, the model is overestimating the performance of the systems compared to what is the actual case is. The simulation software uses performance parameters from the manufacturers, default values, and models to predict the output of the system. This is explained in more detail in section 3.3.2. Some of these factors might be inaccurate.

### 4.1.4 Yield and Irradiance

In this subchapter the relationship between the irradiance and the yield has been studied to verify the results and better understand the data. The irradiance is presented by the incident energy and is plotted vs. the yield in Figure 4.7. A regression line is fitted to the data to study the linear correlation.

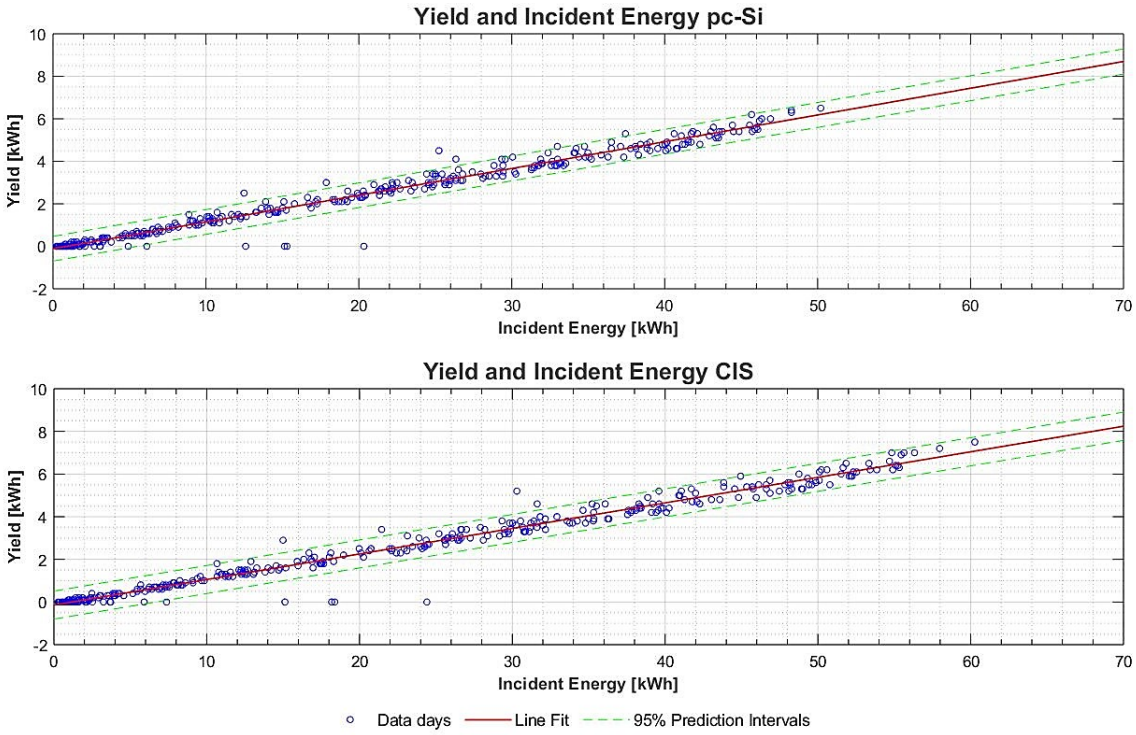


*Figure 4.7: The daily produced yield and incident energy are plotted against each other, for both the pc-Si and CIS systems. The red lines are the fitted regression lines, and the 95% prediction interval is illustrated with the dashed green lines.*

As expected, the yield has a clear dependence on the irradiation. The data follows the regression line closely, and the prediction intervals are narrow. The linear relation is similar for both the pc-Si and the CIS system. The small variation from the line fit can be explained by other factors than the irradiation, such as temperature or wind variations. On the days were the production is above the red line the ambient temperature can have been low enough to cool the modules to under 25°C. However, the days with lower production can have been particularly warm. Since the modules are attached close to the wall, the wind will not be able to contribute to substantial cooling on the rear side of the modules. Although the irradiance and the yield have a clear dependence, the system efficiency is not constant. The efficiency plots for August and November, in Figure 4.8 and Figure 4.9, shows that the system efficiency has daily and monthly variations. For November, there are large variations between days. The efficiency variation is less in August.

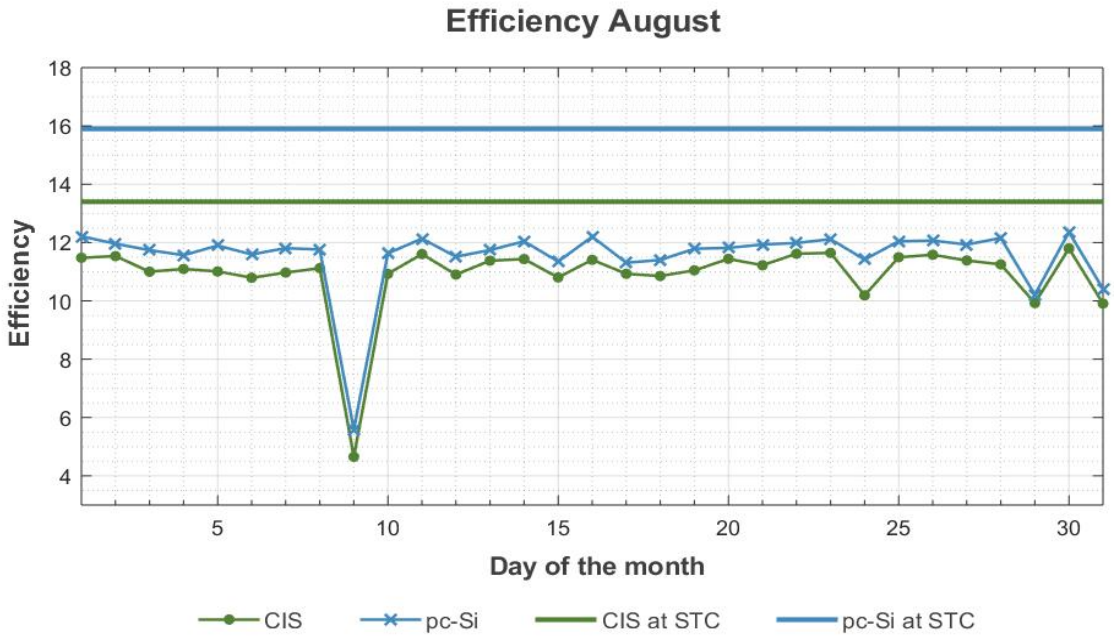


*Figure 4.8: The graph shows the system efficiency for pc-Si and CIS in August, with two lines representing the STC efficiency values of the modules given in the datasheet.*

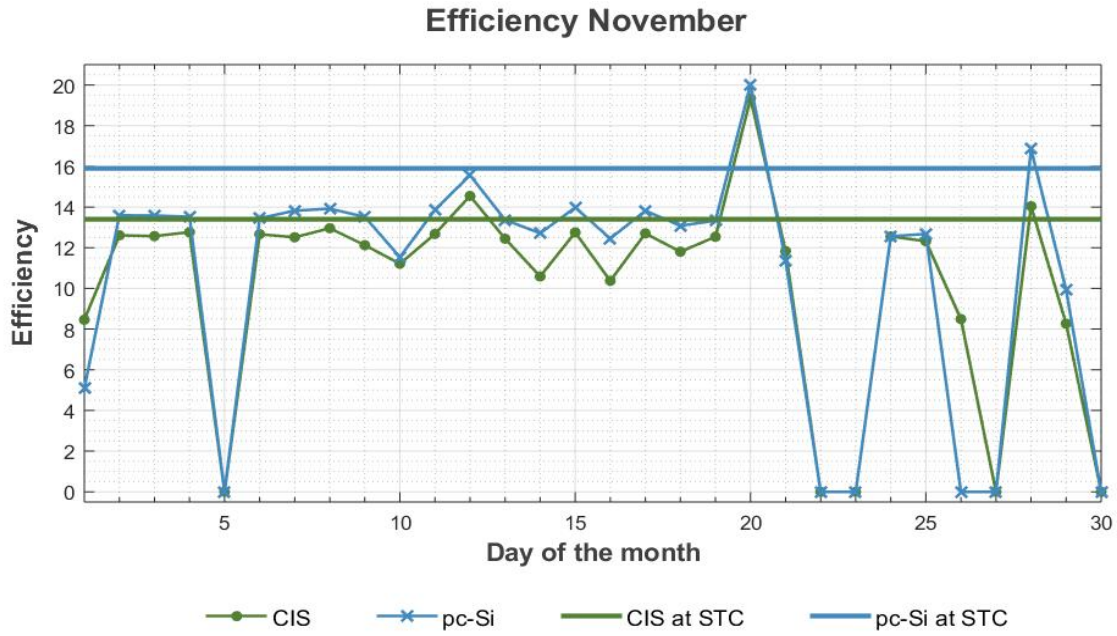


*Figure 4.9: The graph shows the system efficiency for pc-Si and CIS in November, with two lines representing the STC efficiency values of the modules given in the datasheet.*

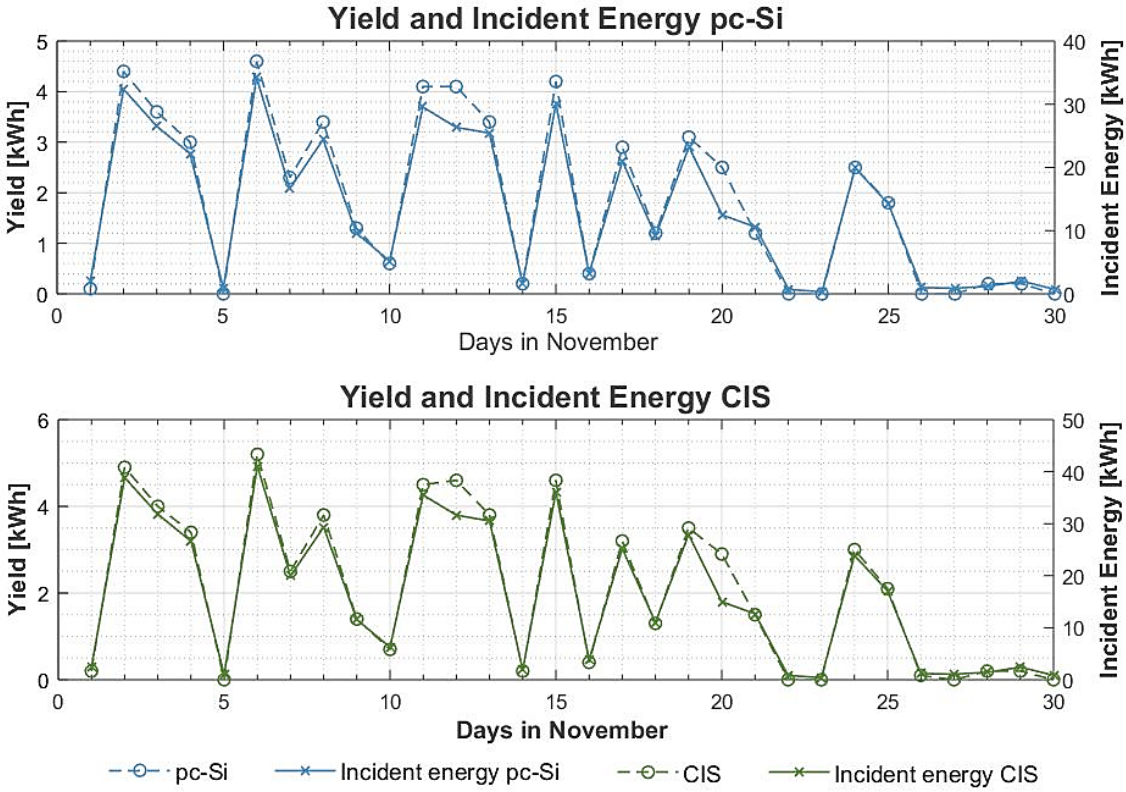


*Figure 4.10: The graph illustrates the variation in produced yield and incident energy during November. In the top graph is the data for the pc-Si system and in the bottom graph is the data for the CIS system.*

The 9th of August had a great drop in efficiency. This is a day where the produced yield is close to zero. Looking at the November efficiency against the yield and irradiation the same month, given in Figure 4.10, the efficiency seems unpredictable when the irradiation is very low. Many of these days the efficiency falls to zero. As the winter months generally have more days with high cloud coverage and low irradiance, the winter months have a higher variety of efficiencies than the summer months. The variation in efficiency can mostly be explained by the fact that both the module efficiency and the inverter efficiency drops extensively at low irradiation. It may also be affected by the startup voltage. As explained in section 3.2.1 the inverter has a startup voltage of 150 V. The $V_{mpp}$ of the pc-Si system is 155.5 V while the $V_{mpp}$ of the CIS system is 342 V. This means that the power production of the pc-Si system must be higher than that of the CIS system before its inverter starts working. Also, the relative uncertainty at low irradiance becomes much greater, than for high irradiance values.

From the November efficiency figure, it is also possible to see that there are some days with especially high efficiency. Day 12 and 20 is two of these days. When looking over at the yield-irradiance curves, they display a larger inconsistence with each other at these exact days. The yield is greater than one would assume looking at the curves. Less than ten days during the year has the same inconsistence. This can occur due to high wind or low temperature. Another possibility is that the pyranometer is registering a lower irradiance than what reaches the modules. These ten

days of inconsistence produces a maximum error of 3% in the calculated monthly system efficiencies.

## 4.2 Light-soaking

### 4.2.1 New performance at STC

Natural degradation is a well-known feature that effects all PV modules, reducing the efficiency of the modules over time. The degradation mechanisms are defined in section 2.5.4, but nearly all are related to water ingress or temperature stress. CIS modules are in addition to degradation, affected by illumination induced changes, also called the light soaking effect. Since degradation and light soaking is altering the performance of PV modules, an accurate model of a system would need fresh measurements of the module performance at STC. Such measurements are not easy to perform since it needs stable STC. A Solar simulator can be used for the measurements, but CIS modules are still difficult to measure precisely because of the light induced metastable changes.

Measurements of the modules' performance at STC was conducted with a pulsed Solar simulator at IFE in Kjeller, to study the degradation and possible light soaking improvements. Each module was measured individually and flashed with a lamp of 1000 W/m$^2$. Temperature corrections were done by the simulator to get the correct values at STC. The performance data at STC measured by the manufacturer, and the measured performance from this study is given in the Tables 4.3-4.6 The reported result of the CIS modules is from the first measurements performed on them.

*Table 4.3: Performance values at STC for the pc-Si modules from the manufacturer. From the left: Module ID, Max Power, Short Circuit Current, Open Circuit Voltage.*

| pc-Si | Values from manufacturer | | |
|---|---|---|---|
| **ID** | **$P_{max}$ [W]** | **$I_{SC}$ [A]** | **$V_{OC}$ [V]** |
| 038 | 261.0 | 9.01 | 31.20 |
| 039 | 260.9 | 8.98 | 31.15 |
| 943 | 261.1 | 8.99 | 31.17 |
| 622 | 262.8 | 9.01 | 31.37 |
| 664 | 262.2 | 9.03 | 30.69 |

*Table 4.4: Measured performance values at STC for the pc-Si modules. From the left: Module ID, Max Power, Deviance from original Power value, Short Circuit Current, Open Circuit Voltage, Fill Factor, Efficiency and temperature during measurements.*

| pc-Si | Measured values | | | | | | |
|---|---|---|---|---|---|---|---|
| **ID** | **$P_{max}$ [W]** | **P-rate** | **$I_{SC}$ [A]** | **$V_{OC}$ [V]** | **FF** | **Eff module** | **Temp [°C]** |
| 038 | 256.5 | -1.76% | 9.082 | 37.72 | 0.749 | 16.50% | 21.1 |
| 039 | 256.7 | -1.64% | 9.072 | 37.77 | 0.749 | 16.51% | 20.6 |
| 943 | 258.0 | -1.19% | 9.110 | 37.70 | 0.751 | 16.60% | 21.2 |
| 622 | 253.5 | -3.69% | 9.085 | 37.77 | 0.739 | 16.31% | 20.0 |
| 664 | 258.9 | -1.29% | 9.121 | 37.76 | 0.752 | 16.66% | 20.9 |

*Table 4.5: Performance values at STC from the manufacturer for the CIS modules. From the left: Module ID, max power. No data for the short circuit current and the open circuit voltage is provided.*

| CIS | Values from manufacturer |
|---|---|
| **ID** | **$P_{max}$ [W]** |
| 432 | 169.6 |
| 442 | 169.2 |
| 456 | 168.9 |
| 392 | 169.7 |
| 438 | 168.4 |
| 434 | 169.7 |
| 402 | 169.4 |
| 446 | 169.4 |

*Table 4.6: Measured performance values at STC for the CIS modules. The values from the first measurement. From the left: Module ID, time of the measurement, elapsed time since disconnection from the power grid, max power, deviance from original power value, short circuit current, open circuit voltage, fill factor, efficiency, and temperature during measurements.*

| CIS | Measured values | | | | | | | |
|---|---|---|---|---|---|---|---|---|
| **ID** | **Time** | **Elapsed** | **$P_{max}$ [W]** | **P-rate** | **$I_{SC}$ [A]** | **$V_{OC}$ [V]** | **FF** | **Temp [°C]** |
| Disconnected | 08.20 | Reference | | | | | | |
| 432 | 09.36 | 1.16 h | 174.2 | 2.73% | 2.152 | 117.2 | 0.691 | 17.6 |
| 442 | 10.28 | 2.08 h | 176.4 | 4.24% | 2.145 | 117.6 | 0.699 | 20.5 |
| 456 | 11.15 | 2.55 h | 170.3 | 0.85% | 2.149 | 114.9 | 0.690 | 20.5 |
| 392 | 13.06 | 4.46 h | 173.8 | 2.43% | 2.117 | 117.3 | 0.700 | 20.5 |
| 438 | 13.59 | 5.39 h | 175.2 | 4.04% | 2.161 | 116.7 | 0.695 | 20.5 |
| 434 | 14.44 | 6.24 h | 172.9 | 1.89% | 2.148 | 116.8 | 0.690 | 20.9 |
| 402 | 15.25 | 7.05 h | 174.5 | 3.02% | 2.076 | 117.3 | 0.716 | 21.1 |
| 446 | 16.12 | 7.52 h | 174.0 | 2.73% | 2.133 | 117.8 | 0.693 | 20.5 |

The value taken most of interest in this study is the maximum power of the modules. The maximum power at STC is the best indication of the module performance, tightly linked to the module efficiency as the measurements are taken at a specific light intensity. The P-rate, is used to describe the change in module performance. The above tables show that the CIS modules have had an improvement of 0.85-4.24%, while the pc-Si modules have degraded by 1.19-3.69%. The result is in correspondence with the theoretical expectations. The pc-Si modules are affected by degradation, while the CIS modules, though also probably affected by degradation, have improved due to the light soaking effect.

The uncertainty of the $P_{max}$ measurements was less than 0.2% during all measurements. The temperatures of the modules during measurements were in most of the tests around 19-21°C. The solar simulator has corrected the results for the inaccurate temperature, but since the modules did not hold a temperature of 25°C the uncertainty of the measurements increases slightly.

### 4.2.2 CIS degradation in dark storage

Earlier research shows that the improvement of CIS modules due to the light soaking effect will be reduced with time when the modules no longer are exposed to light. The effect would according to this research fall rapidly when they are disconnected from the load and stored in darkness (Deceglie et al., 2015). The CIS modules in this study were measured four times to see how they were affected by dark storage after light soaking. The first measurement took place the 6$^{th}$ of March 2018, the same day as the modules were demounted. The other measurements were taken the two following days and lastly one week after the demounting. The measured $P_{max}$ at STC for each module is plotted along a time axis in Figure 4.11. The resulting curves show the darkness induced change in $P_{max}$.

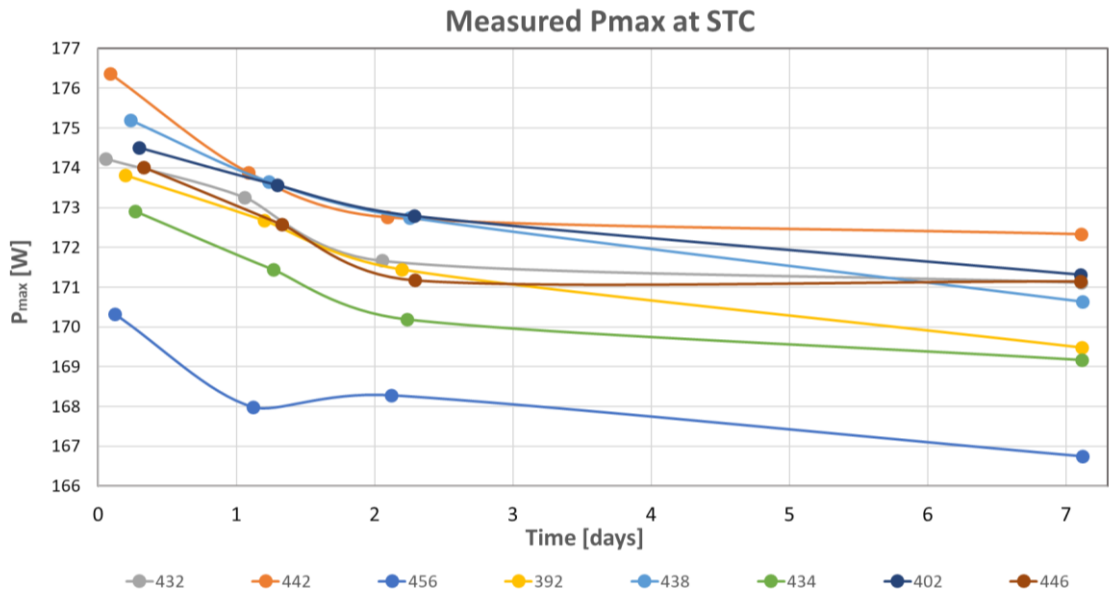


*Figure 4.11: The measured $P_{max}$ at STC taken the first three days and a week after the demounting of the CIS modules. Each line represents one of the modules, eight in total.*

From the figure, it can be seen that all the modules have a similar reduction in $P_{max}$ over the days in dark storage. The most rapid decrease occurred between the first and the second measurement. The first measurements were taken a few hours after the demounting of the modules. The second measurements were done 24 hours after the first measurements. Between the third and fourth measurement, the reduction rate was low, and it was decided to end the measurements. For most of the modules, the $P_{max}$ continued to decrease until the last measurement. The reduction over a week in storage were between 1.7% and 2.6% for all the modules.

Many of the modules have similar performance, but particularly one module stands out from the rest with a lower $P_{max}$ and a lower $V_{oc}$ than the rest of the CIS modules. After the forth measurement the performance of this module was 1.2% lower than the original measurement by the manufacturer. The reduced $V_{oc}$ and $P_{max}$ can be linked to higher series resistance. This can come from corrosion of the metal contacts, possible hotspots on the module, or other defects that can occur over time. The module was inspected during the tests, and no damage was visible. It can also be a consequence of the light soaking not affecting all the modules equally.

A question to consider is whether the same performance drop can occur while the modules are mounted on the wall and connected to a load, with long periods of low irradiation. However, based on literature, the registered performance loss over a long time spent in dark storage is affecting the performance less than 3% after a week. The loss would not be any higher if the modules were mounted outdoors since there is a chance for some current to be generated. Light soaking has been detected at an irradiance of only 10 $W/m^2$, directed towards the CIS modules (Kenny et al., 2006). It is highly unlikely that the irradiance on modules placed outside stays under 10 $W/m^2$ for a week straight. This further reduces the suspicion that a performance drop due to long periods of cloudy conditions can occur.

Another question worth further consideration is the magnitude of the fall in performance the very first hours after the modules were disconnected from the grid. As Figure 4.11 shows, the most rapid drop in performance happened the first day. The first module was measured 1 hour and 16 minutes after disconnection. According to the research done by Kenny, Nikolaeva-Dimitrova, and Dunlop in Italy, light soaking improves the performance of the CIS modules, but the light soaking rapidly loses its effect. Their test showed that the most rapid decrease in performance happened the very first hour after light soaking. Continuous measurements over time showed that the $P_{max}$ dropped with a linear rate on a logarithmic timescale (Kenny et al., 2006). Hence, the light soaking effect on the CIS modules may have been greater than what is reported in this work.

In Figure 4.12 the measurements of $P_{max}$, $V_{oc}$, $I_{sc}$ and $FF$ for two of the modules are given. The top one being the module with the best performance and the bottom one is the module with the worst performance. The $P_{max}$ measured by the manufacturer before delivery is also drawn into the graphs.

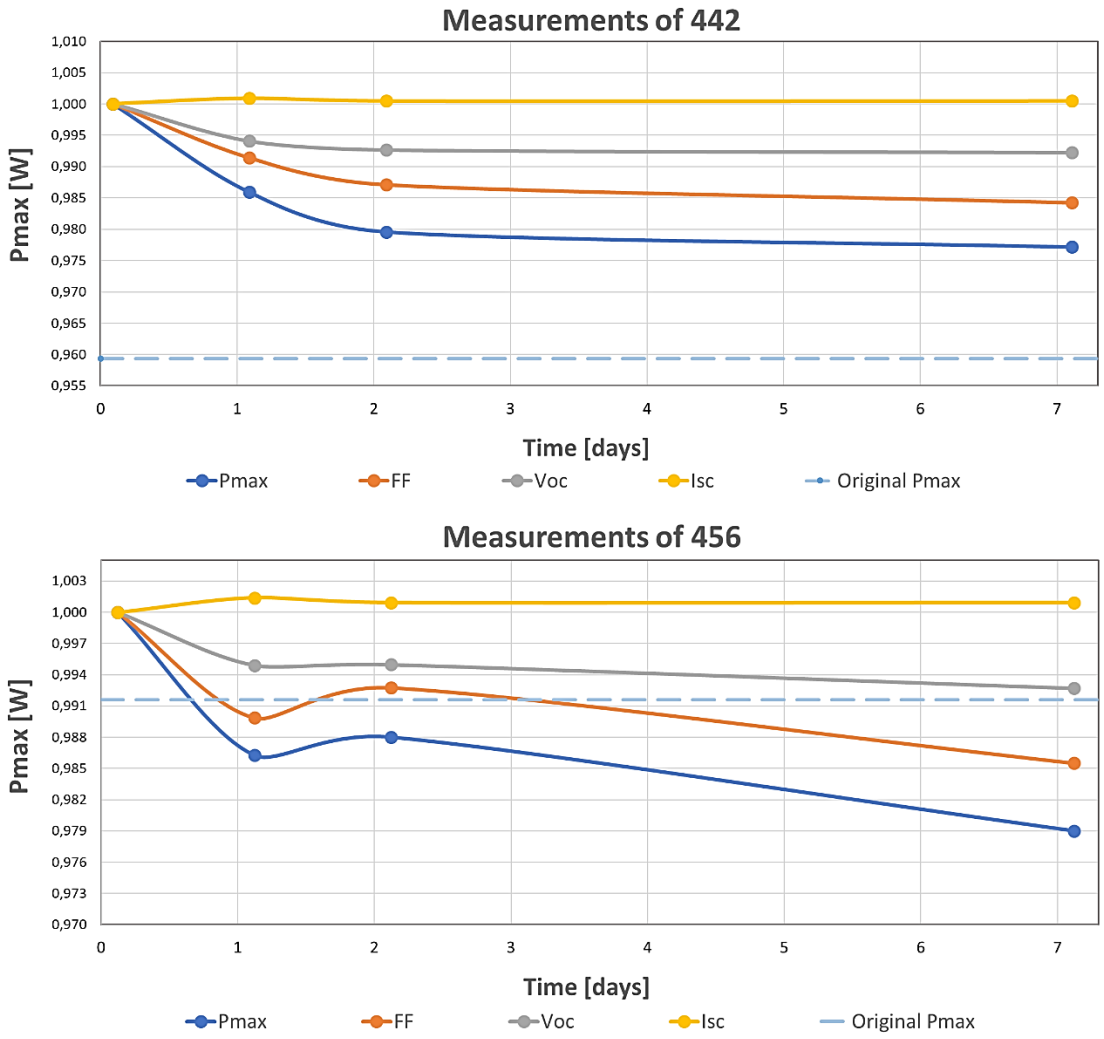


*Figure 4.12: The illustration show the measured performance of module 442 in the top graph and 456 in the bottom graph. The measured $P_{max}$, $V_{oc}$, $I_{sc}$ and FF is taken the first three days and a week after the demounting of the CIS modules. Plotted is also the original $P_{max}$ value from the manufacturer. All the coefficients are measured at STC.*

The overhead graphs illustrate how the four performance parameters change over time in dark storage after light soaking. Earlier research on light soaking has shown a connection between the improvement in $P_{max}$ and a similar improvement in $FF$ and $V_{oc}$ (Del Cueto et al., 2008). The tests done on the CIS modules in this study show a similar connection when measuring the darkness losses. The connection between $P_{max}$ and $FF$ is easy to notice on the graphs, the plots follow the same pattern. $FF$ is not decreasing as much as $P_{max,}$ but it is decreasing substantially enough to observe a connection. $V_{oc}$ also decreases, especially the first day. In comparison, the $I_{sc}$ seems to be increasing a small amount instead of falling. This is probably a consequence of the decreased voltage.

In the graphs there are two blue lines, the darkest showing the $P_{max}$ measurements the lightest is the original $P_{max}$ value from the manufacturer. The first measurements of all the CIS modules had improved performance compared to the measurements done by the manufacturer. As the bottom graph illustrates, not all the modules continued to have a higher performance than originally after the effect of light soaking had decreased. Three of the eight CIS modules ended up with a lower $P_{max}$ than originally after a week of storage. Indicating that the CIS modules are affected by degradation in addition to the light soaking effect.

### 4.2.3 System results after the performance measurements

The results found with the measurements of the solar simulator changes the assumed values of the installed power of the two PV systems given in Table 3.1. The new $P_o$ is calculated summing the measured $P_{max}$ of each module. The module STC efficiency, $\eta_{STC}$, $Y_F$ and $PR$ are also changed. These values have been calculated with the new $P_o$. The results is given in Table 4.7.

*Table 4.7: The tables show the installed peak power from the datasheet, from the measurements at the manufacturer and the new measured values. The corresponding efficiencies are also given. The upper table presents the values for the pc-Si system and the bottom table show the values for the CIS system.*

| **pc-Si (@STC)** | **Datasheet value** | **Original value from manufacturer** | **New measured value** |
|---|---|---|---|
| **Installed Power [W]** | 1300 | 1308 | 1284 |
| **Efficiency [%]** | 15.88 | 15.98 | 15.69 |
| **Final yield [h/year]** | 623.1 | 619.3 | 630.8 |
| **Performance ratio [%]** | 76.8 | 76.3 | 77.7 |

| **CIS (@STC)** | **Datasheet value** | **Original value from manufacturer** | **New measured value** |
|---|---|---|---|
| **Installed Power [W]** | 1320 | 1354 | 1391 |
| **Efficiency [%]** | 13.44 | 13.78 | 14.16 |
| **Final yield [h/year]** | 697.6 | 680.1 | 662.0 |
| **Performance ratio [%]** | 85.9 | 83.8 | 81.6 |

Both the measurements from the manufacturer and the new measured values are addes to the tables. By assuming the $P_o$ from the datasheet is the correct installed power, the CIS system produces 12% more energy per kW installed than the pc-Si system. The measured $P_o$ of the CIS system is higher than the datasheet value, and the measured $P_o$ of the pc-Si system is lower than the datasheet value. The installed power of the two systems is thus not as similar as earlier assumed, and this partly explains why the CIS system produces more energy than the pc-Si system. With the changed values the CIS system produces 5% more energy per kW installed than the pc-Si system. The performance ratio has also become more equal after gathering the new system performance.

These corrections partly explain why the CIS system produced much more than the pc-Si system in the assessment period. The results show that light soaking and degradation does influence the performance of the pc-Si and the CIS systems.

## 4.3 Soiling

The soiling losses were also studied during the testing of the modules. Flash tests of the modules were performed before and after cleaning, and the soil accumulation was measured. The modules had not been manually cleaned since they had been installed. The pc-Si modules were tested the 8th of February 2018 and the CIS modules the 6th of March 2018. Three of each module type was chosen. The flash tests were done at STC. After a module was measured once, the surface was cleaned with a dry rag. The rags were weighed before and after cleaning the modules. This was done with a Mettler Toledo Excellence Plus scale, which had an uncertainty of 0.1 mg. The expected soiling effect was low since all the modules looked clean before measurements. The measured $P_{max}$ before and after cleaning the modules are given in Table 4.8, together with the amount of soil wiped off each module.

*Table 4.8: The measured soil amount, the $P_{max}$ before and after cleaning, the rate of ΔPmax and the standard deviation of the measurements.*

| Module | | Soil | $P_{max}$ Before | $P_{max}$ After | Rate $\Delta P_{max}$ | Std Dev |
|---|---|---|---|---|---|---|
| **pc-Si** | ID: 622 | 1.8 mg | 253.315 W | 253.465 W | 0.06 % | 0.107 % |
| **pc-Si** | ID: 038 | 5.0 mg | 255.636 W | 256.523 W | 0.35 % | 0.115 % |
| **pc-Si** | ID: 039 | 1.1 mg | 256.866 W | 256.674 W | -0.07 % | 0.097 % |
| **CIS** | ID: 456 | 2.8 mg | 170.084 W | 170.328 W | 0.14 % | 0.047 % |
| **CIS** | ID: 392 | 3.5 mg | 173.638 W | 173.344 W | -0.17 % | 0.050 % |
| **CIS** | ID: 438 | 1.4 mg | 175.050 W | 175.204 W | 0.09 % | 0.050 % |

The rate of change between the $P_{max}$ with and without soil is listed in the table, and so is the standard deviation of $P_{max}$ during the measurements. The standard deviation was found according to the description in section 3.4.1.

Two of the pc-Si and two of the CIS modules had an improved $P_{max}$ after they were cleaned. One of each type got a lower $P_{max}$ after the cleaning. The rate of change in $P_{max}$ is small for all the modules, so small in fact that they are very close to the standard deviation of the solar simulator. Two of the measured rates of change is lower than the standard deviation. Since the rate of change is small for all the moduels tested, with all having under 0.35% change in $P_{max,}$ and since the uncertainty of the measurements is almost as large, the soiling effect is in this study assumed neglible.

The uncertainty of the soiling measurements is very high, due to several reasons. Firstly, due to the uncertainty in the solar simulator measurements itself, explained in more detail in section 3.4.1. Secondly, while demounting the modules and carrying them to the solar simulator, dust may have fallen off, especially heavier dust particles. Soil may also have fallen off during the first measurement with the solar simulator since the modules were turned and measured with the front surface faced downwards.

Another aspect that might have affected the results is that the modules were cleaned with dry rags. Since the modules were cleaned with dry rags, some soil may have been left on the modules' surface under the second measurements. If the rags had been soaked in spirit before cleaning the modules, more soil might have been cleaned off. The reason why spirit was not added to the rags during the tests is that soaking them could add uncertainty to whether some of the spirit would evaporate between the first and the second measurement and affected the weight of the rag.

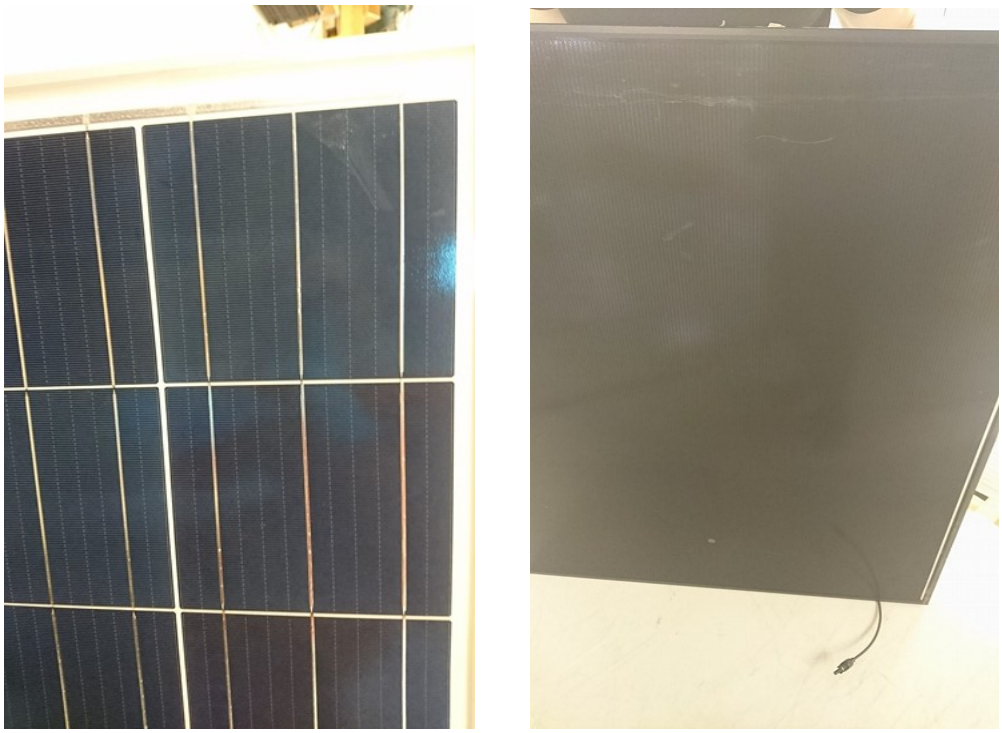

*Figure 4.13: Pictures of one of the pc-Si modules and one of the CIS modules with some soiling marks on them.*

Figure 4.13 show one of the pc-Si modules and one of the CIS modules after they were cleaned. Both had some spots left on the surface after they had been cleaned. A few of the modules had these spots, some of them were caused by fingermarks, other by something that looked like bird droppings, and some spots had probably been made during the assembly of the modules. The spots were still left on the surfaces after they were cleaned with the dry rags. It seemed to be a kind of grease marks. What soiling effect these spots have is not identified. The grease marks were not easy to remove and was still present when the modules were placed back on the test site.

The measured amount of soil on the modules lied between 1.1-5.0 mg. A study on soil accumulation was performed at IFE in Kjeller, Norway, in March and April 2015. The measurements were done on both normal glass, and anti-soiling treated glass fragments of 17×17 cm, placed on a rooftop at IFE at about the same height as the modules of the current test. The measurements were performed over seven weeks, where the glass samples were exposed to natural soiling outside. The soil on the glass was wiped off and weighted every week with the same scale as in the soiling test of this study, and with similar rags. Some of the rags in the earlier tests were soaked with spirit before cleaning the modules, and some were not. The mass difference between the soaked ones and the dry ones was so low that either method would do. The accumulated soil that was measured in the past study lied between densities of 12-85 mg/m$^2$. These numbers are larger than the soil density detected in this study.

The possible reasons to why the soil accumulation discovered were so much smaller than in the past test, could be that the modules of the earlier tests were done on glass that was tilted 45˚. The modules of this experiment were tilted 90˚. The large soil particles probably have a harder time staying on a surface that is tilted 90˚, than one that has a smaller tilt angle because of the gravitational forces. Variations in precipitation conditions can also heavily affect the soiling accumulation. In the past test, the soil level was found to be highest after the weeks with low amounts of precipitation, as expected. In the weeks before the soiling measurements in this study, there had been many days with snowfall. The precipitation can have cleaned the modules. The two factors put together can probably explain much of the difference in the soil density between the new and the past measurements.

Because of varying precipitation levels during the seasons and longer periods with low precipitation levels in the drier months of the year, the effect of soiling might be more apparent in dry periods of the year. Recommendations for further work is to test the soiling effect during different months of the year, to see how much soiling can affect the performance of the systems during dry periods.

## 4.4 Loss mechanisms

### 4.4.1 System and array capture losses

The losses of a system can be separated into two categories, system losses and array capture losses. The array capture losses are the losses due to the array's reduced performance in real conditions.

The system losses are the losses that occur in the system components after the electricity has been generated. The equations used to calculate the system and array capture losses is given in section 3.3.4. Daily average final yield, system losses and array capture losses for the assessment year are presented in Figure 4.14 and Figure 4.15. The presentation of the results is done in accordance with similar performance studies (Ayompe et al., 2011), (Jahn et al., 2000).

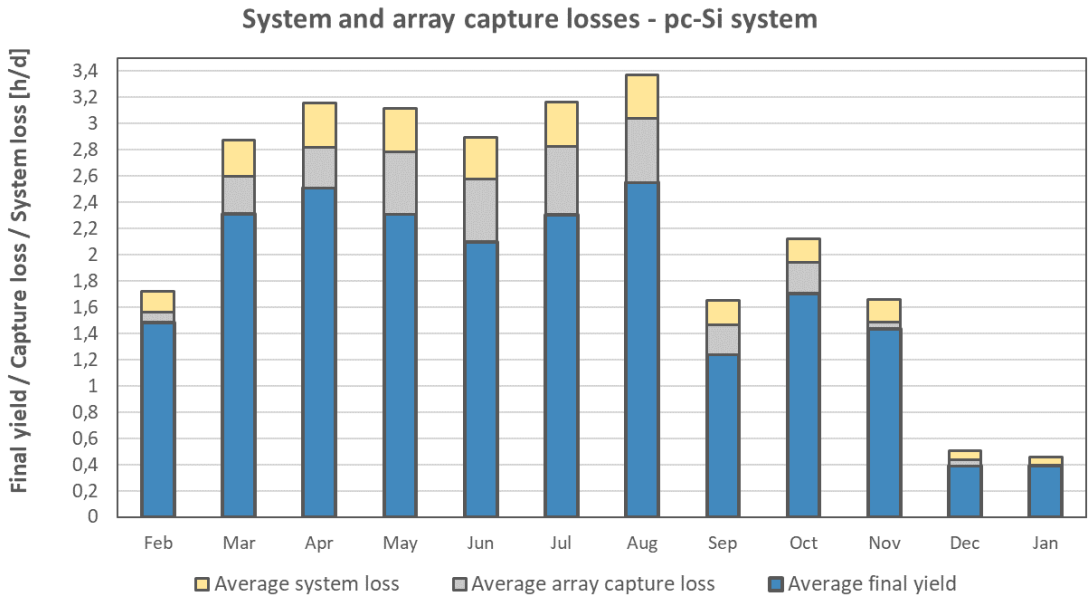


*Figure 4.14: Daily average final yield, array capture losses and system losses during each month for the pc-Si system.*

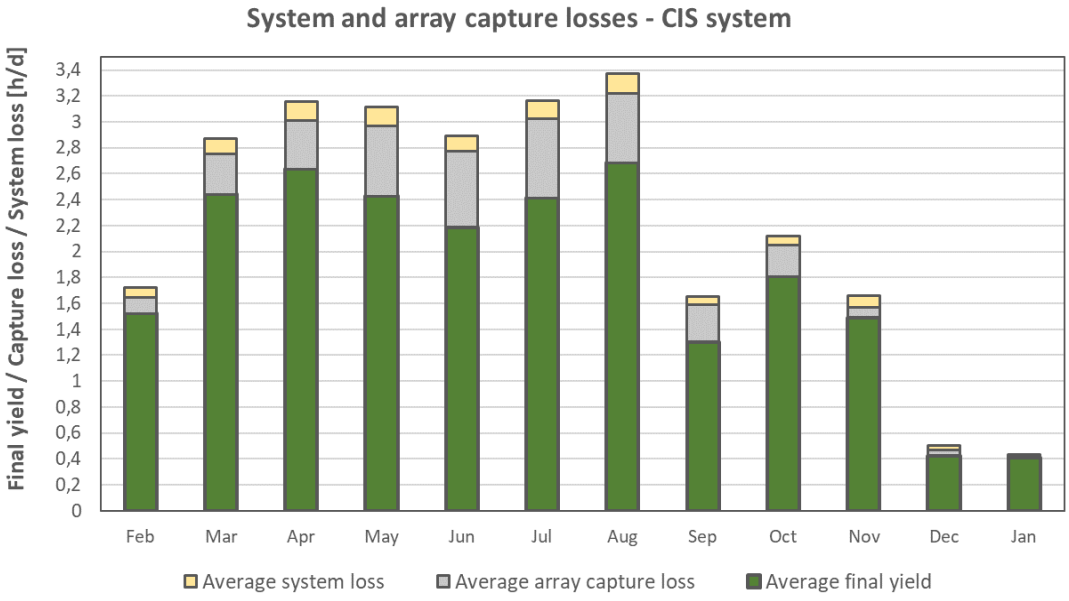


*Figure 4.15: Daily average final yield, array capture losses and system losses during each month for the CIS system.*

The figures clearly show that the array capture losses in general are greater than the system losses, except in some of the winter months. The total losses in the spring and summer months are higher than in the autumn and winter months. The array capture losses of the CIS system are higher than the array capture losses of the pc-Si system. Oppositely, the system losses of the CIS system are lower than that of the pc-Si system. The CIS system probably has lower system losses because it has a higher installed power than the pc-Si system.

*Table 4.9: The average annual system and array capture losses. All the losses are presented as the loss in $Y_F$ and PR.*

| | Final yield loss [h/year] | | Performance ratio [%] | |
|---|---|---|---|---|
| | pc-Si | CIS | pc-Si | CIS |
| **System losses** | 84.2 | 35.8 | 10.4 | 4.41 |
| **Array capture losses** | 96.6 | 114 | 11.9 | 14.0 |

In Table 4.9, the annual losses are shown. The array capture losses are higher than the system losses. The system losses of the CIS system are much lower than that of the pc-Si system, with final yield losses of 35.8 h/year and 84.2 h/year respectively. The difference between the array capture losses of the two systems is not as large, and the pc-Si system is less affected by these losses.

### 4.4.2 Inverter induced loss

In any PV system connected to the grid, there are energy losses due to the conversion of the electricity. The inverter contributes to $L_S$. The magnitude of the inverter losses depends on the efficiency of the inverter. The efficiency varies with the DC input power and the AC output power. The inverter has an optimal operation at a specific power input which make the size of the PV array impact the inverter performance. If the installed power of the array is higher or lower than the optimal input power of the inverter, the inverter is either under- or oversized. The inverter loss will thus be lower for a system that has an optimized design, than one that has an inverter that is under- or oversized.

The manufacturers of inverters usually inform the customer of the maximum efficiency and the EU efficiency of the inverter. PVsyst offers a defalt efficiency profile for many inverters, and the default for the Delta RPI H3 inverter has been used in the analysis of the inverter losses. The eight data points in Figure 3.4 were gathered from the PVsyst inverter profile. With these points, the average inverter efficiency has been estimated for different light intensity increments, which made it possible to estimate the inverter losses that occured during the assessment period. This was done according to the method in section 3.3.5. Figure 4.14 shows the monthly final yields of the system, calculated with the measured installed power, along with the inverter losses.

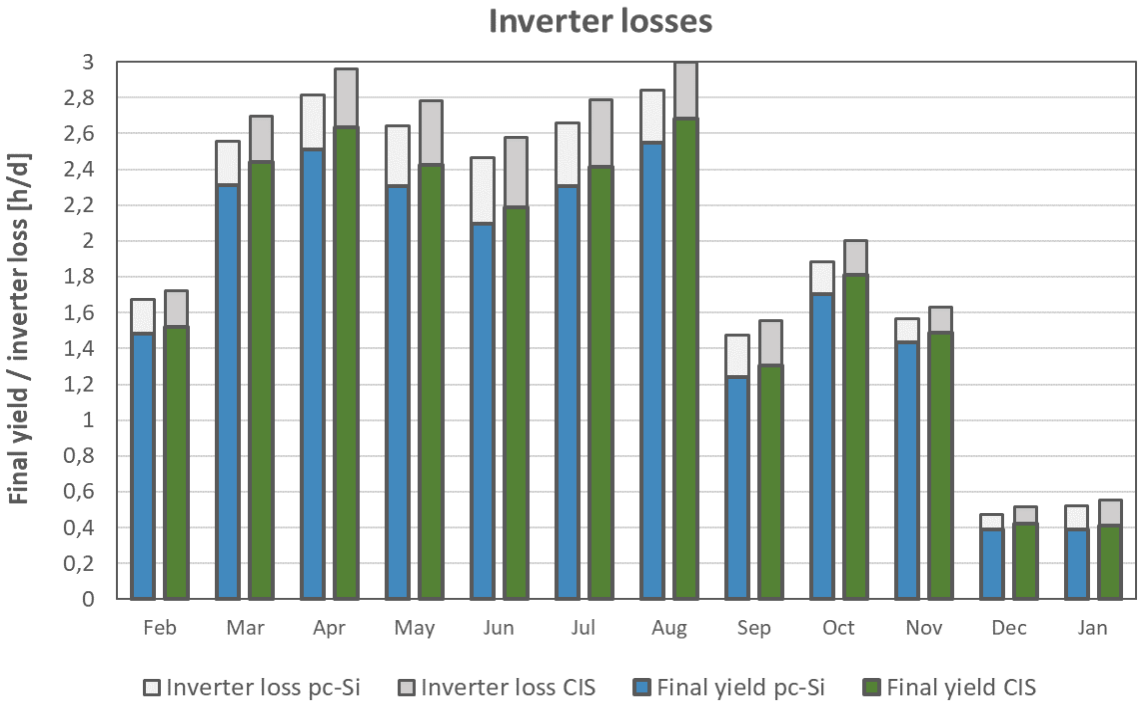


*Figure 4.14: The monthly final yield for the assessment year, with the average inverter loss for each month.*

The average yearly final yield losses due to the inverter were 86.1 h/year for the pc-Si system and 91.8 h/year for the CIS system. This corresponds to an average inverter efficiency of 88% for both systems. January was the month with the lowest average inverter efficiency of 75%. Average monthly inverter efficiency of the two systems differs with less than 0.5%. Since the inverter efficiency estimations are done using the efficiency profile from PVsyst, and because of the simplifications done in the calculations, the uncertainty of the estimates is too high to see a significant difference between the inverter efficiency of the two systems. The final yield losses due to the inverter correspond to the fact that the power production of the CIS system is higher than the power production of the pc-Si system.

### 4.4.3 Irradiance induced loss

A part of the array capture losses is the irradiance induced losses, which represent the lost electricity production due to the varying intensity of the irradiance. The performance of the modules at the true irradiance conditions is compared to the performance at STC, and the deviance is counted as losses or also possible gains. The efficiency profile of a module at varying irradiance intensities differs from module to module, and it is rarely the case that the highest performance is at 1000 W/m$^2$. The efficiency profile is not given by all manufactures, but it is usual that the efficiency at 200 W/m$^2$ is stated in the datasheet of the modules.

In this study, the efficiency profile of the pc-Si modules and the CIS modules at varying light intensities were found by measuring the performance of the modules at different light intensities

in the solar simulator. The method is explained in section 3.3.5, and the resulting efficiency profiles are illustrated in Figure 3.12 along with the relative efficiency at 200 W/m$^2$ specified by the datasheets.

The irradiance induced losses were calculated by estimating an average module efficiency at eleven irradiance intervals of equal width between 0-1100 W/m$^2$. The relative energy contribution of each irradiance interval was calculated from the irradiance data and used to estimate the average efficiency loss or gain for each month and the annual impact. All the results for both the pc-Si and CIS system were negative, which means that the true irradiance conditions on average reduced the performance of the PV systems compared to the performance at 1000 W/m$^2$.

The monthly results are represented as final yield losses in Figure 4.15.

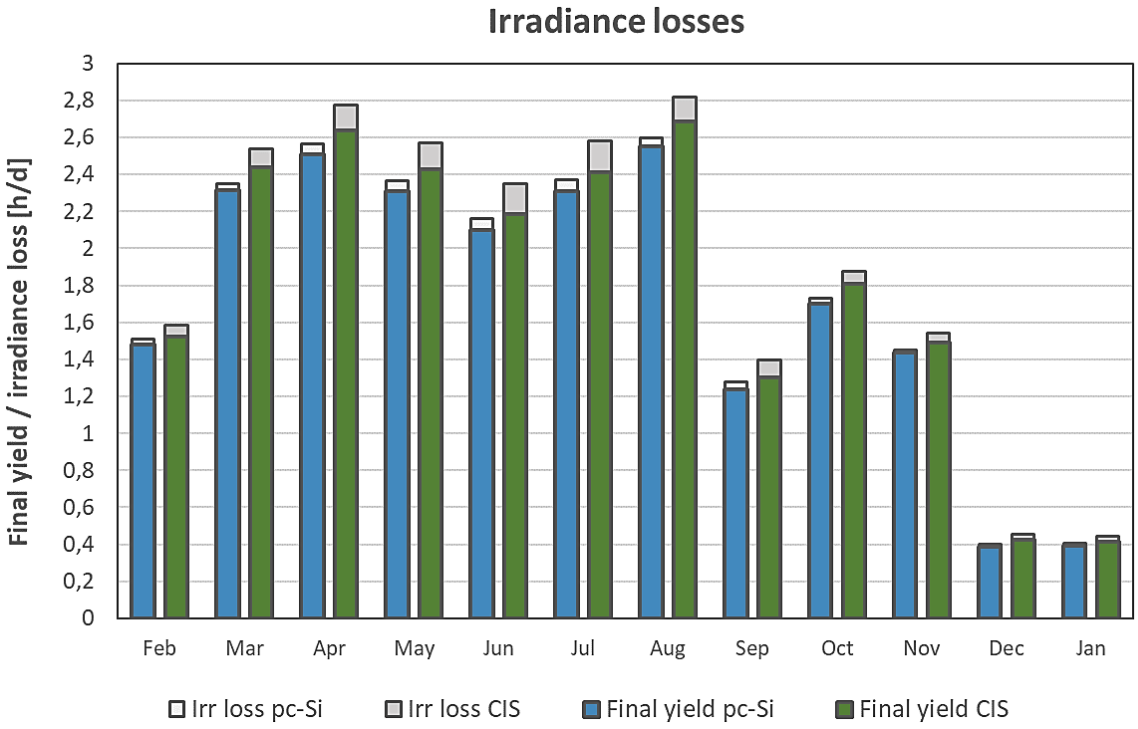


*Figure 4.15: The monthly final yield for the assessment year, with the average irradiance loss for each month.*

The results of the light intensity analysis show that the production loss, represented as final yield losses, of the CIS modules is larger than the production loss of the pc-Si modules, with 35.7 h/year and 13.8 h/year respectively. In the efficiency profiles measured for the modules, the relative efficiency of the CIS modules is less than the relative efficiency of the pc-Si modules at low intensity levels. At intensities of 800 W/m$^2$ and under, the CIS modules has a greater performance reduction than the pc-Si modules. From section 3.3.5 we have that the intensities under 800 W/m$^2$ contribute with over 90% of the incident energy in the POA. During the assessment year, 50% of the incident energy is delivered at intensities lower than 500 W/m$^2$. This supports the result that the CIS system is affected more by the true irradiance conditions than the pc-Si system is.

### 4.4.4 Temperature and irradiance losses

The relation between the irradiance and the yield of the PV systems are presented in Figure 4.7. As earlier explained the relation between them are not perfectly linear, there is some variation that is explained by other factors. Module temperature is a factor that also affects the performance of the module performance. In cold conditions, the performance of the PV system will increase compared to the performance at STC, and oppositely the performance will be reduced when the cell temperature rises above 25°C. To what extent different PV technologies are affected by the cell temperature differs. The CIS modules have a lower temperature dependence than the pc-Si modules. If there is a performance drop due to the cell temperature, it is counted as a part of the array capture losses, if the performance increases the array capture losses decreases.

The cell temperature is affected by several factors, among them are the wind conditions, the ambient temperature and the irradiance in the POA. The correlation between the irradiance and the cell temperature is studied in section 3.3.5. A significant correlation was found. Therefore, the impact of the cell temperature on the performance of the systems is not analyzed independently. Instead, the combined effect of both the cell temperature and the irradiance is studied. The estimated effect of the cell temperature and the irradiance is illustrated in Figure 4.16. The method used to derive these results is explained in section 3.3.5.

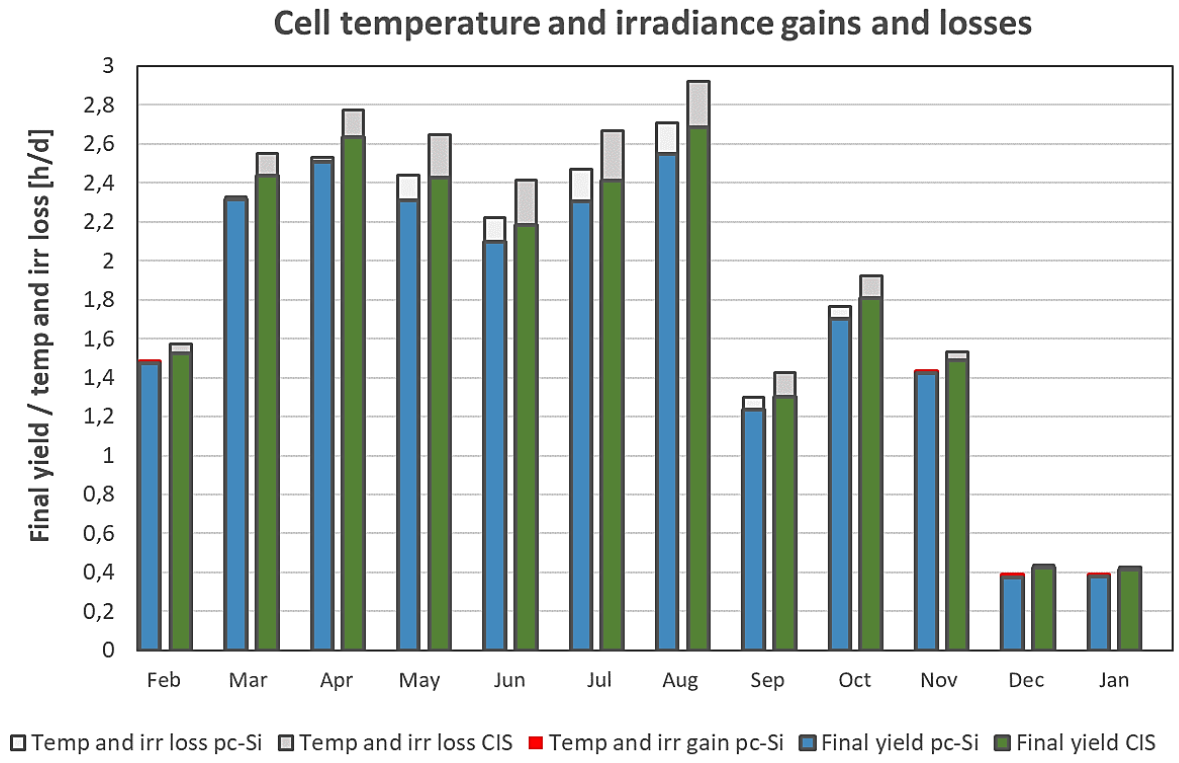


*Figure 4.16: The monthly final yield for the assessment year, with the average irradiance loss for each month. Some months have production gains because of the temperature and irradiance conditions. This gain is drawn as a red column.*

The results from the combined analysis of the cell temperature and irradiance impact on the performance of the systems show that the pc-Si system has the lowest annual $Y_F$ change of 21.3 h/year. The CIS system has an annual $Y_F$ change of 47.2 h/year. The monthly results show that the combined effect of cell temperature and the irradiance is largest in the spring and summer months. In November, December, January, and February the effect is small. In these months the pc-Si system has gained in production because of the real climate conditions. This is probably due to the temperature dependence of the pc-Si modules, that is high compared to that of the CIS modules, in addition to a low ambient temperature and low irradiance that reduces the cell temperature. Although the performance of the modules would be reduced during the same period because of low intensity levels.

The pc-Si system has on average performed better in the real climate conditions than the CIS system. This is more noticeable in Figure 4.17. In this figure, the irradiance induced change in performance of the PV systems is compared to the combined cell temperature and irradiance induced change. The columns represent the lost or gained final yield. The results from the analysis of the combined cell temperature and irradiance impact is placed behind the results from the analysis of only the irradiance impact.

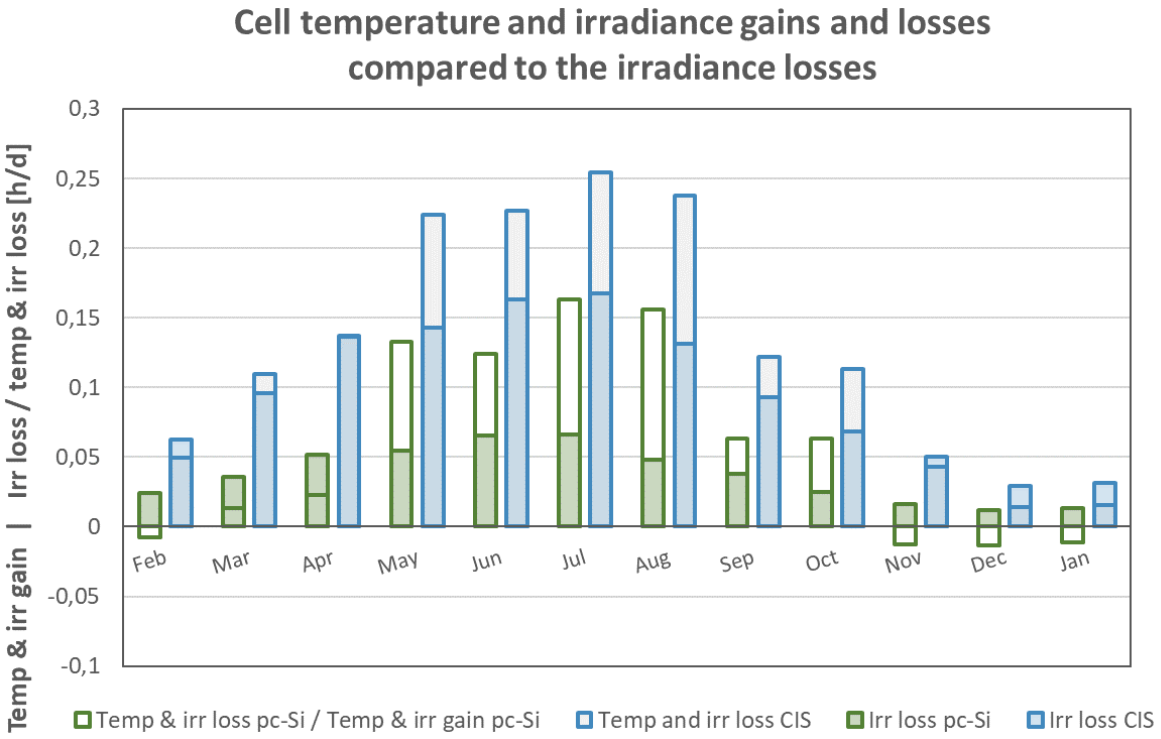


*Figure 4.17: In this histogram the final yield loss or gain due to the combined cell temperature and irradiance effect is compared to the final yield loss due to only the irradiance conditions. The irradiance losses are placed in front of the combined temperature and irradiance losses. All gains are represented as negative values.*

Adding the temperature impact in the analysis uncover that the array capture loss from May to October for both the pc-Si and the CIS systems are greater than found by just analyzing the impact of the irradiance. During these months the losses in the pc-Si system increase more than that of the CIS system. In the winter months, the cell temperature improved the performance of the systems. The overall results show that the annual final yield losses are greater when the temperature effect is added to the irradiance effect. Also, it looks like the local climate has reduced the performance of the CIS system more than it has reduced the performance of the pc-Si system.

### 4.4.5 New understanding of the system performance

In the past three sections, a few key factors that contribute to the system and array capture losses are analyzed for the two systems in this study. The monthly effect of the factors on the performance of the systems is presented in Figure 4.14-4.16. All the factors that were studied reduced the average annual performance of both systems. A summary of the estimated losses is presented with the performance parameters, given in Table 4.10.

*Table 4.10: The estimated losses due to the inverter, the irradiance, and the combination of the cell temperature and the irradiance. All the losses are presented with the performance parameters.*

| | **Final yield loss [h/year]** | | **Performance ratio [%]** | | **Efficiency reduction [%]** | |
|---|---|---|---|---|---|---|
| | pc-Si | CIS | pc-Si | CIS | pc-Si | CIS |
| **Inverter loss** | 86.1 | 91.8 | 10.6 | 11.3 | 1.67 | 1.60 |
| **Irradiance loss** | 13.8 | 35.7 | 1.7 | 4.4 | 0.26 | 0.62 |
| **Temperature and irradiance loss** | 21.3 | 47.2 | 2.6 | 5.8 | 0.41 | 0.82 |

The inverter loss is usually a large part of the system losses, and the temperature and irradiance losses typically covers large parts of the array capture losses. The estimated annual average inverter loss are 86.1 h/year and 91.8 h/year for the pc-Si and CIS systems respectively. Compared to the estimated system losses found in section 4.4.1, the inverter loss is too great, especially for the CIS system. This implies that the estimated loss for the inverter is not accurate.

The temperature and irradiance losses is lower than the array capture losses found in section 4.4.1. The temperature and irradiance induced losses are greater than the losses due to the irradiance alone. This applies to both systems. The CIS system had a higher loss due to the climate factors than the pc-Si system, with *PR* losses of 4.4% and 1.7% respectively.

The additional losses that are not accounted for by the factors analyzed in this study could be callused by factors such as; reflection, the spectral mismatch, shading, soiling, cable resistance, the MPPT and other mismatch related losses.

The uncertainties in the measuring devises and the calculations is difficult to quantify. This makes it difficult to know how incorrect the results are. Comparable studies were not discovered. Further studies should be conducted on the performance of BAPV, and the performance of CIS and pc-Si systems in Nordic climate.

# 5 Conclusions

During the assessment year of this study, the CIS system outperformed the pc-Si system by approximately 14%. The largest production of the two systems took place between March and August. The annual production of the pc-Si and CIS systems was 810.0 kWh and 920.8 kWh respectively. The reference yield of the systems was 811.7 h/year. The average annual final yield was estimated as 623.1 h/year for the pc-Si system and 697.6 h/year for the CIS system, based on the assumption that the installed power of the pc-Si system was 1.30 $kW_p$ and the CIS system was 13.2 $kW_p$. A simulation performed in PVsyst with an imported weather file for the assessment period gave an estimate for the system yield that deviated 1% from the actual yield.

Based on measurements with a pulsed solar simulator, degradation was observed. It was also discovered that the CIS modules had improved due to the light soaking effect. The results from the solar simulator measurements showed that the installed power of the pc-Si system was 1.28 $kW_p$ and the installed power of the CIS system was 1.39 $kW_p$. This renewed the final yield of the pc-Si and CIS systems which were estimated as 630.8 h/year and 662.0 h/year respectively. The result partly explains why the CIS modules outperformed the pc-Si system during the assessment period.

In a study of the loss mechanisms, the soiling effect showed no significant impact on the system performance. The local irradiance and temperature, reduced the performance of the pc-Si system by 21.3 h/year and the CIS system by 47.2 h/year. The array capture losses were also estimated and supported the result that the CIS system was more affected by the Nordic climate conditions than the pc-Si system.

The losses due to the inverter were estimated, but the calculation of the average system losses exposed that the results were inaccurate. The system losses of the pc-Si system was far higher than that of the CIS system. This may have been influenced by an oversized inverter.

The study shows that the system efficiency of the pc-Si system was larger than the system efficiency of the CIS system, even though the CIS system produced a higher yield than expected. This suggests that the pc-Si system produces more electricity per area of installed PV than the CIS modules.

The results also show that the CIS system produces more electricity per installed $kW_p$ than the pc-Si system. Analysis has shown that this partly is due to the lights soaking effect and the oversized inverter.

# 6 Further work

- A new study should be performed on the systems with an expanded time period, using measured data for more than one year. For this study, the logger for the weather data should be substituted with a logging device that has an accurate clock.
- The expanded dataset should be used in an improved analysis of the loss mechanisms of the two systems. The method for estimating the inverter loss should be changed.
- Additional analysis of the reflection, shading, spectrum, and albedo should be performed to closer investigate the impact of the Nordic climate on the performance of the systems.
- The soiling losses should be studied further in other seasons of the year. Especially in the dryer months, when soiling might have an increased effect on the system performance.
- New measurements of all the modules should be done with the solar simulator in a temperature controlled room. This will reduce the uncertainty of the measurements taken both at STC and at varying light intensities. The relative efficiency of the CIS modules at different light intensities can be measured after the metastable changes have vanished so that these will not affect the result.

# 7 References


Ayompe, L., Duffy, A., McCormack, S. & Conlon, M. (2011). Measured performance of a 1.72 kW rooftop grid connected photovoltaic system in Ireland. *Energy conversion and management*, 52 (2): 816-825.

Bjørn Thorud. (2017). *Solenergi i Norge – endelig take off?* Unpublished manuscript.

Commission, I. E. (1987). Standard IEC 60904-3: photovoltaic devices. *Part 3: Measurement Principles for Terrestrial Photovoltaic (PV) Solar Devices With Reference Spectral Irradiance Data*.

Deceglie, M. G., Silverman, T. J., Emery, K., Dirnberger, D., Schmid, A., Barkaszi, S., Riedel, N., Pratt, L., Doshi, S. & Tamizhmani, G. (2015). Validated method for repeatable power measurement of CIGS modules exhibiting light-induced metastabilities. *IEEE Journal of Photovoltaics*, 5 (2): 607-612.

Del Cueto, J., Rummel, S., Kroposki, B., Osterwald, C. & Anderberg, A. (2008). *Stability of CIS/CIGS modules at the outdoor test facility over two decades*. Photovoltaic Specialists Conference, 2008. PVSC'08. 33rd IEEE: IEEE.

Dirnberger, D. (2017). Photovoltaic module measurement and characterization in the laboratory. In *The Performance of Photovoltaic (PV) System*, pp. 23-70: Elsevier.

Frontier, S. (2016). *CIS power modules by Solar Frontier*. Germany: Solar Frontier. Unpublished manuscript.

Google maps. *Kjeller*. Available at: https://www.google.no/maps/@59.9731247,11.051425,18z (accessed: 22.04.2018).

Gostein, M. & Dunn, L. (2011). *Light soaking effects on photovoltaic modules: Overview and literature review*. Photovoltaic Specialists Conference (PVSC), 2011 37th IEEE: IEEE.

Honsberg, C. & Bowden, S. (2014). *PVeducation.org*. Available at: http://pveducation.org/pvcdrom/2-properties-sunlight/solar-radiation-outside-earths-atmosphere (accessed: 20.03.2018).

International Renewable Energy Agency, I. (2018). *Renewable power generation costs in 2017*. Abu Dhabi: International Renewable Energy Agency (IRENA).

Jahn, U., Mayer, D., Heidenreich, M., Dahl, R., Castello, S., Clavadetscher, L., Frölich, A., Grimmig, B., Nasse, W. & Sakuta, K. (2000). *International Energy Agency PVPS Task 2: Analysis of the operational performance of the IEA Database PV systems*. 16th European Photovoltaic Solar Energy Conference and Exhibition, Glasgow, United Kingdom.

Jonas Skaare Amundsen, G. B., Harald Endresen, Torgeir Ericson, Audun Fidje, David Weir and Eirik Veirød Øyslebø. (2017). *Kraftmarkedsanalyse 2017-2030*. Norway: The Norwegian Water Resources and Energy Directorate.

Kenny, R. P., Nikolaeva-Dimitrova, M. & Dunlop, E. D. (2006). *Performance measurements of CIS modules: outdoor and pulsed simulator comparison for power and energy rating*. Photovoltaic Energy Conversion, Conference Record of the 2006 IEEE 4th World Conference on: IEEE.

Kratochvil, J. A., Boyson, W. E. & King, D. L. (2004). *Photovoltaic array performance model*: Sandia National Laboratories.

Multiconsult & Viak, A. (2018). *Solcellesystemer og sol i systemet*. Norway: Solenergiklyngen.

Müllejans, H., Zaaiman, W. & Galleano, R. (2009). Analysis and mitigation of measurement uncertainties in the traceability chain for the calibration of photovoltaic devices. *Measurement Science and Technology*, 20 (7): 075101.

Nave, C. R. (2016). *Hyper Physics, Scattering Concepts*. Available at: http://hyperphysics.phy-astr.gsu.edu/hbase/atmos/blusky.html#c2 (accessed: 20.03.2018).

Nelson, J. (2003). *The physics of solar cells*: World Scientific Publishing Company.

Pico technology. *PT100 platinum resistance thermometers*. Available at: https://www.picotech.com/library/application-note/pt100-platinum-resistance-thermometers (accessed: 24.04.2018).

PVsyst6 Help. (2018). *Meteonorm data and program*. Available at: http://files.pvsyst.com/help/meteo_source_meteonorm.htm (accessed: 09.05.2018).

PVsyst 6 Help. (2018a). Component database.

PVsyst 6 Help. (2018b). *Inverter model: efficiency*. Available at: http://files.pvsyst.com/help/index.html?inverters_general.htm (accessed: 23.04.2018).

Sandia National Laboratories. *Plane of Array Irradiance*. Available at: https://pvpmc.sandia.gov/modeling-steps/1-weather-design-inputs/plane-of-array-poa-irradiance/ (accessed: 20.03.2018).

Shockley, W. & Queisser, H. J. (1961). Detailed Balance Limit of Efficiency of p-n Junction Solar Cells. *Journal of Applied Physics*, 32 (510). doi: 10.1063/1.1736034

Skoplaki, E. & Palyvos, J. A. (2009). On the temperature dependence of photovoltaic module electrical performance: A review of efficiency/power correlations. *Solar energy*, 83 (5): 614-624.

Smets, A. H., Jäger, K., Isabella, O., Van Swaaij, R. A. & Zeman, M. (2016). *Solar Energy: The physics and engineering of photovoltaic conversion, technologies and systems*: UIT Cambridge Limited.

Solar, S. (2016). *Spi-Sun Simulator 5100SLP Blue System: Operation and Maintenance Manual*: Spire Solar.

Statistics Norway. (2017). *Electricity*. Available at: https://www.ssb.no/en/energi-og-industri/statistikker/elektrisitet/aar (accessed: 06.05.2018).

Timeanddate. (2018). *Lillestrøm, Norge — Soloppgang, solnedgang og dagens lengde, mars 2017*. Available at: https://www.timeanddate.no/astronomi/sol/norge/lillestrom?maaned=3&year=2017 (accessed: 01.03.2018).

Willett, D. & Kuriyagawa, S. (1993). *The effects of sweep rate, voltage bias and light soaking on the measurement of CIS-based solar cell characteristics*. Photovoltaic Specialists Conference, 1993., Conference Record of the Twenty Third IEEE: IEEE.

# 8 Appendix

Electrical and mechanical specifications for the PV modules at the test site.

*Datasheet for the IBC PolySol 260 CS modules.*

Smart Systems for Solar Power

IBC SOLAR


**IBC EcoLine – For particulary stable output**

## IBC PolySol 250 CS, 255 CS, 260 CS

**Solar modules made by polycrystalline silicon**

Whether for single family homes, industrial roofs or open spaces – the trusted solar modules IBC PolySol CS are perfectly suited for anyone placing high demands on quality and cost efficiency. IBC SOLAR defines the most stringent specifications for components, ensuring you the best results. Thanks to the modules' positive power tolerance and linear performance guarantee, you'll benefit from high output and returns.
Thanks to the anti-reflective coating on the front glass panels, these modules capture even more light to be more efficient and produce optimum yields.

**Highlights:**

- 10-year product warranty*
- 25 years power warranty*
- Positive power tolerance: – 0/+5 Wp
- Highly effective with low-iron photovoltaic glass and anti-reflective coating (3.2 mm)
- Tested according IEC 61215 for snow loads up to 5400 Pa (ca. 550 kg/m²)
- IEC 61730, application class A for system voltages up to 1000 V, protection class II
- Produced in ISO 9001 and ISO 14001 certified factories
- 100% end control with individual registration of the electrical characteristics
- Quality tested by IBC SOLAR in own laboratory with climate chambers and flasher with integrated electroluminescence measurement

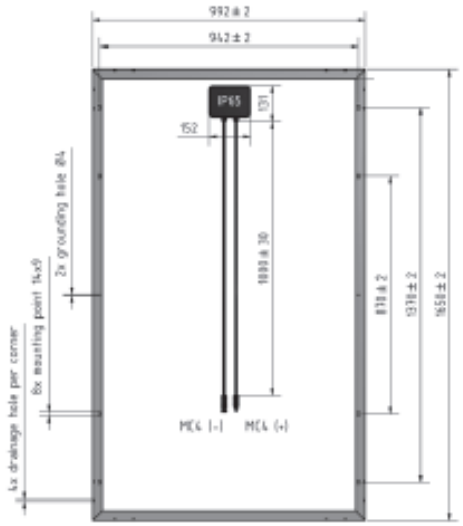


Progression of the power warranty

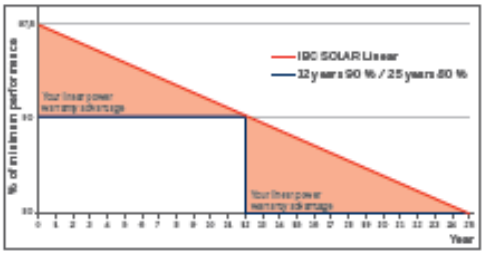


## TECHNICAL DATA

| IBC PolySol | 250 CS | 255 CS | 260 CS |
|---|---|---|---|
| STC Power Pmax (Wp) | 250 | 255 | 260 |
| STC Nominal Voltage Umpp (V) | 30.4 | 30.9 | 31.1 |
| STC Nominal Current Impp (A) | 8.23 | 8.25 | 8.37 |
| STC Open circuit voltage Uoc (V) | 37.6 | 37.8 | 38.1 |
| STC Short circuit current Isc (A) | 8.81 | 8.83 | 8.98 |
| 800W/m² NOCTAM1.5 Power Pmax (Wp) | 183.07 | 186.77 | 190.64 |
| 800W/m² NOCTAM1.5 Nominal Voltage Umpp (V) | 27.78 | 27.96 | 28.16 |
| 800W/m² NOCTAM1.5 Open Circuit Voltage Uoc (V) | 35.05 | 35.57 | 36.04 |
| 800W/m² NOCTAM1.5 Short Circuit Current Isc (A) | 6.92 | 6.96 | 7.00 |
| Rel. efficiency reduction @ 200W/m² (%) | 3.9 | 4.23 | 4.29 |
| Tempcoeff Isc (%/°C) | +0.064 | +0.064 | +0.064 |
| Tempcoeff Uoc (mV/°C) | −117.7 | −120.7 | −121.7 |
| Tempcoeff Pmpp (%/°C) | −0.43 | −0.43 | −0.43 |
| Module Efficiency (%) | 15.3 | 15.6 | 15.9 |
| NOCT (°C) | 48 | 48 | 48 |
| Max. System Voltage (V) | 1000 | 1000 | 1000 |
| Max. Reverse Current Ir (A) | 20 | 20 | 20 |
| Current value String fuse (A) | 15 | 15 | 15 |
| Fuse protection from parallel strings | 4 | 4 | 4 |
| Height (mm) | 45 | 45 | 45 |
| Weight (kg) | 20.5 | 20.5 | 20.5 |
| Article number | 2203800007 | 2203800005 | 2203800006<br>2203800008 |

2014-08-01

Presented by:

* The linear power warranty is only valid for installations within Europe and Japan. For further information, please refer to the corresponding product and power warranty in accordance with the version of the full warranty conditions received from your specialized IBC SOLAR partner at the time of installation. This warranty is valid only when the product is installed in accordance with the applicable installation instructions. Electrical values under standard test conditions: 1000 W/m²; 25°C, AM1.5. 800 W/m², NOCT. Specifications according EN 60904-3 (STC). All datas according DIN EN 50380. Subject to modifications that represent progress.

*Datasheet for the SF165-S modules.*

Solar Frontier Europe GmbH

# Product Data Sheet SF165-S

## Electrical Characteristics

### Electrical Performance at Standard Test Conditions (STC)*1

| | | SF165-S |
|---|---|---|
| Nominal Power | Pmax | 165 W |
| Power tolerance | | +5 W / 0 W |
| Open circuit voltage | Voc | 110.0 V |
| Short circuit current | Isc | 2.20 A |
| Voltage at nominal power | Vmpp | 85.5 V |
| Current at nominal power | Impp | 1.93 A |

### Electrical Performance at Nominal Operating Cell Temperature (NOCT) Conditions*2

| | | SF165-S |
|---|---|---|
| Nominal Power | Pmax | 123 W |
| Open circuit voltage | Voc | 100 V |
| Short circuit current | Isc | 1.76 A |
| Voltage at nominal power | Vmpp | 80.2 V |
| Current at nominal power | Impp | 1.53 A |

### Performance at Low Irradiance

Efficiency reduction of maximum power from an irradiance of 1,000 W/m² to 200 W/m² at 25 °C is typically 2.0 %.
The standard deviation for the reduction of efficiency is 1.9 %.

*1 Standard Test Conditions (STC): 1,000 W/m² irradiance, module temperature 25 °C, air mass 1.5. Isc and Voc are ±10 % tolerance of STC rated values. Module output may rise due to the Light Soaking Effect. Subject to simulator measurement uncertainty (using best-in-class AAA solar simulator and applying Solar Frontier preconditioning requirements): +10 % / -5 %.
*2 Nominal Operating Cell Temperature Conditions: Module operating temperature at 800 W/m² irradiance, air temperature 20 °C, wind speed 1 m/s and open circuit condition.

## Typical I-V Characteristics at STC

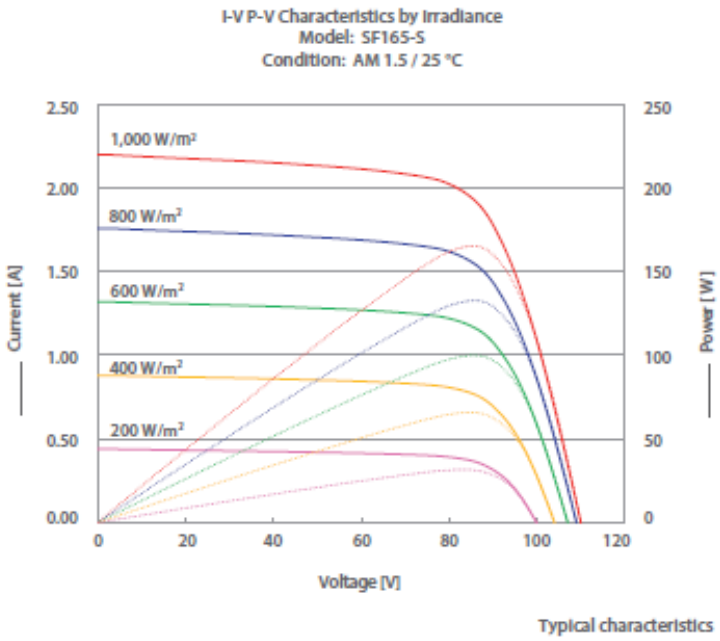


Typical characteristics

## Thermal Characteristics

| | |
|---|---|
| **NOCT** | 47 °C |
| **Temperature coefficient of Isc** | +0.01 %/K |
| **Temperature coefficient of Voc** | -0.30 %/K |
| **Temperature coefficient of Pmax** | -0.31 %/K |

These thermal characteristics are typical data.

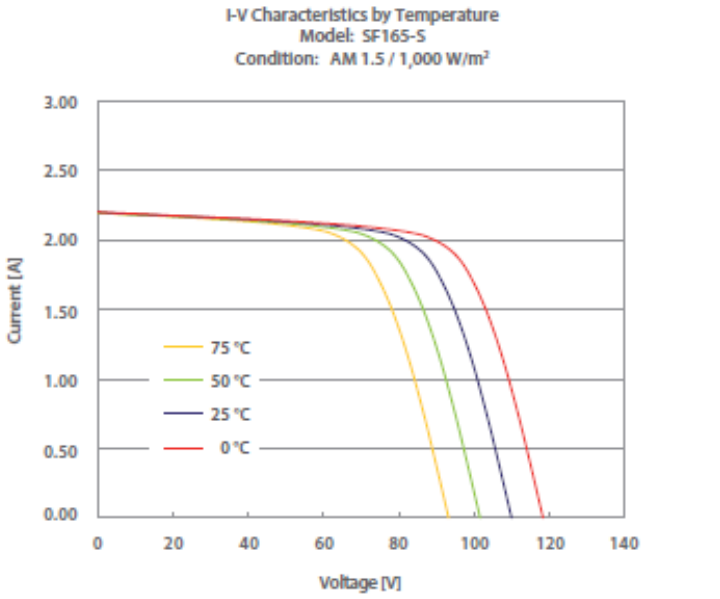


Typical characteristics

SOLAR FRONTIER

## Characteristics for System Design

| | | |
|---|---|---|
| Maximum system voltage | Vsys | 1,000 V DC (UL 600 V DC) |
| Limiting reverse current | Ir | 7 A |
| Maximum series fuse rating | Isf | 4 A |

## Mechanical Characteristics

| | |
|---|---|
| Dimensions (L x W x H)*3 | 1,257 x 977 x 35 mm (49.5 x 38.5 x 1.4 inch) |
| Weight | 20 kg (44.1 lbs) |
| Module operating temperature | -40 °C to 85 °C |
| Application class on IEC61730 | Class A |
| Fire safety class on IEC61730 | Class C |
| Safety class on IEC61140 | II |
| Snow load (to the front of the module)*4 | 2,400 Pa (IEC61646) / 1,600 Pa design load (UL1703) |
| Wind load (to the back of the module) | 2,400 Pa (IEC61646) / 1,600 Pa design load (UL1703) |
| Cell type | CIS substrate glass (cadmium free) |
| Front cover | Clear tempered glass, 3.2 mm |
| Encapsulant | EVA |
| Back sheet | Weatherproof plastic film (color: black & silver) |
| Frame | Anodized aluminum alloy (color: black) |
| Edge sealant | Butyl rubber |
| Junction box | Protection rating: IP67 (with bypass diode) |
| Adhesive | Silicone |
| Output cables (Conductor) | 2.5 mm²/ AWG14 (halogen free) |
| Cable lengths (symmetrical) | 1,200 mm (47.2 inch) |
| Connectors | MC4 compatible |

## Qualifications and Compliance

| |
|---|
| IEC 61646 / IEC 61730 / UL 1703 / MCS 005-2.3 |
| CE-Mark declaration |
| Solar Frontier is certified as: ISO 9001 / ISO 14001 / OHSAS 18001 |
| RoHS compliant |

Electrical and mechanical specifications for the inverters at the test site.

*Datasheet for the Delta RPI H3 inverter.*

# RPI H3

High efficiency single phase transformerless inverters for the European market - Perfect choice for residential PV systems

**Versatile applications**

- Aluminium housing ensures long lasting protection against moisture and corrosion
- Wide input voltage range
- Suitable for indoor and outdoor applications (IP65)
- Compact design for simplified installation

**Maximum profitability**

- Peak efficiency of 97 %
- Fanless design for reduced maintenance costs
- Affordable residential inverter with all essential functions and reliable performance

www.solar-inverter.com

# 3.0 kVA transformerless solar inverters

## Technical data RPI H3

| INPUT (DC) | RPI H3 |
|---|---|
| Max. recommended PV power | 3.78 kW$_p$ |
| Max. power | 3.2 kW |
| Nominal power | 3.15 kW |
| Voltage range | 125 ... 600 V [1] |
| MPP operating voltage range | 125 ... 550 V |
| Startup voltage | 150 V |
| Voltage range for maximum power | 320 ... 500 V |
| Max. current | 10 A |
| Number of MPP trackers | 1 |

| OUTPUT (AC) | |
|---|---|
| Maximum apparent power | 3 kVA [2] |
| Nominal apparent power | 3 kVA [2] |
| Voltage range | 230 -20%/+22%, 1 Phase (L, N, PE or L, L, PE) [3] |
| Nominal current | 13 A |
| Nominal frequency | 50 / 60 Hz |
| Frequency range | 50 / 60 Hz ± 5 Hz [3] |
| Power factor adjustable | 0.8 cap ... 0.8 ind |
| Total harmonic distortion (THD) | < 3 % @ nominal apparent power |

| GENERAL SPECIFICATION | |
|---|---|
| Model name | RPI H3_110 |
| Part number Delta | RPI302N63E0000 |
| Max. efficiency | 97.0 % |
| Efficiency EU | 96.2 % |
| Operating temperature | -25 ... +60 °C |
| Full power without derating | -25 ... +40 °C |
| Storage temperature | -25 ... +60 °C |
| Humidity | 0 ... 95 % non-condensing |
| Max. operating altitude | 2000 m (above sea level) |
| Standard guarantee | 5 years (guarantee extension available upon request) |

| MECHANICAL DESIGN | |
|---|---|
| Size (H x W x D) | 367 x 420 x 157 mm |
| Weight | 15 kg |
| Cooling | Natural convection |
| AC connector | Wieland RST25I3S B1G M01 |
| DC connector | 2 pairs of Multi-Contact MC4 |
| Communication interfaces | 2 x RS485, 1 x dry contact, 4 x digital inputs |
| DC disconnector | Integrated |
| Display | 2 LEDs, 2-line LCD |

| SAFETY / STANDARDS | RPI H3 |
|---|---|
| Protection degree | IP65 |
| Safety class | I |
| Configurable trip parameters | Yes |
| Insulation monitoring | Yes |
| Overload behavior | Current limitation; power limitation |
| Anti-islanding protection / Grid regulation | VDE 0126-1-1; VDE-AR-N 4105; Synergrid C10/C11 06/2012 / VDE 126 A1; VFR 2013 / 2014; VDE 16 1-1 A1; UTE 15-712; French Islands 50 Hz/60 Hz; EN 50438 2013:Netherlands; UK G83-2 |
| EMC | EN61000-6-2; EN61000-6-3 |
| Safety | IEC62109-1 / -2; CE compliance |

1) No risk of electrical damage till 630 V
2) Cos Phi = 1 (VA = W)
3) AC voltage and frequency range will be programmed according to the individual country requirements.


**United Kingdom**
Email: sales.uk@solar-inverter.com
Tel: 0800 051 4280 (Free Call)

**International**
Email: sales.europe@solar-inverter.com
Tel: +49 7641 455 547


www.solar-inverter.com

Electrical and mechanical specifications for the solar simulator.

*Pages from the solar simulator manual.*

spire

# Spi-Sun Simulator™ 5100SLP Blue System

## A Photovoltaic Module Tester


*Operation and Maintenance Manual*

(Note: your product may vary slightly from photo above.)

Spire Solar, LLC
Fax (978) 649-6225
Phone (978) 649-6111
support@spiresolar.com



The Spi-Sun Simulator™ system manuals are issued by Spire Solar for the exclusive use of its customers.

# 3 Specifications

## 3.1 Spi-Sun Simulator™ 5100SLP Blue System Specifications

The Spi-Sun Simulator™ 5100SLP system conforms to the requirements of this specification and information in this manual. Any deviation from the product specification must be noted as a contract requirement.

**Table 5: Specifications of the Spi-Sun Simulator™ 5100SLP System**

| | |
|---|---|
| **Maximum Module Dimensions** | |
| Maximum Module Length | 2100 mm |
| Maximum Module Width | 1300 mm |
| **Light Source** | |
| Number of Lamps | 1 |
| Lamp Type | Single long pulse filtered xenon tube |
| Pulse Duration | 10 to >50 ms at 1000 W/m$^2$ |
| Spectrum | ≤ ± 18%, AM 1.5G, 300-1200 nm (exceeds Class A) |
| Irradiance Temporal Stability | ≤ 0.2% at 1,000 W/m$^2$ (exceeds Class A) |
| Irradiance Spatial Uniformity | ≤ 1% |
| Lamp Life | >150,000 flashes |
| **Measurement Range and Performance** | |
| Range of Light Intensity | 200-1,100 W/m$^2$ |
| Measurement Duration | < 1 second |
| Power/ Module (max) | 600 W |
| Voltage Ranges | 5 ranges (2.5, 10, 25, 100, 250 V full-scale) |
| Current Ranges | 4 ranges (3, 6, 12, 25 A full-scale) |
| I/V Resolution | 0.003% |

**Table 5: Specifications of the Spi-Sun Simulator™ 5100SLP System**

| | |
|---|---|
| Repeatability<br>Defined as $C_v$ = Standard Deviation / Mean * 100% where $C_v \leq 0.15\%$ is based on SPC data (5 flashes with a 50-second delay between flashes). | $\leq 0.15\%$ $P_{max}$, $I_{sc}$, $V_{oc}$, FF |
| **Throughput** | |
| Continuous Typical Cycle Time | 30 seconds |
| **System Specifications (not including control cabinet)** | |
| Length x Width x Height | 2740 x 2007 x 1040 mm |
| Weight | 702 kg (1,547 lb) |
| **Control Cabinet Dimensions** | |
| Length x Width x Height | 1716 x 635 x 1380 mm |
| Weight | 316 kg (697 lb) |
| **Utilities Requirements** | |
| Electricity | 208-240 VAC ±10%, 30 A, 50/60 Hz, 1 Ph |
| **Environment** | |
| Temperature | 23 ±5 °C |
| Humidity | 40–55% r.h. non-condensing |

## 3.2 Certifications

**Figure 3: CE Certification**

CE

## 3.3 Handling, Transportation, and Storage

The following guidelines will help ensure that the Spi-Sun Simulator™ 5100 system is handled correctly during transportation and storage.

- Carefully crate the tool for transport of any kind.
- If transporting the simulator by truck, air ride is required.

Production results

**p-Si**

| | Yield [kWh] | Energy [kWh] | Eff | Sim Yield [kWh] | Sim Energy [kWh] | Sim Eff | Sim2 Yield [kWh] | Sim2 Energy [kWh] | Sim2 Eff | Yield Rate | Energy Rate | Eff diff |
|---|---|---|---|---|---|---|---|---|---|---|---|---|
| Feb | 53,300 | 394,879 | 13,50 % | 44,508 | 335,158 | 13,28 % | 51,2925406 | 389,9101532 | 13,15 % | 1,198 | 1,178 | 0,22 % |
| Mar | 92,1 | 728,1324393 | 12,65 % | 105,1827265 | 795,35231 | 13,22 % | 93,7923367 | 731,7184225 | 12,82 % | 0,875619059 | 0,915484157 | -0,58 % |
| Apr | 96,7 | 774,186194 | 12,49 % | 102,6864361 | 817,0271545 | 12,57 % | 98,2738452 | 781,1215305 | 12,58 % | 0,941701783 | 0,947564827 | -0,08 % |
| May | 91,9 | 789,459373 | 11,64 % | 98,0789631 | 821,6494842 | 11,94 % | 93,1587263 | 787,658638 | 11,83 % | 0,937000118 | 0,960822575 | -0,30 % |
| Jun | 80,8 | 710,1652558 | 11,38 % | 93,3484667 | 800,6534969 | 11,66 % | 82,4788355 | 714,0332405 | 11,55 % | 0,865573939 | 0,88698202 | -0,28 % |
| Jul | 91,8 | 802,1576248 | 11,44 % | 88,1441075 | 772,0915235 | 11,42 % | 93,9901848 | 809,7881438 | 11,61 % | 1,041476312 | 1,038941111 | 0,03 % |
| Aug | 101,5 | 855,0692814 | 11,87 % | 80,1285655 | 689,6938911 | 11,62 % | 103,5375333 | 866,6415251 | 11,95 % | 1,266714303 | 1,239780854 | 0,25 % |
| Sep | 47,7 | 405,9181684 | 11,75 % | 82,8783326 | 677,397616 | 12,23 % | 48,4271907 | 410,549436 | 11,80 % | 0,575542467 | 0,599231764 | -0,48 % |
| Oct | 67,8 | 537,8917522 | 12,60 % | 56,8601654 | 450,744314 | 12,61 % | 66,1241124 | 523,2579634 | 12,64 % | 1,192398923 | 1,193341181 | -0,01 % |
| Nov | 55,3 | 407,5312928 | 13,57 % | 22,6554479 | 177,2744604 | 12,78 % | 49,7283064 | 373,0986696 | 13,33 % | 2,440914002 | 2,298871997 | 0,79 % |
| Des | 15,5 | 127,863731 | 12,12 % | 13,3676619 | 103,8552047 | 12,87 % | 12,2564754 | 97,45853138 | 12,58 % | 1,159514664 | 1,231173068 | -0,75 % |
| Jan | 15,6 | 109,5521858 | 14,24 % | 18,2648534 | 142,7252927 | 12,80 % | 11,3739188 | 93,8867457 | 12,11 % | 0,854099382 | 0,767573733 | 1,44 % |
| SUM | 810,000 | 6642,806 | 12,19 % | 806,104 | 6583,623 | 12,24 % | 804,434 | 6579,123 | 12,23 % | | | |

**CIS**

| | Yield [kWh] | Energy [kWh] | Eff | Sim Yield [kWh] | Sim Energy [kWh] | Sim Eff | Sim2 Yield [kWh] | Sim2 Energy [kWh] | Sim2 Eff | Yield Rate | Energy Rate | Eff diff |
|---|---|---|---|---|---|---|---|---|---|---|---|---|
| Feb | 59,300 | 474,057 | 12,51 % | 50,260 | 402,362 | 12,49 % | 57,6931938 | 468,0922844 | 12,33 % | 1,180 | 1,178 | 0,02 % |
| Mar | 105,2 | 874,1326021 | 12,03 % | 118,9353748 | 954,8309441 | 12,46 % | 106,4312105 | 878,4376224 | 12,12 % | 0,884513965 | 0,915484157 | -0,42 % |
| Apr | 110 | 929,4207424 | 11,84 % | 117,2959804 | 980,8518808 | 11,96 % | 112,3859236 | 937,7467055 | 11,98 % | 0,937798547 | 0,947564827 | -0,12 % |
| May | 104,6 | 947,7563954 | 11,04 % | 112,8699071 | 986,4010487 | 11,44 % | 107,3626745 | 945,5945893 | 11,35 % | 0,926730629 | 0,960822575 | -0,41 % |
| Jun | 91,2 | 852,5627613 | 10,70 % | 108,0211095 | 961,1950888 | 11,24 % | 95,5143774 | 857,2063279 | 11,14 % | 0,844279423 | 0,88698202 | -0,54 % |
| Jul | 104 | 963,0008143 | 10,80 % | 102,6324795 | 926,9060628 | 11,07 % | 109,1419893 | 972,1613529 | 11,23 % | 1,013324442 | 1,038941111 | -0,27 % |
| Aug | 115,8 | 1026,521956 | 11,28 % | 92,9740952 | 827,9866178 | 11,23 % | 119,4936134 | 1040,414587 | 11,49 % | 1,245508222 | 1,239780854 | 0,05 % |
| Sep | 54,4 | 487,3101179 | 11,16 % | 95,504263 | 813,2247773 | 11,74 % | 55,8181257 | 492,8700158 | 11,33 % | 0,569608081 | 0,599231764 | -0,58 % |
| Oct | 78 | 645,7461467 | 12,08 % | 64,7790737 | 541,1244972 | 11,97 % | 75,3724857 | 628,1780903 | 12,00 % | 1,204092549 | 1,193341181 | 0,11 % |
| Nov | 62,2 | 489,246695 | 12,71 % | 25,6051527 | 212,8203291 | 12,03 % | 56,2416374 | 447,9098765 | 12,56 % | 2,429198557 | 2,298871997 | 0,68 % |
| Des | 18,3 | 153,5020964 | 11,92 % | 15,2382291 | 124,6795438 | 12,22 % | 13,7821968 | 117,000253 | 11,78 % | 1,20092695 | 1,231173068 | -0,30 % |
| Jan | 17,8 | 131,5188448 | 13,53 % | 20,8505849 | 171,3435974 | 12,17 % | 12,5989836 | 112,7122772 | 11,18 % | 0,853693078 | 0,767573733 | 1,37 % |
| SUM | 920,800 | 7974,777 | 11,55 % | 924,967 | 7903,726 | 11,70 % | 921,836 | 7898,324 | 11,67 % | | | |

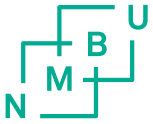


**Norges miljø- og biovitenskapelige universitet**
Noregs miljø- og biovitskapelege universitet
Norwegian University of Life Sciences

Postboks 5003
NO-1432 Ås
Norway